
**VEGETATION INFLUENCE IN STRENGTHENING CHANNEL BANKS IN THE
PENNSYLVANIAN JOGGINS FORMATION, NOVA SCOTIA**

Chinemerem Iheanyichukwu Dennar

Submitted in Partial Fulfilment of the Requirements

for the Degree of Bachelor of Science, Honours

Department of Earth Sciences

Dalhousie University Halifax, Nova Scotia

March 2012

Distribution License

DalSpace requires agreement to this non-exclusive distribution license before your item can appear on DalSpace.

NON-EXCLUSIVE DISTRIBUTION LICENSE

You (the author(s) or copyright owner) grant to Dalhousie University the non-exclusive right to reproduce and distribute your submission worldwide in any medium.

You agree that Dalhousie University may, without changing the content, reformat the submission for the purpose of preservation.

You also agree that Dalhousie University may keep more than one copy of this submission for purposes of security, back-up and preservation.

You agree that the submission is your original work, and that you have the right to grant the rights contained in this license. You also agree that your submission does not, to the best of your knowledge, infringe upon anyone's copyright.

If the submission contains material for which you do not hold copyright, you agree that you have obtained the unrestricted permission of the copyright owner to grant Dalhousie University the rights required by this license, and that such third-party owned material is clearly identified and acknowledged within the text or content of the submission.

If the submission is based upon work that has been sponsored or supported by an agency or organization other than Dalhousie University, you assert that you have fulfilled any right of review or other obligations required by such contract or agreement.

Dalhousie University will clearly identify your name(s) as the author(s) or owner(s) of the submission, and will not make any alteration to the content of the files that you have submitted.

If you have questions regarding this license please contact the repository manager at dalspace@dal.ca.

Grant the distribution license by signing and dating below.

Name of signatory

Date

ABSTRACT

Channel stability has been linked to the emergence of vegetation in the Paleozoic resulting in the evolution of single, deeper channels that meandered slowly across floodplains and narrow, probably anastomosing systems. This study reports an investigation on vegetation influence in stabilizing fluvial channel banks visible in the Joggins Fossil Cliffs. This long-standing issue has been difficult to evaluate because *in situ* plants and root systems are rarely well preserved in the fossil record. Joggins Fossil Cliffs is one of the best places for this study because of its well preserved upright trees associated with channels. The ability of vegetation to stabilize channel banks depends on plant vigour, density of vegetation cover, and root depth. Methods such as photomosaic tracing, petrographic observation, X-ray diffraction and electron microprobe observation were used in investigating and analysing data relevant to the hypothesis.

Field observations at Joggins provide evidence of root architecture and root mat impact on channel-bank stability. Root systems of upright trees form the baseline and margin line of some channels, suggesting that root architecture had an impact on channel-bank form and stability. Upright trees rooted at the top of preserved meandering-channel banks, tilted towards the channel at one locality, show evidence of bank resistance to erosion. Presence of narrow distributary channels with upright trees at both margins and extending out as an apparently dense cover into the adjoining floodplain deposit also indicates vegetation stability of channel banks. The presence of trees projecting up into the base of channels and causing bars to form around them show evidence of vegetation influence on channels, although this probably did not have any impact on the channel bank. Field observations and results, together with past research, have shown evidence for the impact of root mats in stabilizing channel banks, and abundant root casts and long roots on channel tops at some of the localities suggest possible root mat impact on the

channels. Past literature studies indicate that the binding power of root mats increases the cohesion of the soil, thereby increasing strength. This hypothesis forms the working hypothesis for research on root mats in this study. Results indicate that vegetation has significant effects on channel forms and stability. Vegetation increases channel stabilization and reduces cross-sectional area.

Thin section, X-ray diffraction and microprobe analysis has shown evidence of calcite and siderite influence in channel bank stability. Calcite crystallization around roots resulted in expansion and fragmentation of quartz, resulting in cementation of sediment as rhizoliths and compaction of the adjoining sediment. Although the timing of this cementation is difficult to constrain, such rhizoliths commonly form around growing roots in modern settings. Calcite acts as general cement in the sandstones and, if precipitated early, would have increased the strength of the bank, making it resistant to erosion. Siderite, which occurs as nodules around roots on some preserved channel banks, may have formed erosion-resistant armour. Thus, early calcite and siderite crystallisation may play an important role in the stabilization of channel banks. In general, vegetation works together with other factors such as mineral formation to create an effective impact on channel bank stability.

TABLE OF CONTENTS

ABSTRACT	I
TABLE OF CONTENTS	III
LIST OF FIGURES	VII
LIST OF TABLES	IX
ACKNOWLEDGEMENT	X
CHAPTER 1 – Introduction	1
1.1.0 Introduction – Joggins Formation	1
1.2.0 Study area	1
1.3.0 Previous Work	3
1.4.0 Objectives	4
CHAPTER 2 – Regional geology	6
2.1.0 Background	6
2.2.0 Depositional setting for Joggins Formation	9
2.3.0 Lithologies	9
2.4.0 Facies Assemblage	10
<u>2.4.1 Open-water assemblage</u>	11
<u>2.4.2 Poorly drained floodplain assemblage</u>	11

<u>2.4.3 Well drained floodplain assemblage</u>	15
CHAPTER 3 – Methodology	16
3.1.0 Introduction – Research Methods	16
3.2.0 Tracing observations	16
3.3.0 Microscopic observations	17
3.4.0 XRD observations	17
3.5.0 Electron Microprobe observations	19
CHAPTER 4 – Results	22
4.1.0 Tracing 1	22
<u>4.1.1 Description</u>	22
<u>4.1.2 Interpretation</u>	24
4.2.0 Tracing 2	25
<u>4.2.1 Description</u>	25
<u>4.2.2 Interpretation</u>	30
4.3.0 Tracing 3	32
<u>4.3.1 Description</u>	32
<u>4.3.2 Interpretation</u>	37

4.4.0 Tracing 4	38
<u>4.4.1 Description</u>	38
<u>4.4.2 Interpretation</u>	45
4.5.0 Tracing 5	46
<u>4.5.1 Description</u>	46
<u>4.5.2 Interpretation</u>	54
4.6.0 Petrography	56
<u>4.6.1 Description</u>	56
4.7.0 X-ray diffraction	59
<u>4.7.1 Description</u>	59
<u>4.7.2 Interpretation</u>	62
4.8.0 Electron microprobe	63
<u>4.8.1 Description</u>	63
<u>4.8.2 Interpretation</u>	72
CHAPTER 5 – Discussion	74
5.1.0 Vegetation and Sediment Influence	74
5.2.0 Cementation and compaction	79

5.3.0 Literatures on similar issues	81
5.4.0 W DFA verses PDF A	83
CHAPTER 6 – Conclusions	85
6.1.0 Summary and Conclusions	85
6.2.0 Recommendation for future work	87
References	88
Appendix A – Photographs	93
Appendix B – Petrographic data	97
Appendix C – XRD charts	104
Appendix D – Longitudinal root dimension and volume estimation data	113
Appendix E – Trace location on stratigraphic log	117
Appendix F – Microprobe data	124

LIST OF FIGURES

Figure 1.1	Study Areas	2
Figure 1.2	Map of the cliff section showing the trace localities	5
Figure 2.1	Geological map of showing Joggins	7
Figure 2.2	Stratigraphic position of Joggins Formation in Cumberland Group	8
Figure 4.1	Interpretative tracing and photograph of Trace 1	23
Figure 4.2	Interpretative trace and photograph of Trace 2	26
Figure 4.3	Photographs of calamite stems on siltstone beneath mudstone	27
Figure 4.4	Interpretative trace and photograph of Joggins of Trace 2b	28
Figure 4.5	Sketch of tree trunks and sediment mounds around them	31
Figure 4.6	Interpretative trace and photograph of Trace 3	33
Figure 4.7	Calamite imprint on cliff	34
Figure 4.8	Interpretative trace and photograph of Trace 3b	35
Figure 4.9	Fossilised stems on Trace 3 cliff	36
Figure 4.10	Illustrative trace and photograph of Trace 4	39
Figure 4.11	A closer view on root on Trace 4 cliff	40
Figure 4.12	Preserved roots on fallen cliff boulder.	42
Figure 4.13	Illustrative trace and photograph of Trace 4b	43

Figure 4.14	Illustrative trace and photograph of Trace 4c	44
Figure 4.15	Illustrative trace and photograph of Trace 5	47
Figure 4.16	Illustrative trace and photograph of Trace 5b	49
Figure 4.17	Illustrative trace and photograph of Trace 5c	51
Figure 4.18	Illustrative trace and photograph of tree trunk in Trace 5	52
Figure 4.19	Illustrative trace and photograph of vegetation remains in Trace 5	53
Figure 4.20	Thin section X	57
Figure 4.21	Thin section Y	58
Figure 4.22	Thin section Z	60
Figure 4.23	Electron microprobe image of siderite in sample X	65
Figure 4.24	Electron microprobe image of quartz in sample X	67
Figure 4.25	Electron microprobe image of alkali feldspar in sample X	67
Figure 4.26	Electron microprobe image of calcite in sample X	69
Figure 4.27	Electron microprobe image of kaolinite in sample X	70
Figure 4.28	Electron microprobe image of pyrite, rutile, and zircon in sample X	71

LIST OF TABLES

Table 2.1	Table of Logs/plant fragments	12
Table 4.1	Mass percentage summary	66
Table 5.1	Summary of evidences	75

AKNOWLEDGEMENTS

I would like to thank Dr. Martin Gibling for his help throughout this study. I wouldn't have been able to accomplish this without his guidance, patience and enthusiasm. I also want to say a big thanks to Zabrina for her help and company during the field work, and also to Arden Bashforth for providing vegetation identification. Big thanks to Thomas Duffett for helping me out with the XRD sample preparation and also to Keith Taylor for helping out with the XRD equipment and data. I want to send my gratitude to Gordon Brown for the thin and polished section preparation, and also to Dan MacDonald for his assistance in the microprobe work. I also want to show appreciation to Yana Fedortchouk and Zhang Zhiihai for their help in capturing thin section sample photographs. I would like to thank my lovely wife, daughter and extended family for their support and encouragement throughout this study. Finally, I would like to thank the Almighty God for seeing me through this study and being with me all through the stress period.

CHAPTER 1 - Introduction

1.1.0 Introduction

The existence of vegetation in our everyday life has resulted in the ignorance of its importance in shaping landscape in geologic time. Past and current researches have shown evidence that vegetation shaped and stabilized fluvial landscapes. Studies have also shown that rivers were wide, broad and shallow braided channels that spread and migrated across landscapes during the Ordovician but became more “tamed” later in the Palaeozoic as vascular plants began to evolve (Gibling, pers. comm. 2011). The Devonian and Carboniferous saw many complex and varied plant taxa flourish, leading to an association with the evolution of single, deeper channels that meandered slowly across floodplains and only occasionally broke their banks to carve out new channels (Gibling and Davies, 2012).

The significance of vegetation as a control of channel form and process is increasingly being recognized in fluvial research. An unresolved scientific question is the degree to which vegetation influences river channels. Over the past decade, there has been a large body of research that shows roots to be immensely strong in binding modern river banks (Gibling and Davies, 2012). However, because trees and roots are difficult to preserve in the rock record, there has been little information about vegetation influence in the past. This thesis addresses these unresolved questions of vegetation effect on river channel banks, and also raises awareness of the importance of vegetation in rock records.

1.2.0 Study area

The study area is situated in Joggins rural community which is located at 45° 42' 0" North and 64° 26' 0" West in Cumberland County, Nova Scotia (Fig. 1.1). The main focus of the study

area is the Joggins Fossil Cliffs (Fig. 1.1) which are situated in the Cumberland Basin, a sub-basin of the Maritimes Basin. The coastal section of the well exposed 15 km cliff section is famous for its magnificent fossil record preserved in its natural environment. This area is a representative of the Coal Age Pennsylvanian terrestrial tropical environment and ecosystem of the Carboniferous. Joggins attained UNESCO World Heritage status in 2008. Although there has been over 150 years of continuous research, many discoveries have been occurring in the Joggins Fossil Cliffs in recent years, resulting in more intense sedimentological and palaeoecological studies (Davies et al., 2005).

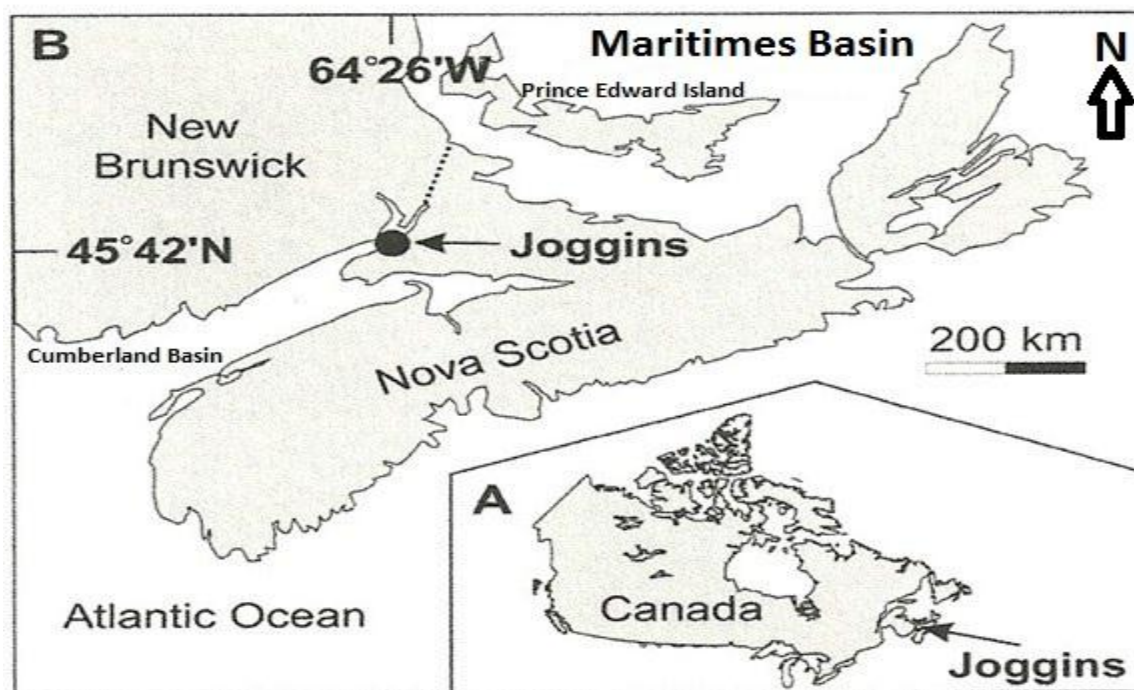


Figure 1.1-Location of study area represented by arrow in Canadian map (A), and dot in Nova Scotian map (B) (Modified from Falcon-Lang, 2003).

1.3.0 Previous Work

Significant research has been done in the Joggins Formation by many scientists from the 1800s till present. Some of the earliest scientists who contributed to the palaeontology of Joggins include Sir Charles Lyell, Sir Charles Darwin and a Canadian geologist, Sir William Dawson. The Joggins section was brought to the attention of the world through early accounts by Jackson and Alger (1829), Brown and Smith (1829), and Gesner (1836). This early awareness led to Lyell's visit to Joggins during his first visit to North America in 1845. Lyell created more awareness after his visit in 1845, describing Joggins as the finest example in the world of a Carboniferous exposure (Falcon-Lang, 2003). William Logan recorded a 14,570 foot (4441m) continuous section along Chignecto Bay and defined eight stratigraphic divisions from the top downwards. The first stratigraphic log and descriptions of the Joggins Formation were done by Logan (1845) and Dawson (1854) (Davies et al., 2005).

In the 1900s and 2000s, further research was published by Ryan, Smith, Boehner, Calder, Rygel, Teniere, Gibling, Davies and many others. The history of the stratigraphic nomenclature of Cumberland Basin was summarized by Ryan et al. (1991), Ryan and Boehner (1994) and Calder (1998). Researches of the 1900s and 2000s are focused mainly on palaeontology and sedimentology. Rygel (2005) investigated channel bodies, and Smith (1991) investigated the paleosols. Davies and Gibling (2003) worked on the sequence stratigraphy, and coal composition and carbonaceous strata were researched by Gibling and Kalkreuth (1991) and Hower et al. (2000). Falcon-Lang also did detailed work at Joggins in 2003 in which he focused on late Carboniferous tropical dryland vegetation in an alluvial-plain setting. A detailed visual log of the Joggins Formation was presented by Davies et al., (2005).

Recent research carried out relevant to the Joggins Formation includes work done by DiMichele et al. (2010) on the cyclic changes in Pennsylvanian palaeoclimate and effects on floristic dynamics in tropical Pangaea. Another significant recent work was carried out by Rygel and Gibling (2006) in which they studied fluvial architecture of the Pennsylvanian Joggins formation by recording natural geomorphic variability in a high-accommodation setting. The most recent work to be published by Gibling and Davies (2012) with reference to the study area is a summary of vegetation effects on rivers with a Palaeozoic perspective.

1.4.0 Objectives

This thesis examines representative parts of the fluvial channel systems of the Joggins Formation, as seen in the cliffs and along the coast. The main objective is to investigate the influence of vegetation on the support and stabilization of fluvial channel banks. Joggins is one of the few places in the world where this issue can be evaluated effectively in the rock record, in view of the extraordinary preservation of the upright trees. A study of various channel bodies has been carried out with a major interest in localities where upright tree trunks are positioned on or close to visible channel banks. Vegetation study with focus on roots and tree types is of immense importance to the study, and was studied systematically with the channel body study in order to explore the relationship between vegetation and sedimentation. In order to carry out these objectives successfully, stratigraphic sections that encompass strata in the cliff localities were measured, and the analysis included keeping records of the various lithologies and sedimentary structures of some of the successions in the Joggins section. Some of the sedimentary structures present in the channel sections serve as palaeoclimate indicators to show the general setting of the fluvial channels. The information mentioned in this section provides evidence relevant to the hypothesis of vegetation / sediment interaction explored in this thesis, and also creates awareness

of the importance of vegetation in stabilization of fluvial channel banks. The various localities and cliff sections traversed are represented by Trace 1 through Trace 5 in Figure 1.2.

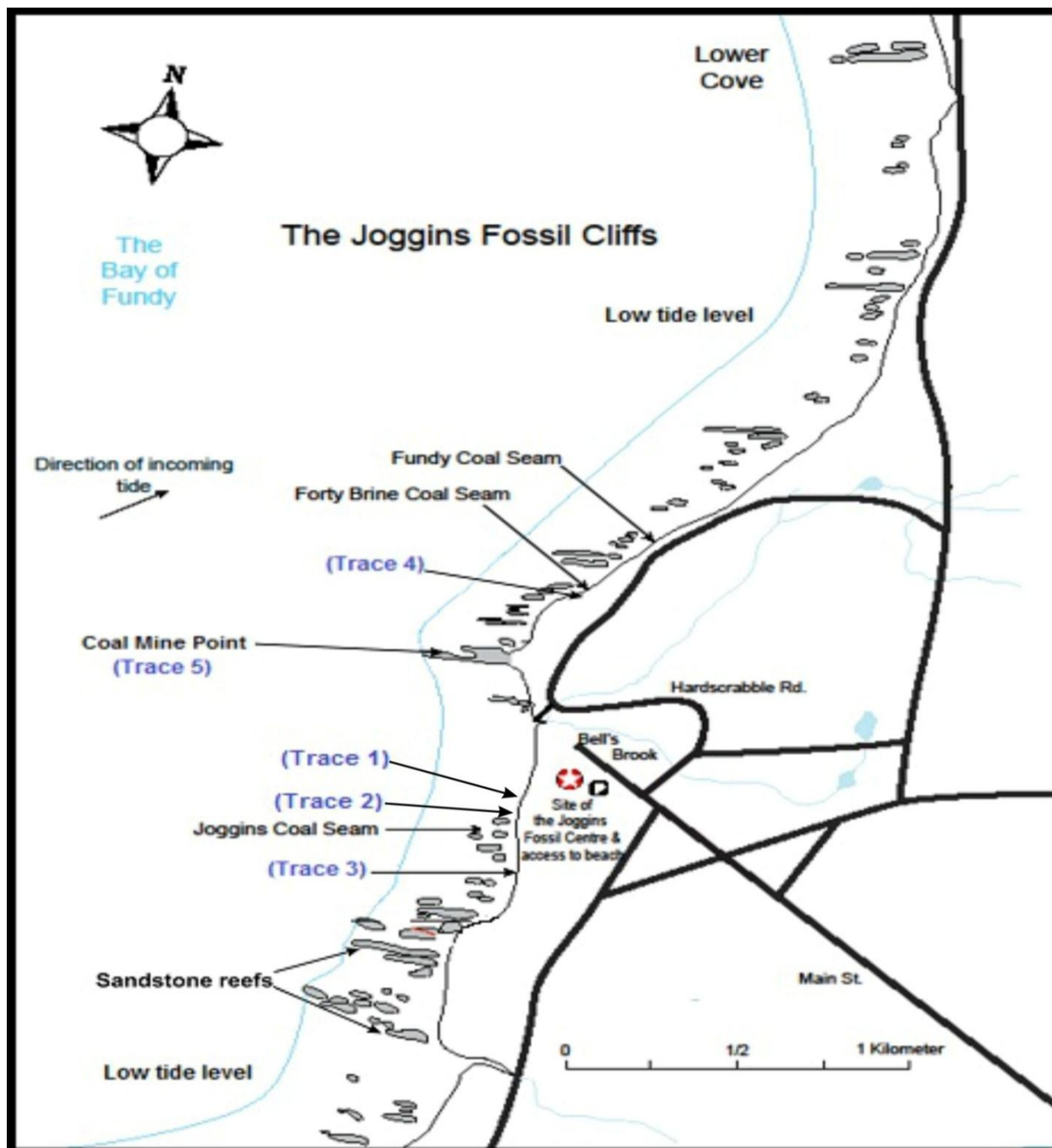


Figure 1.2-Measured section of Joggins Formation from Lower Cove to South of Bells Brook with Trace 1-5 representing the traverse localities and cliff sections.

CHAPTER 2 – Regional geology

2.1.0 Background

The Joggins Formation was deposited within the Cumberland Basin of Nova Scotia, a local depocentre within the regional Maritimes Basin of Atlantic Canada (Fig 2.1) (Ryan and Boehner, 2011). Cumberland Basin is a depocentre oriented northeast-southwest containing a succession of sedimentary strata in excess of 8 km thick. The Joggins Formation is stratigraphically positioned between Springhill Mines Formation at the top and Little River Formation at the bottom, with Polly Brook Formation laterally equivalent to the three formations (Fig. 2.2). Within the western part of the Cumberland Basin, the Athol Syncline runs to the Athol Fault to the south. This Athol Syncline hosts the Joggins Formation on its northern limb (Rygel and Gibling, 2006). The syncline is about 25 km wide by 75 km long and is bounded by the Caledonia Highlands Massif to the west and Cobequid Highlands Massif to the south, the salt-cored Minudie Anticline to the north, and two unnamed salt diapirs to the east (Calder, 1994; Rygel and Gibling, 2006). These salt diapirs and structures had great influence on the creation of accommodation in the Athol Syncline, especially in the Pennsylvanian (Waldron and Rygel, 2005).

The continuous exposure of the cliff section at Joggins is a result of high tides of the modern Bay of Fundy, recognized to have the highest tides in the world. The present appearance of the Joggins Fossil Cliffs is as a result of three major geological events that took place millions of years ago. It is not clear exactly when the first event resulting in the tilting took place. It could have been during the Carboniferous, when tectonics continued to influence the newly deposited strata or during the Mesozoic (Wach, pers. comm. 2009). The second event took place during the

Pleistocene, when glacier ice covered Nova Scotia, leaving glacial tills overlying the Carboniferous strata after melting. The last event occurred at about 8000 years ago during which sea level rose after the melting of the glaciers. This last event took place after the creation of the Bay of Fundy (Wach, pers. comm. 2009).

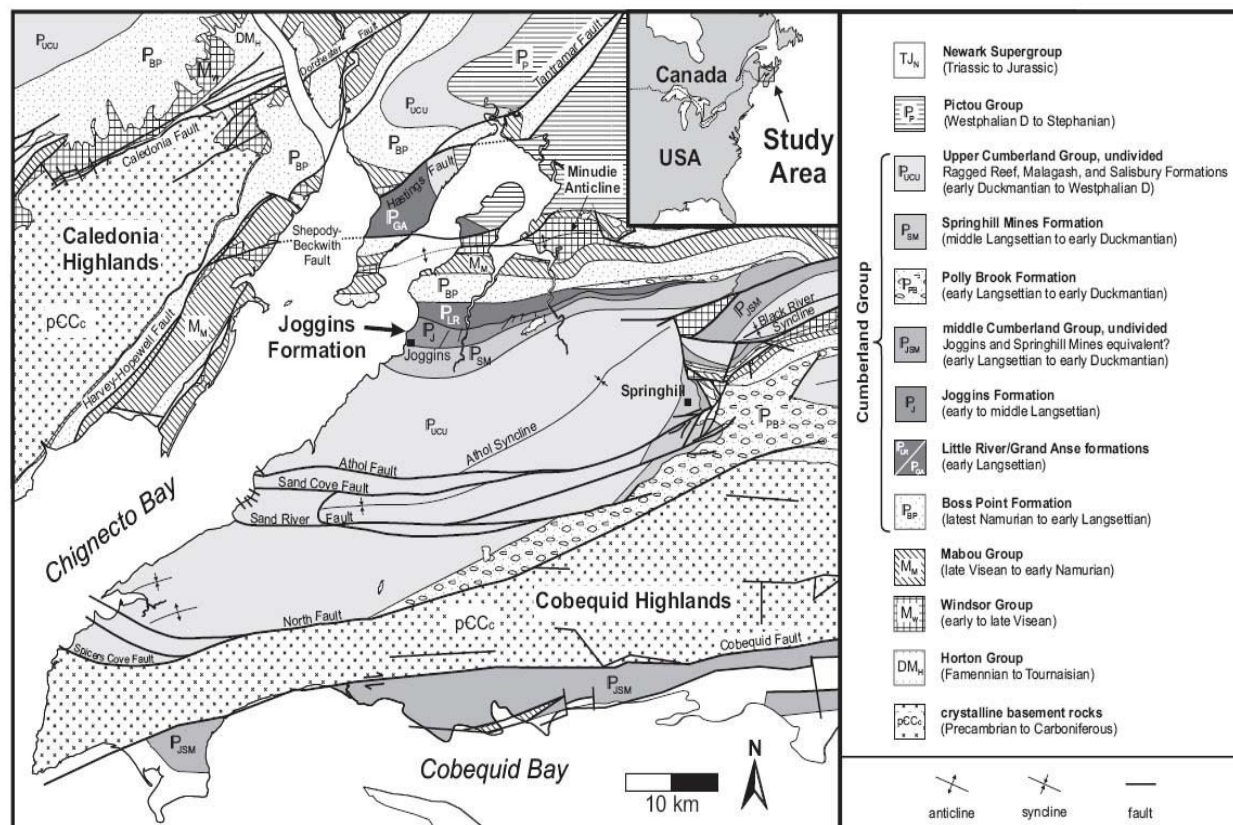


Figure 2.1-Geological map of western Cumberland Basin and adjacent areas showing the distribution of the Joggins Formation. Modified from Ryan et al. (1990) and St. Peter (2001) by Davies et al. (2005).

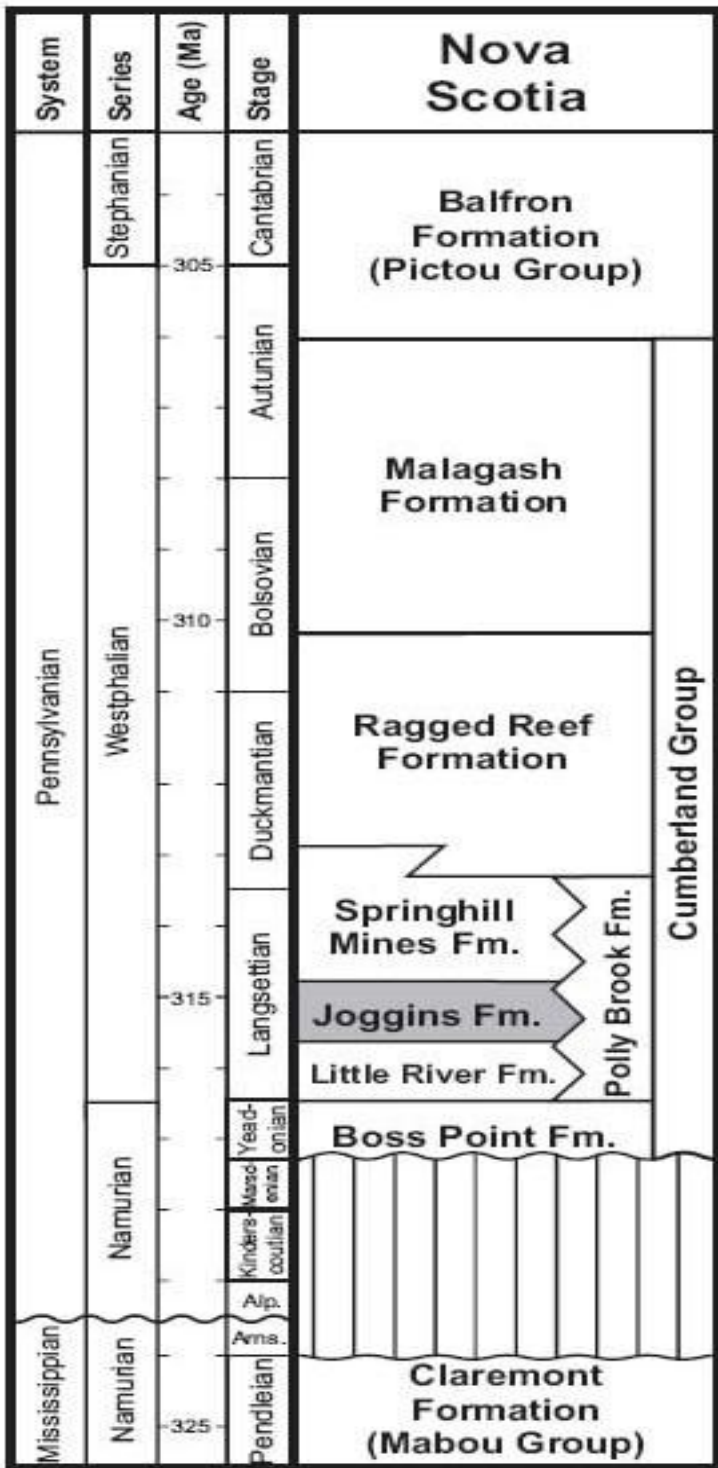


Figure 2.2- Stratigraphic position of Joggins Formation within Cumberland Group. Modified from Ryan et al. (1990) and St. Peter (2001) by Davies et al. (2005).

2.2.0 Depositional setting for Joggins Formation

The Joggins Formation can be divided into open water, poorly drained and well drained facies associations with the poorly drained facies being the site for the major preserved fossil forests. The Joggins environment is also a redox environment which is identified by the presence of oxidation and reduction in the cliff marked by red and grey sandstone of the poor and well drained floodplain assemblage. The presence of coal in this environment indicates the presence of swamps in Joggins at certain periods. The presence of swamps at Joggins aided the growth of a wide range of vegetation, including lycopsid trees such as *Sigillaria* and *Lepidodendron*, as well as bamboo-like plants such as *Calamites* which grew near streams and filled in gaps in the forest during the death of the larger trees in the Joggins forest. Trees such as *Cordaites* grew on hill tops and sandy banks of rivers above the swamps of Joggins. This plant is commonly permineralized in the fossil record.

During the Carboniferous, Joggins experienced flooding of various magnitudes resulting in the swamp forest. This swamp forest was rich in diversity and housed varieties of life, including land-dwelling reptiles, amphibians, and many others (Davies et al., 2005). Joggins environment contains both meandering and anastomosing fluvial channels resulting in fixed and multi-storey channels.

2.3.0 Lithology

The Joggins cliff comprises beds of sandstone, siltstone, shale, mudstone, coal and a small amount of limestone. Sand, silt and mud were derived from erosion of pre-existing rocks by wind, rivers and rain during the Carboniferous period. This cliff is undergoing serious erosion due to Fundy tides which result in exposure of many fossils. The rocks of this cliff have varying

resistance to erosion depending on their degree of lithification. The grey and reddish-brown sandstone is the most resistant rock on the cliff due to its high degree of cementation. Siltstone, mudstone and shale are less resistant because of the fineness of the grains and lesser degree of cementation. Coal and limestone are found together in the cliffs south of Little River to the area near the fossil centre. The beds of this cliff strike approximately 095° and dip at 15° towards the south. The cliff contains channel fills of fine- to medium-grained sandstone and mudstone with fossil trees standing vertical or tilted adjacent to some of the visible channel forms. These ancient river channels cut through accumulating floodplain deposits.

The most famous part of Joggins cliff is the Fundy forest where many tree stumps are found. This area used to be a coal mine area, which results in sulphur and heavy metal contamination of spring water running out of the rock. Many of the beach rocks have ripple marks on them. These ripple marks are asymmetrical with short wavelength and low amplitude showing that they formed in shallow water. Some parts of the Joggins cliff show evidence of parasequences. The parasequences coarsen upwards with the mudstones as the dominant floodplain deposit. The base of the cycle in the cliff is a regime of initial major transgression while the start of the major regression is within the cycle.

2.4.0 Facies Assemblages

Sedimentary and stratigraphic studies of the Joggins Formation show three major facies assemblage including open water brackish bay units and two terrestrial units: poorly drained floodplain and well drained floodplain assemblages.



2.4.1 Open-water facies assemblage



The open-water assemblage represents flooding events that flooded most of the Cumberland Basin (Davies et al., 2005). This assemblage comprises mainly coal, dark limestone, laminated grey siltstone and sandstone. The coal is overlain by the dark limestone, which is in turn overlain by meters of siltstone, grading up into sandstone (Davies et al., 2005). The dark limestone is rich in bivalves, ostracodes, arthropods, articulated fish and plant fragments, contributing to its dark colour. Many of these organisms such as bivalves, ostracodes and plant fragments are also present in the siltstone unit. The siltstones appear to be weathered in some regions, with discoidal siderite nodules. The sandstone units are mostly sheet-like and preserve sedimentary structures such as asymmetrical ripple cross-lamination, mud drapes, lineated plane beds, wave ripples and a few hummocky cross-laminae, suggesting both wave and current activity (Davies et al., 2005). Trace fossils present in this sandstone display grazing, walking and resting traces. A few channels are seen cutting the sandstone bodies in some parts of the cliff. The presence of bivalves, ostracodes, foraminifera and trace fossils suggests brackish conditions, whereas mineralogical and geochemical data from some bivalve shells suggest freshwater influence (Brand, 1994). There is also good evidence for marine conditions from echinoderm and brachiopod fragments in limestones (Grey et al., 2011).

2.4.2 Poorly drained floodplain assemblage

The poorly drained floodplains assemblage is the most famous part of Joggins because of the presence of the fossil forests. The lithology of this unit includes sandstone, green/grey mudstone, coal, shale and minor limestone with siderite nodules. The sandstones and mudstones of this assemblage are sheet-like and heterolithic, extending across the cliff and foreshore. Many

sandstone and mudstone beds contain buried erect trees, some of which are associated with channel bodies (Davies et al., 2005). Small distributary channels traversed the coastal plain and brought sand and mud to the adjacent fresh to brackish bays during repeated flood events (Davies et al., 2005). Poorly drained floodplain assemblages contain varied types of vegetation such as lycopsids, calamites, sphenosids, cordaitalean gymnosperms, pteridosperms, and ferns (Table 2.1).

Images	Log/Plant Type	Description
	<p style="text-align: center;">Type A Calamite stem preserved in a conglomerate. {SPHENOSID}</p>	<p>Jointed with equally spaced ridges and furrow.</p>
	<p style="text-align: center;">Type B {CORDAITALEAN}</p>	<p>Smooth deeply rugose surface which is probably the actual bark impression, with deep furrows and ridges which may be the actual wood surface with bark removed.</p>

	<p>Type C Sigillaria {LYCOPSID}</p>	<p>Deeply rugose with parallel furrows. Actual impression of outer bark.</p> <p>Right hand front fragment: 4.3 cm wide.</p>
	<p>Type D TREE FERN AND PTERIDOSPERM</p>	<p>Surface finely rugose, with wide and coarse striations running longitudinally along axis. Parallel to sub-parallel ridges and furrows.</p> <p>Width of fragment: ~ 2 cm wide.</p>



	<p>Type E {LYCOPSID}</p>	<p>Finely rugose to almost smooth surface with no continuous longitudinal ridge and just swollen lenses that spiral around axis. Sporangial form or puds present on the lower right corner of the picture.</p>
	<p>Cone of a giant tree.</p>	<p>Spore bearing cone of a lycopsid tree held in abundance in the crown branches and often fall off (abscised in botanical terms) from the tree after the spores were released. The cone also contains small spores that are very similar to pollen of seed plants.</p>

Table 2.1 - Plant fragments and imprints from fallen channel cliff boulders. Arden Bashforth, unpublished information, 2011 modified by Chinemerem Dennar.

The trees present in the fossil forests vary in size with the maximum observed height of about 6 m (Davies et al., 2005). The preservation of these trees implies rapid sedimentation, and flow events aided in the creation of scour hollows around the trunks (Rygel et al., 2004). Hollowing out of the trunks in the fossil forest was caused by wildfire in some cases, thereby

making homes for tetrapods and other organisms found in tree trunks (Davis et al., 2005). The vegetation was dense enough to form peat, which became coal during burial over geologic time. These coals represent flooding surfaces and mark the end and beginning of some of the cycles.

2.4.3 Well drained floodplain assemblage

The well drained floodplain assemblage is dominated by a red bed assemblage comprising mainly stratified red mudstone and sandstone, with minor grey mudstone and ostracode-bearing limestone. The channel bodies present in this assemblage are narrow and about 6 m thick with an aggradational style of filling (Rygel, 2005; Davies et al., 2005). Heterolithic sheets of sandstone and mudstone, laid down as levee and crevasse splay complexes, are noticed thinning away from most of the channel bodies (Davies et al., 2005). The dominant channel body represented in this assemblage is a multistory, narrow channel indicating the former presence of anastomosing channels. Preservation of trees is very poor in this assemblage, but some of the roots present tend to be filled with sediments and minerals. The red floodplain muds are immature, cumulative palaeosols that formed under a humid seasonal climate (Smith, 1991; Davies et al., 2005). There are remains of the oldest known snail, *Dendropupavetusta*, in conglomerate situated in the base of a sandstone channel body with an abandoned mudstone channel fill above the sandstone channel body. The existence of soil carbonate nodules reworked into conglomerate with fragments of wood and charcoal clasts implies wildfire. Plants such as cordaitaleans, calamitaleans and macerated plant material are present in this assemblage with sedimentary structures such as ripple marks and trough cross-bedding also visible. Although there is poor preservation of tree stumps in this assemblage, small log jams are preserved in some of the channel bodies.

CHAPTER 3 – Methodology

3.1.0 Introduction – Research Methods

Four major methods were used in this thesis which involved field study and tracing of photo mosaics, petrographic observations, X-ray Diffraction observation, and electron microprobe analysis. The tracing method applied in this thesis involved an exercise of patience and work with care. The other methods were carried out in the laboratory for mineral identification of root coatings and root fillings. Minor tools such as Windows Paint and Corel Draw were used for modification of maps and photographs.

3.2.0 Tracing observations

Over 50 photographs of outcrops of interest were taken in the field and screened for the photographs which best fit the purpose of the research. A series of observations and tracings were made on the photographs outlining interesting features such as tree trunks, channels, and bar forms. The tool used for this tracing was CorelDraw X5 software. After initial photography and tracing, additional field work was carried out using the traced photographs as a reference to document additional important features in the actual cliffs. Corrections were made on the traced photograph in the field and transferred to the working copy by retracing the corrected area on the photograph.

This tracing method was designed to investigate the environmental relationship between all the features in the photograph with a major emphasis on tree trunks and their likely effects on channels. The positions of features are identified in the thesis with reference to the horizontal and vertical meterage shown on the tracings.

3.3.0 Microscopic observations

Three rock samples bearing roots with nodules were collected from the traced outcrops and the roots were cut into thin sections in order to check the root and nodule mineralogy. The selected rock samples were broken down into smaller size and cut into slabs by a technician. The equipment used in preparation of the thin sections include: motorized flat lap with diamond lap, motorized diamond saw, glass microscope slides and clear epoxy glues.

The thin sections were analysed with the aid of a petrographic microscope. Detailed analysis of minerals using optical properties in thin section, textural and structural relationship are important to understanding the origin and influence of the mineral coatings associated with the roots. Microscopic characteristics used in identification of the minerals include colour, colour variation under plane-polarised light (pleochroism), textural characteristics of grains, refractive index, and optical symmetry (birefringence).

3.4.0 XRD Observations

X-ray diffraction (XRD) is a technique used for phase identification of unknown minerals in powdered form based on their crystal and chemical properties, and interplanar spacing. Before a sample is analysed in X-ray diffraction, it undergoes a series of processes to make the material suitable for the analysis. The first process involved the crushing of the sample into fragments of about 1 – 15 mm diameter in a jaw crusher. The second process involved further grinding of the sample into finer grains in a Braun pulveriser called the disk mill. This second process was done several times using a thread knob with locking levers to adjust the gap between 0.2032 m diameter grinding plates to control particle size output. Acetone is used to clean the grinding plate before and after use due to its non-corrosive properties. This third process ground the

sample into powdered form in a Fritsch pulverisette 5 called the planetary ball mill. After the sample passed through the second process, it was emptied into a beaker and weighed in a weighing balance. The weight of the sample and the beaker was used to balance the mill and the sample weight by setting the mill counterbalance weight to the weight of the sample and the beaker. The weighed sample was placed in a container of its size containing balls, and put in the Fritsch pulveriser where it was ground into powdered form ($<1\mu\text{m}$) by the movement of the balls. The pulveriser was set to a rotational speed of 250 rpm at an interval of 15 minutes after which it was ready for X-ray diffraction analysis.

X-ray diffraction is based on constructive interference of monochromatic X-rays which are generated by a cathode ray tube. The X-ray beam is filtered to produce monochromatic radiation which is essential for diffraction, collimated to concentrate and directed towards the sample. Copper is the target material used for single crystal diffractometer (Appendix C). With conditions satisfying Bragg's law, constructive interference is produced when the incident ray interacts with the sample. The atomic spacing of most mineral structures is similar to the wavelength used in the X-ray diffractometer (Nesse, 2000). Reflection angle can be determined from the Bragg equation ($n\lambda = 2d\sin\theta$) if the wavelength λ , integer n representing order of reflection and the spacing between planes in the crystal lattice are known. The sample in the X-ray diffractometer rotates in the path of the collimated X-ray beam at an angle θ , whereas the X-ray detector collects the diffracted X-rays and rotates at an angle of 2θ . A goniometer is used to maintain the angle and to rotate the sample. X-ray signal is recorded and processed by a detector and converted to an intensity count rate which is then output to a computer monitor in graph plot of intensity/count versus 2θ . The peak intensities, positions and widths provide important

information about the structure of the mineral. The peak intensities are directly related to the d-spacing and are used to identify possible mineral matches.

X-ray diffraction is used to identify unknown minerals and to confirm minerals identified in the thin section. The analysis is necessary for the identification of minerals that are too fine to be identified using the petrographic microscope, such as clay minerals. For mixed materials, the detection limit is about 2% of sample, which implies that materials less than 2% of the sample might not be detected. Measurement parameters, peak lists, identified phases and graphic representation are outputs for the various samples. Mixing of peak with the noise can result in lack of identification of minerals that are in low proportions.

Semi-quantitative analysis carried out on the minerals helped determine the approximate proportion of the minerals in the samples. The analysis was done in six steps; identification of the diagnostic peak for the mineral, measurement of the peak height above the middle baseline, measurement of the peak width at a position of half the peak height, calculation of peak area by multiplying peak height by width at half peak height, multiplication of each area by the intensity factor of the mineral and taking the total, and final calculation of the proportions of each mineral out of 100% (Appendix C). Results and data for the X-ray analysis are present in Chapter 4 and Appendix C.

3.5.0 Electron Microprobe observations

Electron microprobe (EMP) is an analytical tool used to non-destructively determine the chemical composition of major and trace elements of materials (1-5 micron) in situ. The EMP is similar to the SEM, but with the range of electron spectrometer that allows for quantitative and qualitative chemical analysis. Before any sample is passed through the EMP, it is first prepared

into a polished section and then coated with a thin layer of carbon that is light enough to allow minimal interface with the electron beam and emitted X-rays.

Before an EMP is used, samples are first loaded into a sample chamber through a vacuum interlock and mounted on the sample stage. The sample chamber is pumped to obtain a high vacuum before beginning the analysis. Suitable analytical conditions are required, such as accelerating voltage and electron beam current. There are two major types of electrons generated in the EMP, primary and secondary electrons. The source of the generated primary electrons for the case study is tungsten-filament cathode, whereas secondary electrons are generated after the primary electrons interact with the sample. The electron beam must be focused and standardized for the desired material. The electron beam generated from the source is condensed and focused by a series of electromagnetic lenses. The sample is bombarded by an accelerated and focused electron beam which has enough energy to produce both energy and matter from the sample. Heat, electrons and X-rays are produced by the electron-sample interaction. The two major imaging tools commonly used in EMP are secondary-electron imaging (SEI) and back-scattered electron (COMP), although it has the capability of performing cathodoluminescence imaging. There are two possible collisions in an EMP which are elastic and inelastic collisions. Inelastic collision of the incident electrons with electrons in the inner shells of atoms in the samples results in generation of X-rays with characteristic energies. The produced X-rays by each element in the sample are counted and compared to X-rays produced by a standard of known composition. With this counting and comparison, it is possible to determine the chemical composition of a spot with great accuracy.

For the case study, EMP was used in only one sample analysis to determine the chemical constituents of unidentified minerals in the XRD. The EMP analysis involves selection of

minerals of interest and focusing suitable areas within the selected mineral. Focusing and testing of the mineral on the monitors allows for satisfaction of Bragg's equation, which is necessary for accurate reading on the peak instead of the flanks.

CHAPTER 4 - Results

4.1.0 Tracing 1

4.1.1 Description

At about 830 m level in the stratigraphic section (Davies et al., 2005), south of Coal Mine Point, an outcrop contains two well exposed small mudstone channel fills with a fossilized tree trunk about 1.73 m high exposed on the bank between the two channels fill (Fig. 4.1). The first in the sequence of events recorded in this cliff is the deposition of sandstone, which is overlain by the mudstone bed, with the tree trunk rooted in the top of the mudstone. The mudstone bed forms a mound with the tree trunk standing on the top and two mudstone-filled channels on either side of the ridge. It is probable that the sloping mound surface represents root positions. The tree trunk has been coalified as evidenced by preserved periderm close to the root. The next event was the filling of the shallow channels on either side of the tree with about 0.43 m of mud, followed by deposition of alternate beds of sandstone and mudstone (~ 6 m thick), which tend to be continuous and laterally linked with the sediments in the tree trunk. The bed immediately overlying the topmost visible part of the tree trunk forms a cone-like top cover over the tree trunk. The mudstone below the trunk contains abundant siderite nodules (Fig. 4.1: purple ovals), which are mainly noticed close to the root system of the trunk, suggesting that the siderite may be associated with the roots.

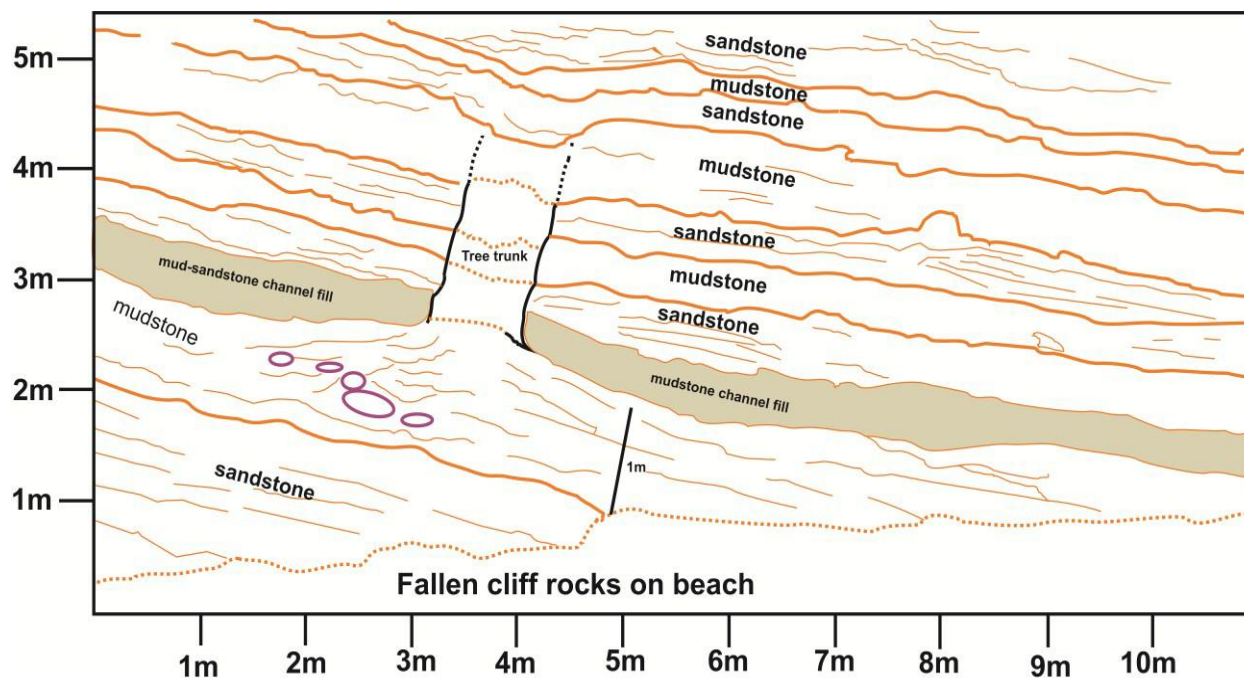


Figure 4.1- Interpretative tracing and photograph of a cliff section showing a standing tree between two channel fills and the sequence of deposition in a sheet-like pattern; the purple ovals represent various nodules present.

4.1.2 Interpretation

The sequence of deposition of the cliff section started with the deposition of sand under high flow velocity, followed by a lower velocity flow resulting in mud deposition in horizontal layers. The growth of the tree trunk followed the mud deposition, which was followed by channel formation and fill. The presence of the tree accounts for the creation and stabilization of the ridge. It is probable that the tree trunk had great influence on the stabilization and creation of the two channels. The position of the tree trunk on the ridge with mud-filled channels on both sides of the tree and ridge is an indication of a positive impact of the tree trunk on the channel bank. The fact that the margin of the mudstone channel is bordered by the bottom of the tree trunk and takes the shape of the diverging root system on the right (Fig. 4.1) is also an indication of the possibility that the tree trunk contributed to the stability of the bank.

Sediment infill of the channel was followed by hollowing of the tree trunk after the death of the tree, which was followed by deposition of alternating sand and mud beds which probably entered the tree trunk through holes in the periderm. Traceable layers of the interbed in the trunk appear from the top of the tree exposure to the bottom. The continuity of layering from outside through the trunk fill is probably a result of sediment filling the trunk through holes created by decay or possibly by fire, implying that the trunk was hollow at the time of sedimentation. The cone-like top cover (Fig. 4.1) over the tree trunk implies that the sediment layer filled in the top of the tree trunk.

The pattern of deposition of alternate beds with contrasted grain size shows that the fluvial flow velocity fluctuated. There is a possibility that the channel was deeper than its present depth, and that some of the sandstone and mudstone were laid down within standing water,

resulting in drowning of the tree. The alternating beds are crevasse splays breaking out from channels in flood and depositing on the floodplain either on dry surface or standing water. Siderite nodules below the mudstone mound seem to be related to the roots of the tree, some probably as coatings on the roots. The nodules may have formed early in the history of the section, possibly even during the life of the tree, and this early cementation may be linked to the bank stability of the channels. The connection of the siderite nodules and roots in relation to bank stabilization will be discussed in more detail in the discussion.

4.2.0 Tracing 2

4.2.1 Description

At about the 840 m level of the stratigraphic section (Appendix E), south of the Interpretation Centre, is a sandstone channel-fill about 1.39 m thick with many plant roots and calamite stems at the extreme right end of the channel body (Fig. 4.2). Between 4 m and 5 m below the sandstone channel fill is a thin siltstone and mudstone bed with various calamite stems (Fig. 4.3). The mudstone contains many nodules, which are randomly distributed. Some of the roots preserved on the cliff are encased in calcite and siderite nodules. There are also two vertical tree trunks (~ 0.38 m long and 1 m long) growing on the flooding surface beneath the channel body. These trunks are rooted on an irregular wavy surface (Fig. 4.4). The tree trunk between the horizontal 1 m and 2 m position is filled with siltstone whereas the other (7-8 m position) is filled with sandstone (Fig. 4.2).

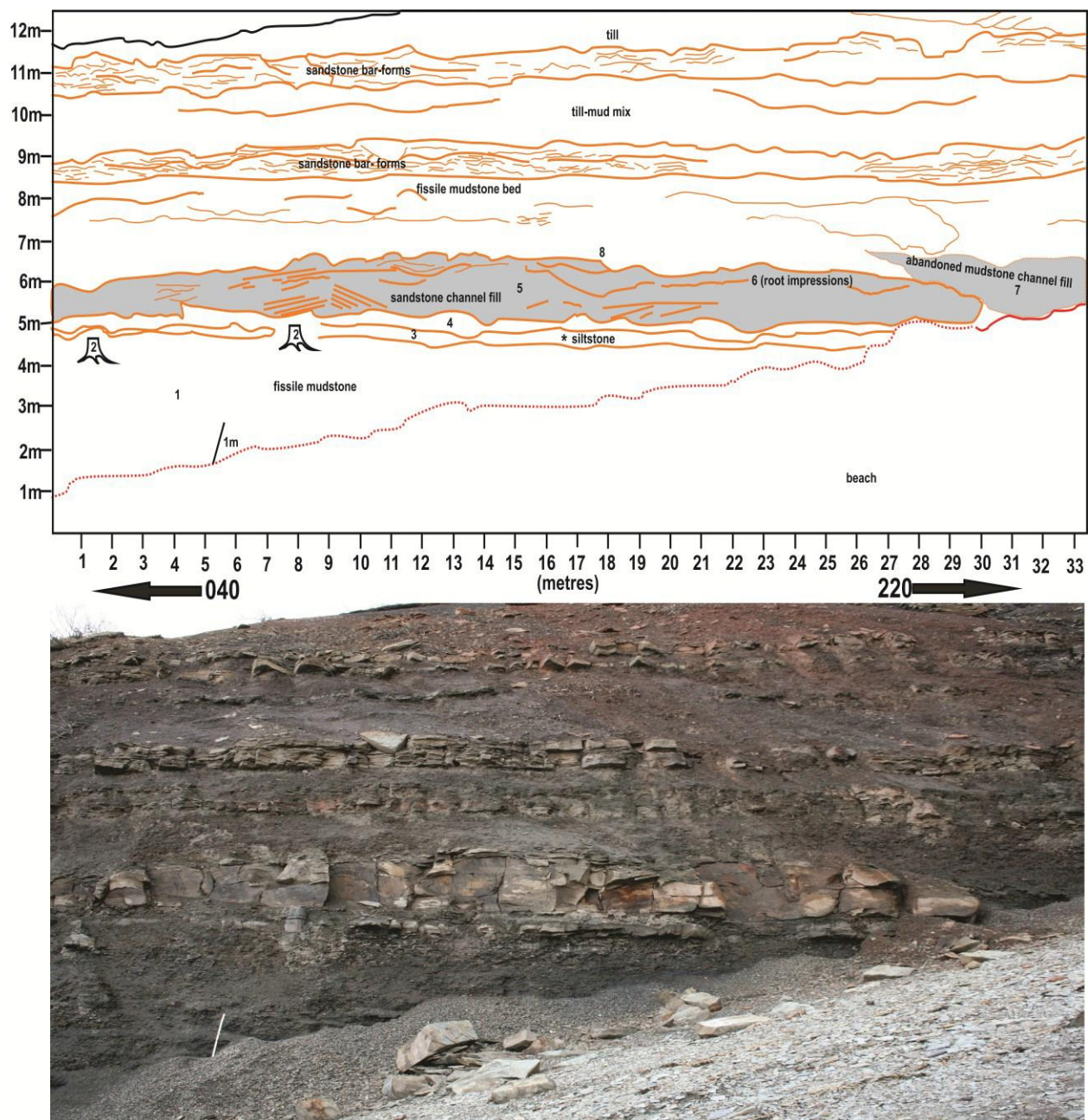


Figure 4.2- Interpretative trace and photograph of Joggins cliff section showing two lycopsid tree trunk interactions with the sandstone channel fill and the host mudstone bed. Asterisk before siltstone indicates the presence of a calamite. The cliff trend represented by thick-black arrow and orientation. The letter markings, 1 to 8, represent the series of events up until the mudstone above the abandoned channel, with 2 and 6 representing vegetation growth.



Figure 4.3- Photographs of calamite stems on siltstone beneath mudstone. (a) Calamite stem imprint on siltstone. (b) Two calamite imprints with mineral filling in the cavity created by the stem in the right-hand. (c) Well preserved upright calamite stem underneath a cavity created by a stem. (d) Fully preserved flat laying (fallen) calamite stem.

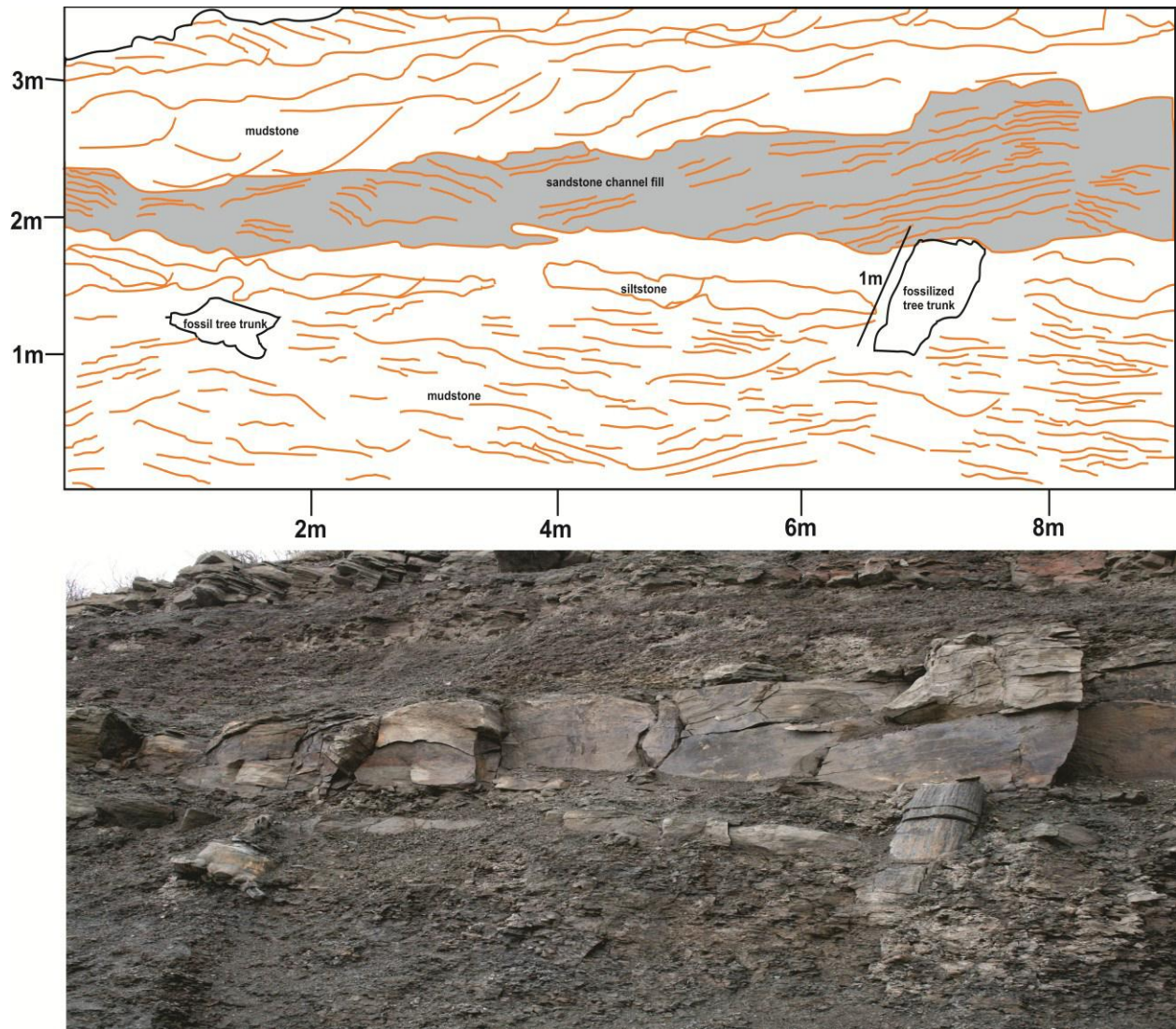


Figure 4.4- Interpretative trace and photograph of Joggins cliff section showing closer view of two tree trunk interactions with the sandstone channel fill.

The sandstone channel body portrays inclined surfaces of two bars, implying lateral bar accretion. The lateral bars were accreted in opposite directions resulting in varying slope in both right and left direction which gives the appearance of a V- shape in the tracing (Fig. 4.4). The sandstone channel body records about 11 traceable dipping beds within each bar. The vertical thickness of the accreted bars ranges from 0.44 m to 1.29 m, and the bar deposits with dipping layers extend horizontally to about 9 m in each case. It is difficult to determine which bar accreted first as a result of lack of definite evidence on the cliff.

Next to the sandstone channel is an abandoned mudstone channel fill about 7.7 m in apparent length and 1.5 m thick. The sedimentary structures present in the sandstone are ripple cross-lamination, some of it deposited as climbing ripples with trough forms. Trough cross-lamination on an extension of the channel sandstone beneath the abandoned channel body was used to determine the paleoflow of the channel to be approximately 110° , into the cliff line. The cliff trends 040° to 220° (Fig. 4.2). The difference between the NE-SW outcrop trend and the paleoflow is 70° which is oblique to the cliff trend; however, it implies that the flow direction is approaching normal to the cliff face. Strike and dip taken from the dipping margin of the abandoned channel are 090° and 40° with a strike-paleoflow difference of 20° , which is derived from comparing 70° paleoflow and 90° strike, implying a flow movement direction close to the orientation of the abandoned channel. These measurements show that the cliff face is exposing a near cross-section of the channel body.

4.2.2 Interpretation

The outcrop records about eight events up to the mudstone bed above the sandstone channel (Fig. 4.2). The events begin with mud deposition, followed by tree and calamite growth. The third event is marked by the deposition of a thin layer of silt with calamite imprints on it, followed by deposition of a thin mud layer and then sandstone channel fill. The sixth event is evidenced by roots in the sandstone channel fill which implies vegetation abundance. The roots are high in the channel body, indicating their growth after sand accumulation. Vegetation growth was followed by the creation and filling with mud of an abandoned channel, which was followed by mud deposition above the abandoned channel fill.

The cliff section records a period of flooding which is marked by the thick mudstone at the base of the cliff. Deposition of the sediments occurred in a fluvial environment with progressively increasing energy resulting in the sequential deposition of mudstone, siltstone and sandstone with progressive grain-size increase. The two tree trunks grew after the flooding event and before the formation of the channel represented by the sandstone channel-body above. The two tree trunks are positioned within the mudstone beneath the siltstone (Fig. 4.2). They are about 6 m apart and approximately 22 m away from the abandoned channel body (Fig. 4.2).

It is difficult to state if the two tree trunks have any effect on the channel because there is no clear evidence proving it. The tree trunks appear to have been already broken before the arrival of the channel at this site or broken by the channel migration and erosion into the site. Although this is not apparent in the cliff-face view, the two tree trunks actually project from the cliff and are not directly under the sandstone, and a careful visual inspection (Fig. 4.4) suggests that the tree trunks may have extended up into the sandstone originally. These projected trees

probably influenced the accumulation of sediment mounds in the channel, but have no impact on bank stability. There is a possibility of the tree trunks being completely buried by the sandstone channel fill before being broken during erosion of the cliff, which has eroded back far enough to have removed any evidence of tree bark-imprints on the sandstone. The channel sandstone shows evidence of inclined surfaces dipping away in opposite directions (left and right) above the right- and left-hand tree trunk (Fig. 4.3), implying that the tree projected up above the channel base, and sediments were deposited in mounds around them (Fig. 4.5). The sandy fill of the channel may have been created by the growth of the two overlapping bars. As exposed, the right-hand bar appears larger than the left-hand bar, and its inclined surfaces overlap with those from the left-hand bar, resulting in the V-shaped inclined beds. The interaction of the tree trunks with flowing water would have influenced bank erosion by disturbing the flow field, so that the tree trunks would have acted much as a bridge piling acts to modify flow. There is no evidence for vegetation influence on channel bank stability at this site, but the trees in the channel would have caused intensive turbulence up-flow and reduced velocity down-flow.

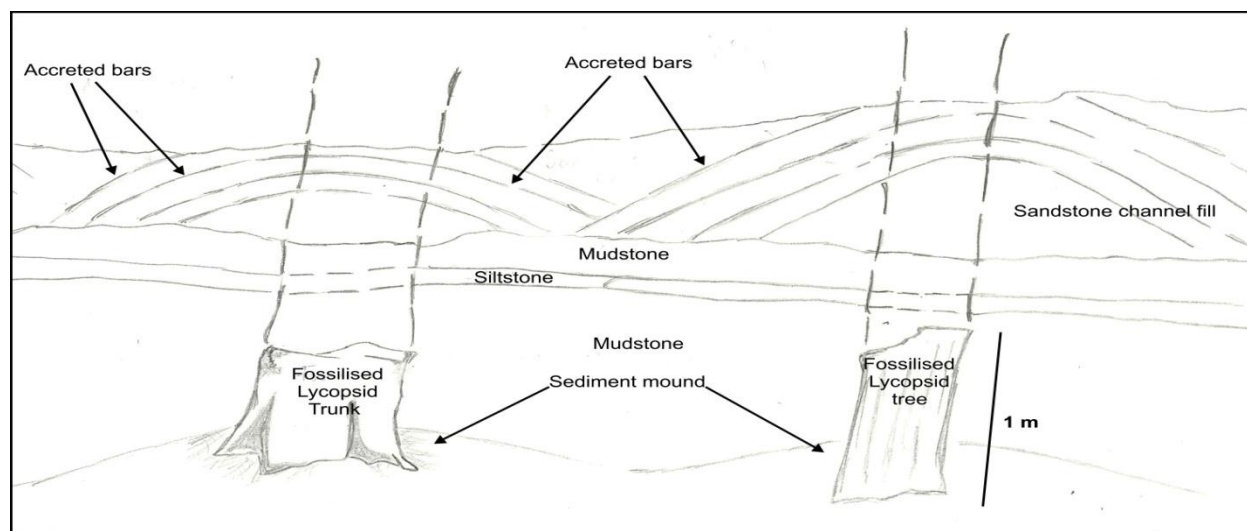


Figure 4.5- Schematic diagram of sediment mounds formed around standing trees.

4.3.0 Tracing 3

4.3.1 Description

Further to the south of Coal Mine Point is a 10 m high cliff within the Poorly Drained Facies Association at about the 900 m level in the measured section (Davies et al. 2005) and comprising fissile mudstone, sandstone-mudstone interbeds, blocky sandstone and channel sandstone fill (Fig. 4.6). The channel bodies lie at the top of a broadly coarsening upward succession about 6.3 m thick. The sandstone channel body comprises three stacked channel fills with an approximate apparent horizontal extension of 20 m. The first sandstone channel fill has a thickness of about 2.2 m, whereas the second and third channel fills have an approximate thickness of 1 m and 2 m. The three sandstone channel fills have a tectonic dip, and an imprint of a calamite stem is present close to the left-hand bank of the third channel fill, probably rooted on the former bank between the first and third channels (Fig. 4.7). The right-side bank of the second and third sandstone channel fills contains tree stumps, coalified stems and roots over a horizontal distance of about 2.3 m, implying that a considerable amount of vegetation was present from the bank into the floodplain away from the channel (Fig. 4.8). The cliff section shows preserved tree and stem exposure of approximately 15 to 20 cm long (Fig. 4.9).

The first channel fill has an indistinct margin, making it difficult to determine the position of the left bank. The cliff was illustrated by Rygel and Gibling (2006), who also show two lycopsid trunks on the right-hand margin of the second channel body; these are presently absent due to erosion of the cliff resulting in the trunks falling down the cliff. Above this channel deposit are gently dipping deposits, and below it are sandstone and mudstone representing a poorly drained floodplain deposit.

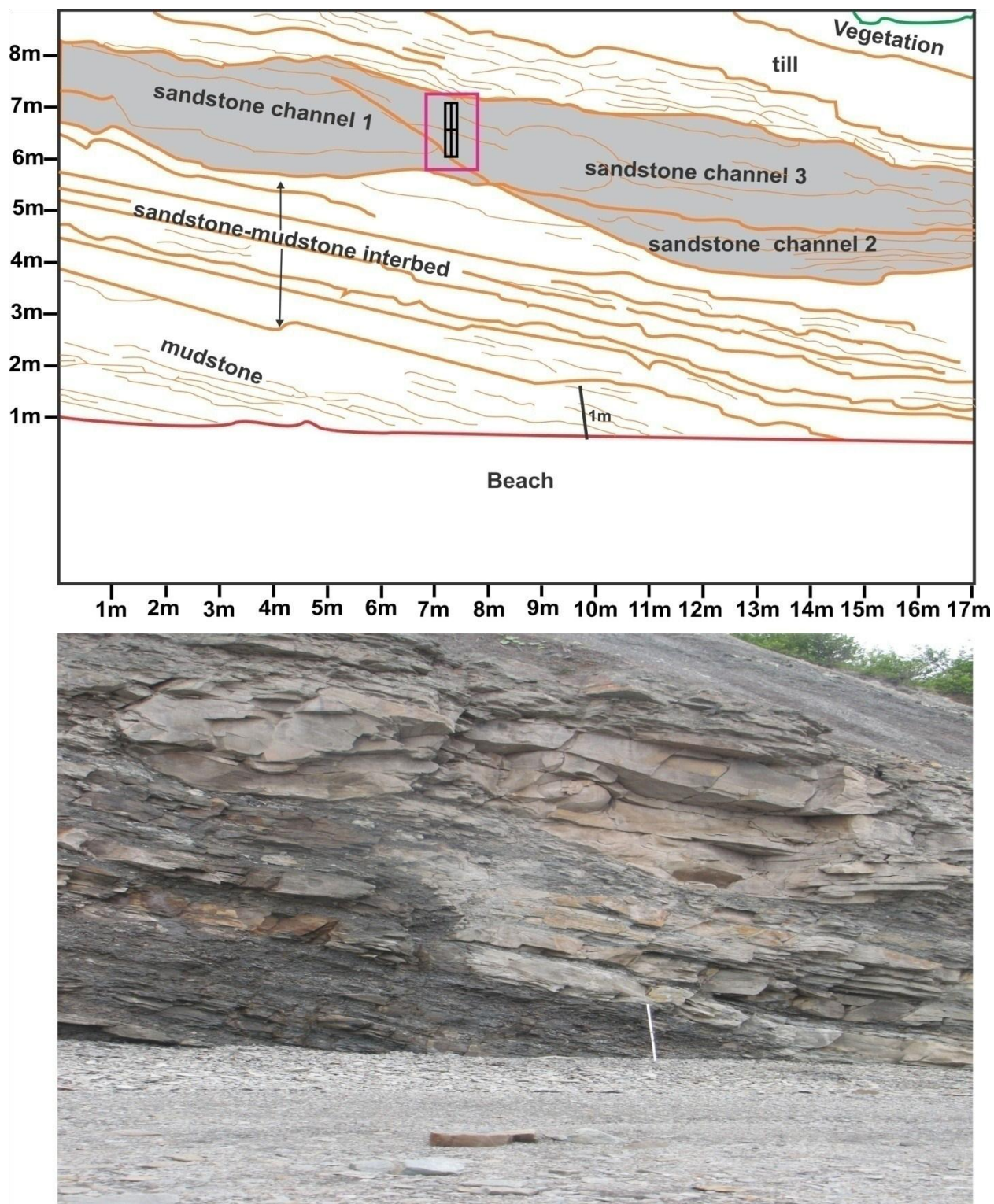


Figure 4.6- Interpretative trace and photograph of sandstone-filled, fixed-channel bodies with the purple box representing position of calamite imprint.

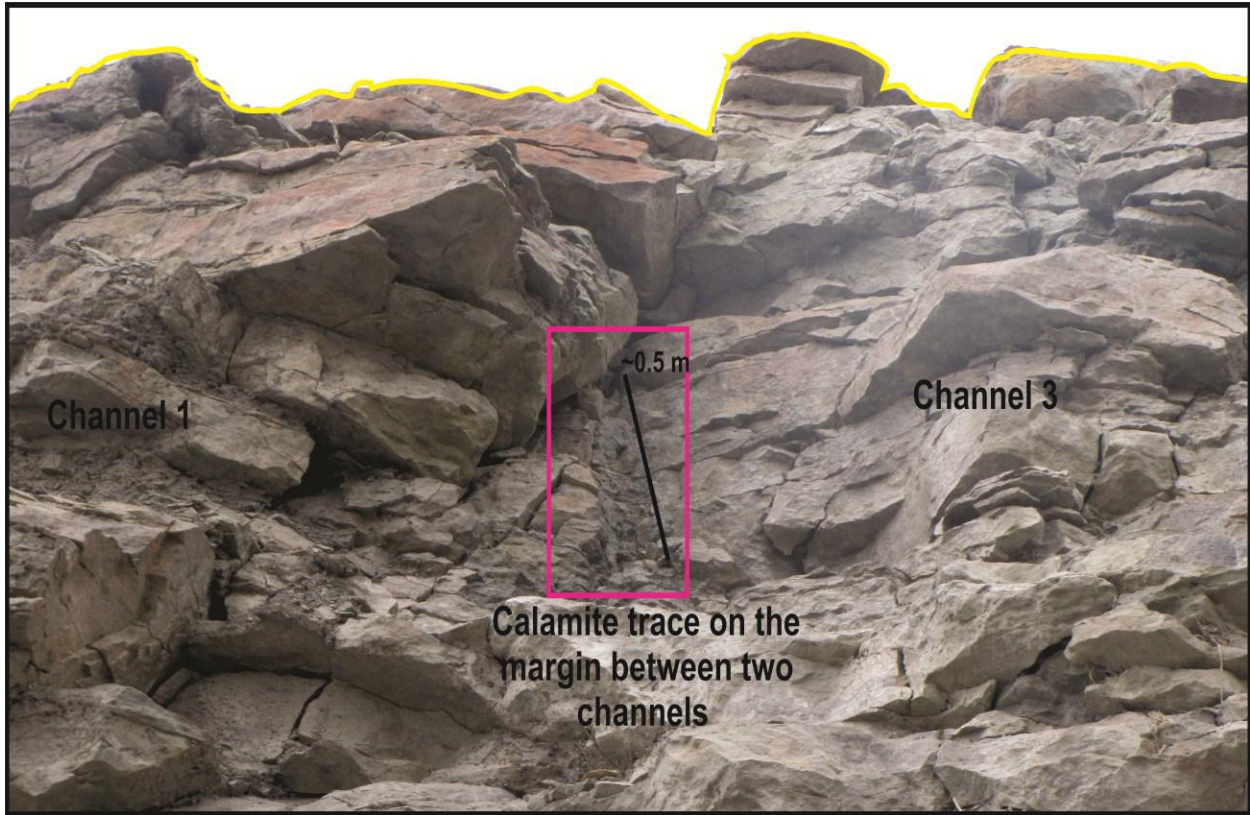


Figure 4.7- Calamite imprint between the first and the third sandstone channel fill

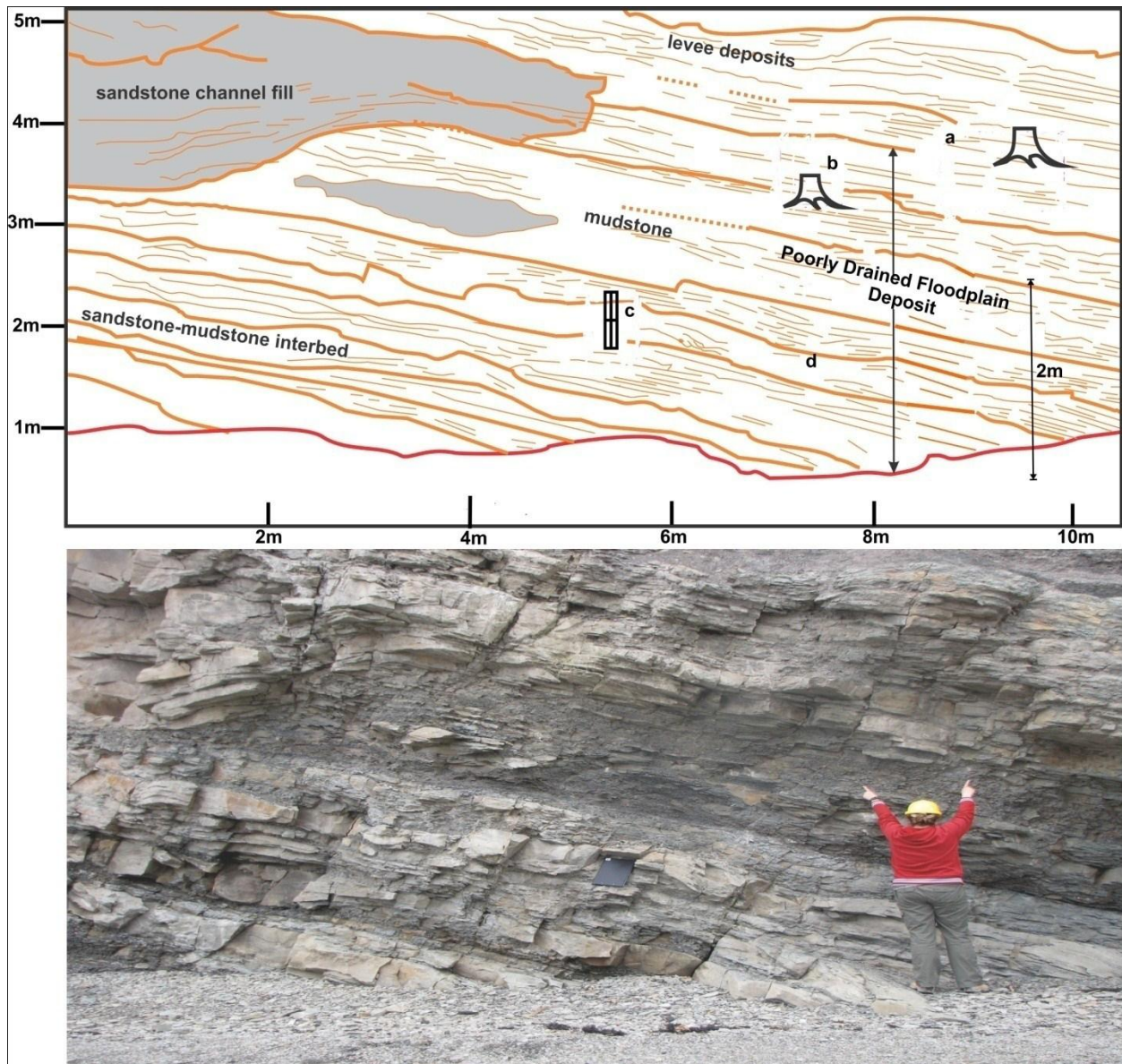


Figure 4.8- Interpretative trace and photograph of a closer view of the bank of the second and third channel bodies with the alphabetical markings (a, b, c, d) representing the various positions of roots and stems.



Figure 4.9- Fossilised stems on the cliff close to the bank of the third sandstone channel. (a) Three fossilised stems on the cliff representing the bank of the third channel. (b) Calamite stem imprint on the cliff representing the bank of the third channel. (c) Coalified plant bark on sandstone bed below the channel body. (d) Coalified stem with visible roots. The heights of the stems are tens of cm in scale.

4.3.2 Interpretation

The sandstone channel of the cliff section comprises three distinct channel deposits. The broadly upward coarsening succession below the channel bodies is interpreted as a coarsening upward delta succession, and the small channel bodies were interpreted as delta distributaries by Rygel and Gibling (2006). The three channel fills have incised bases, and the channels filled by layers without additional channel widening, implying that the three channels were essentially cut and fill events. The presence of tree stumps, stems and roots on the bank of the second and third sandstone channels to the right provides evidence for extensive vegetation. The vegetation ran from the bank onto the floodplain as evidenced by the presence of the roots and upright-stems from the channel through the adjacent bedding connecting the channel to the rest of the cliff to the right. A calamite imprint on the bank between the first and third channel bodies shows evidence of vegetation between the channel bodies, implying that the small, narrow channel bodies may have been locked into place by vegetation on both sides. Vegetation featured plants of various sizes as evidenced by stems, trunks and roots of various sizes. Identified plants present in this forest are calamite and lycopsid, which have different root architectures. The combined effects of roots from the two identified and unidentified plants may have been capable of stabilizing the channel banks. The abundance of preserved vegetation in the area suggests dense forestation which has significant impact on bank stability.

4.4.0 Tracing 4

4.4.1 Description

At the 572.5 – 581 m level in the section (Davies et al. 2005), north of Coalmine Point, is a large sandstone channel body interpreted as a delta distributary channel fill by Rygel and Gibling (2006), comprising three sandstone channel fills (storeys) and an abandoned mudstone channel, with erosional surfaces separating the channel bodies. The distributary channel fill is a narrow channel body of about 8 m thick that ends just a little way out from the cliff onto the foreshore. The three channel fills have varying thickness of 2.6 m, 4.4 m, and 1.8 m, from the bottom storey to the top. The first and second sandstone channel fills are vertically positioned on top of each other, and the third channel fill is situated above an abandoned mudstone channel fill and a mudstone bed which is above the second sandstone channel fill.

The first sandstone channel body contains tree roots about 6 m long and 0.4 m wide diverging from a central position which is assumed to be the position of a large tree trunk, no longer preserved (Fig. 4.10). The assumed tree trunk would have been situated within channel fill 2 with its root system growing in channel fill 1. The roots between the first channel fill and the second channel fill are large and radiating from the former trunk position (Fig. 4.11).

Fallen boulders at the base of the cliff contain more information about the vegetation from the channel region, including both roots and stems (Table 2.1). The stems noticed in the boulders range from tens of centimetres to a meter long, and are from different trees. The trees represented are lycopsids, cordaitaleans, and calamites, based on comparisons with stem types, and they are mainly associated with sandstone. Some of these stems appear to be flattened and

are imprints, whereas others are fully preserved. These stems range in size from about 15 cm to 50 cm long with width range of about 5 cm to 10 cm.

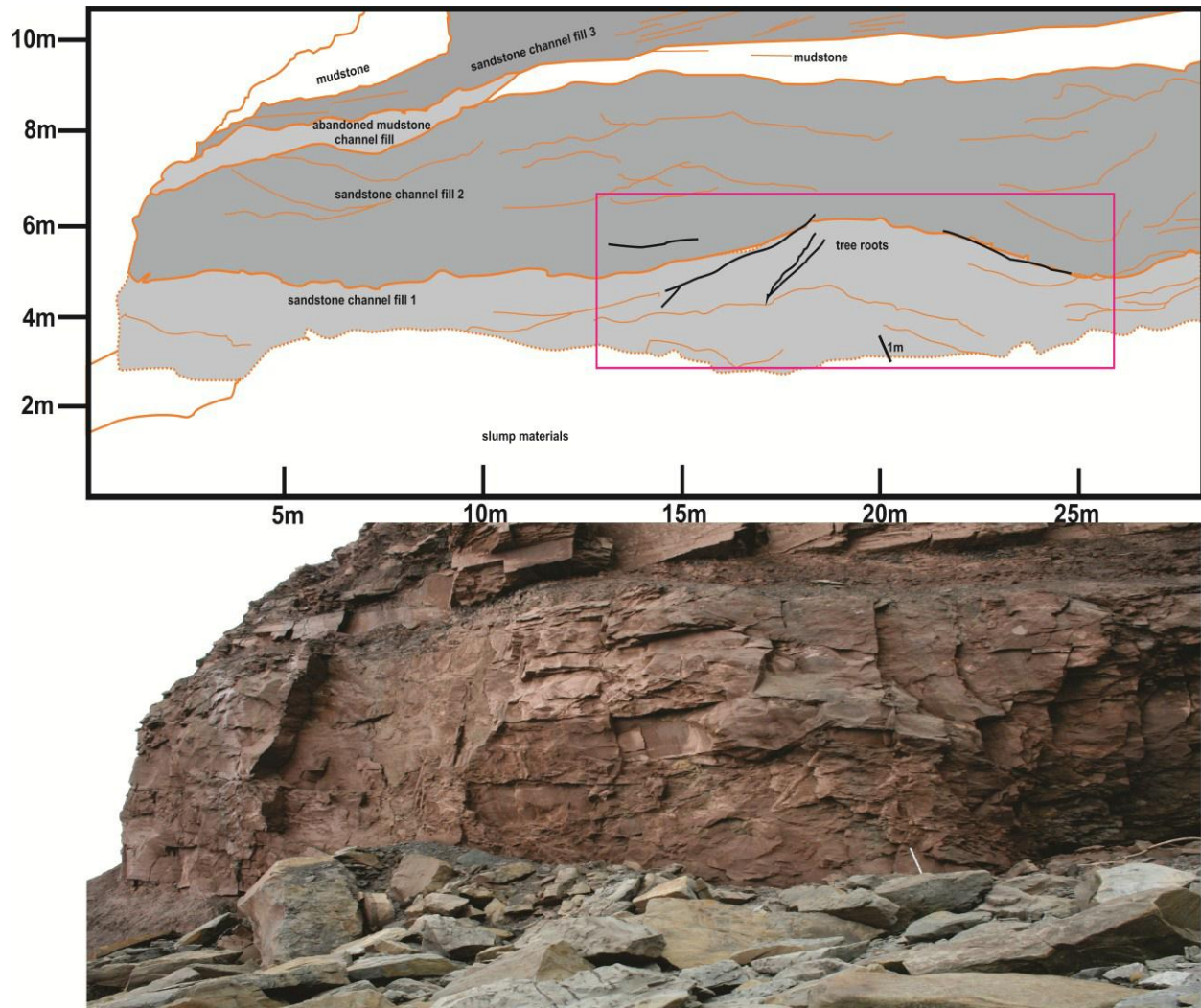


Figure 4.10-Illustrative trace and photograph of a delta distributary channel showing three sandstone channel fills and an abandoned mudstone channel fill. Purple box represents position of the tree trunk and root system which is enlarged in Figure 4.11.

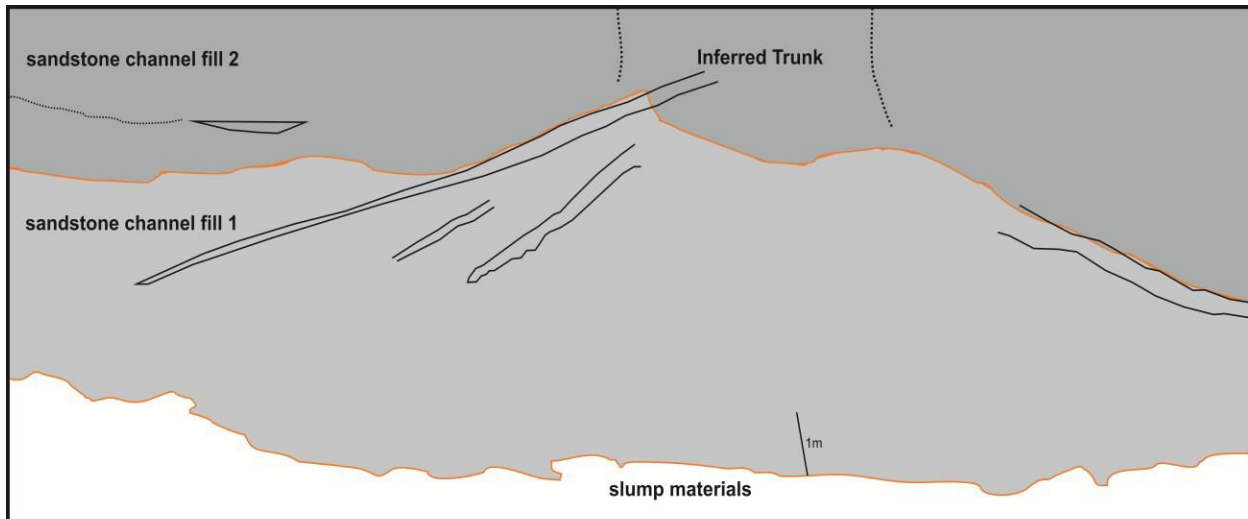


Figure 4.11- Illustrative trace and photograph showing closer view of the tree roots and their position with respect to the first and second channel fill.

The roots in the boulders are approximately 45 cm long and show evidence of various root types such as fibrous roots and root mats (Fig. 4.12). Estimation of root cast volume on the rock surface was calculated using photomosaic and graph calibration. The transverse section of these roots has a diameter range of 3 to 4.5 cm with a mineralised rim and a core that marks the former root position before decay. It is probable that the decay of the roots created a cylindrical

cavity that was filled by cement from groundwater (Appendix A; C and D). Some fallen boulders also contain climbing ripples, indicating rapid sedimentation. Some of the sandstone boulders have calcite cement, which is evidenced by the rapid effervescence of the rock on contact with HCl. The fallen boulders probably belonged to the third sandstone channel before falling off the cliff as a result of erosion. There are roots in position, in the top part on the third sandstone channel body, showing evidence for the origin of the blocks.

Hundreds of meters away from the cliff is a smaller sandstone channel body (~1.5 m thick) along the beach, with two large upright tree trunks of about 1 m and 0.5 m tall on the bank. This small sand-filled channel can be assumed to be linked to the first sandstone channel body on the cliff, with the bank area of the large channel body separating them (Fig. 4.13). It can also be assumed to be a separate channel of its own with the bank area being one of its margins (Fig. 4.14). The sizes of the trunks are large with diameter ranging from 0.4 m to 0.6 m (Appendix A; E and F).

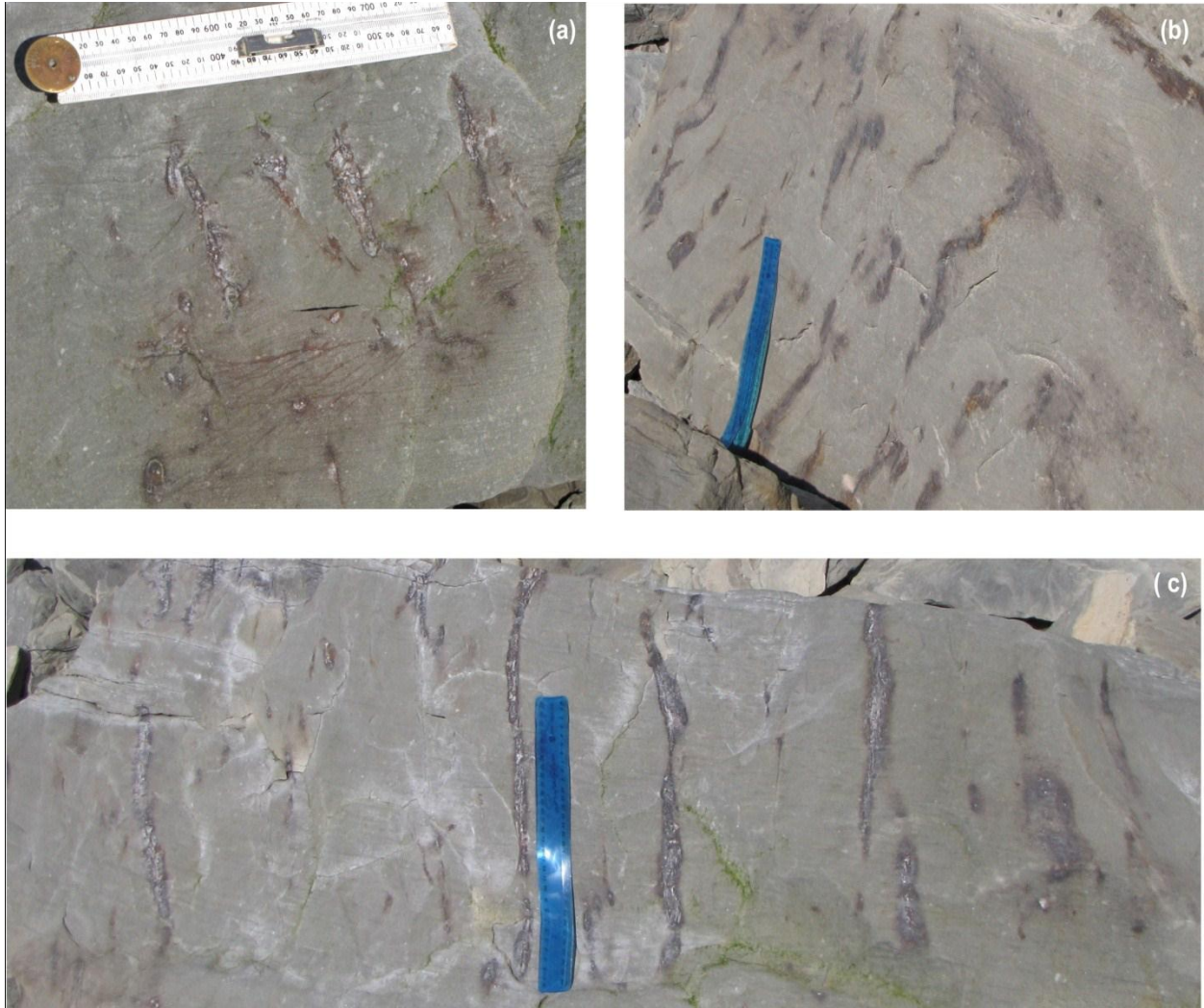


Figure 4.12- Preserved roots on fallen cliff boulder with thirty centimeters ruler scale. (a) Fibrous roots on the beach boulder. (b) Root mat with two extended roots. (c) Parallel roots on fallen cliff boulder.

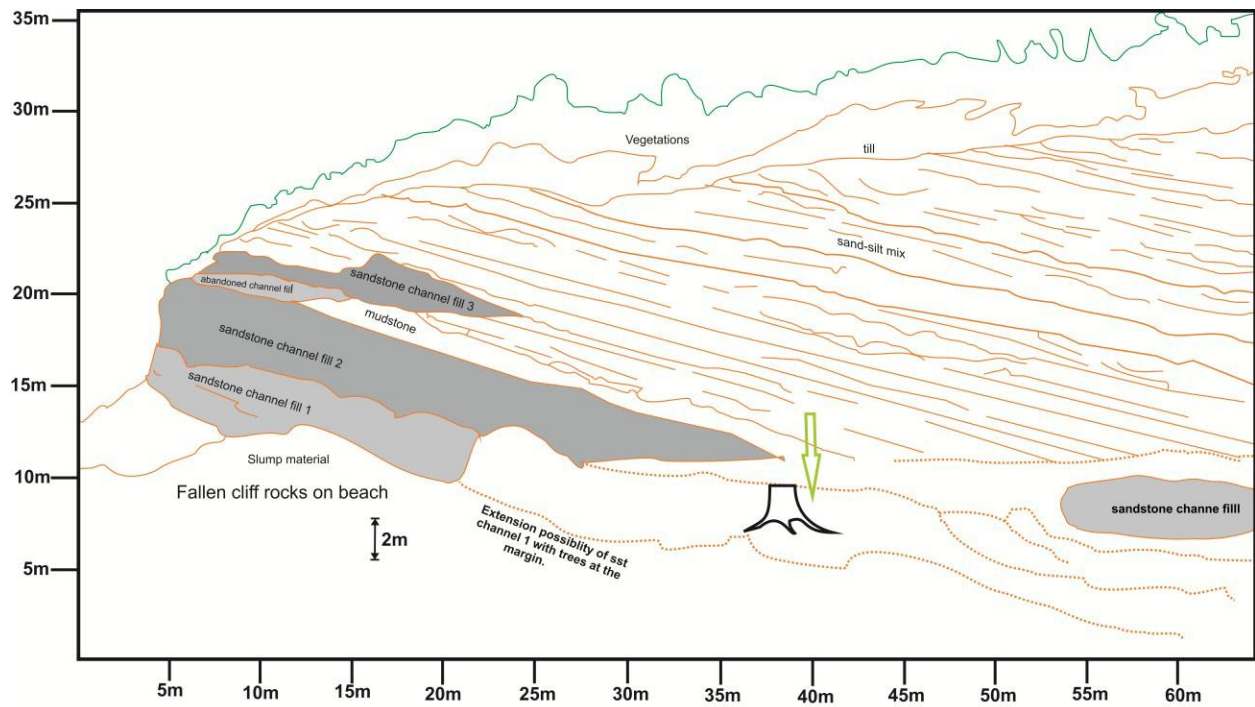


Figure 4.13- Illustrative trace and photograph showing two parallel sandstone channels with the tree trunk representing the position of the first tree trunk and the green arrow representing the position of the second tree trunk inside the bank outcrop separating the two sandstone channels.

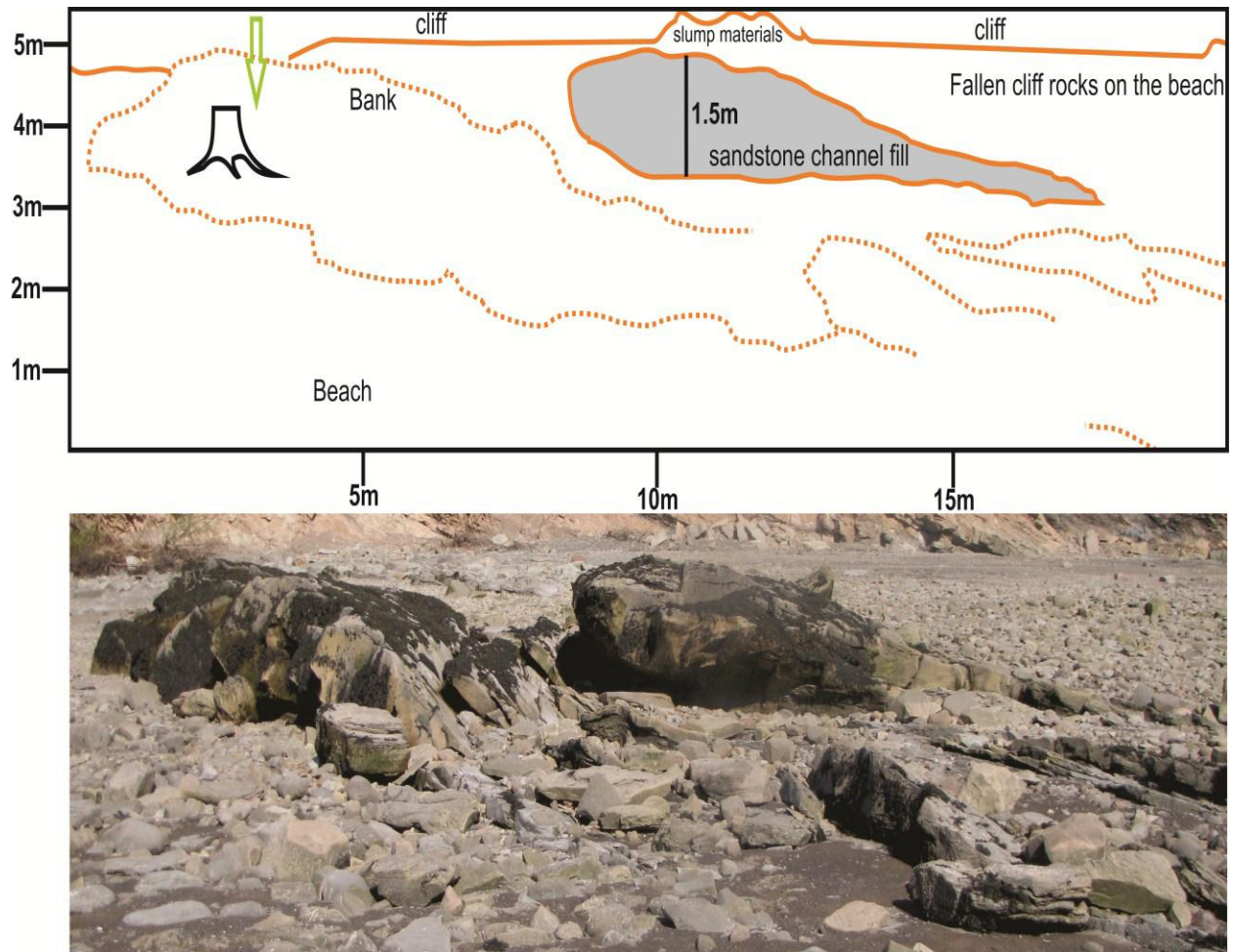


Figure 4.14- Illustrative trace and photograph of the beach sandstone channel fill with the bank to the left containing two large tree trunk fossils represented by the trunk and the green arrow.

4.4.2 Interpretation

This deep delta distributary channel (~9 m thick) contains visible evidence of rooting related to its architecture (Fig. 4.10). Stems on beach boulders from the cliff are not clear evidence of vegetation types within a fossil forest associated with the channel body, since they are not *in situ* (Table 2.1). The stems may have been transported and therefore may not represent the actual vegetation growing on the river bank. According to Rygel (2006), the types of vegetation preserved within the channel body are typical of vegetation growing on the floodplains around the channel body, raising the possibility that the transported vegetation was actually growing along the channel banks. Evidence from longitudinal root sections on fallen cliff boulder shows varying root sizes, which shows rooting architecture similar to those of modern trees with the roots getting finer away from the trunk (Appendix D).

The root architecture associated with the former tree on the cliff face shows a pattern of rooting along and below the channel sediments at the boundary between two storeys. The length of the roots gives some measure of the depth to which root stabilization might be expected to extend. Based on vegetation classification in Table 2.1, the roots of the inferred trunk on the cliff probably belong to a cordaitalean tree. Estimation of root cast volume on the rock surface has shown that the root casts on fallen beach boulders in Tracing 4 locality occupy about 21% of the rock volume (Appendix D). The fact that the tree trunk is situated in the second channel fill and its roots penetrate the first channel fill implies that the tree was growing on the first channel fill before being buried by the second channel fill. The large and radiating roots between the first and second channel fill give direct evidence of the size and extent of roots: large and extensive, likely to influence a large volume of sediment. The termination of the channel close to the inferred tree trunk position is evidence of the tree position being close to the original channel

bank. The tree trunk is about 7 m from the margin of the channel body. It is also probable that the tree trunk grew in the channel bank in seasonal climates. Considering the tree position to be at or close to the bank, it is reasonable to infer that the tree roots played a role in stabilizing the channel bank.

The base of the second sandstone channel fill traces directly along the root-line of the two oppositely diverging roots of the tree (Fig. 4.11). The top of the first sandstone channel fill takes the shape of the rooting architecture, probably due to the root influence during sediment deposition and stabilization. These are clear lines of evidence that the roots have impacted the stabilization of the channel materials.

A small channel along the beach with two big tree trunks on its bank may have been separate from or broadly connected with the distributary channel. Whether connected or not, there is a convincing evidence that the tree trunks influenced bank strength since the trees are preserved next to the small channel body. It is reasonable to assume that the tree trunks still preserved on the shore resembled those represented only by roots within and on top of the channel body in the cliff, on account of the large size of vegetative material in both positions. The root-shoot relationship also plays a very important role on the stability of the bank by maintaining rigidity, resisting and reducing flow velocity and thereby reducing erosion.

4.5.0 Tracing 5

4.5.1 Description

Coal Mine Point cliff is a 10.5 m thick, meandering channel-body with a longitudinal view of two major channel bodies in the cove on the north side of the point: channel-body 1 and channel-body 2 with a cliff orientation of about 312° (Fig. 4.15).

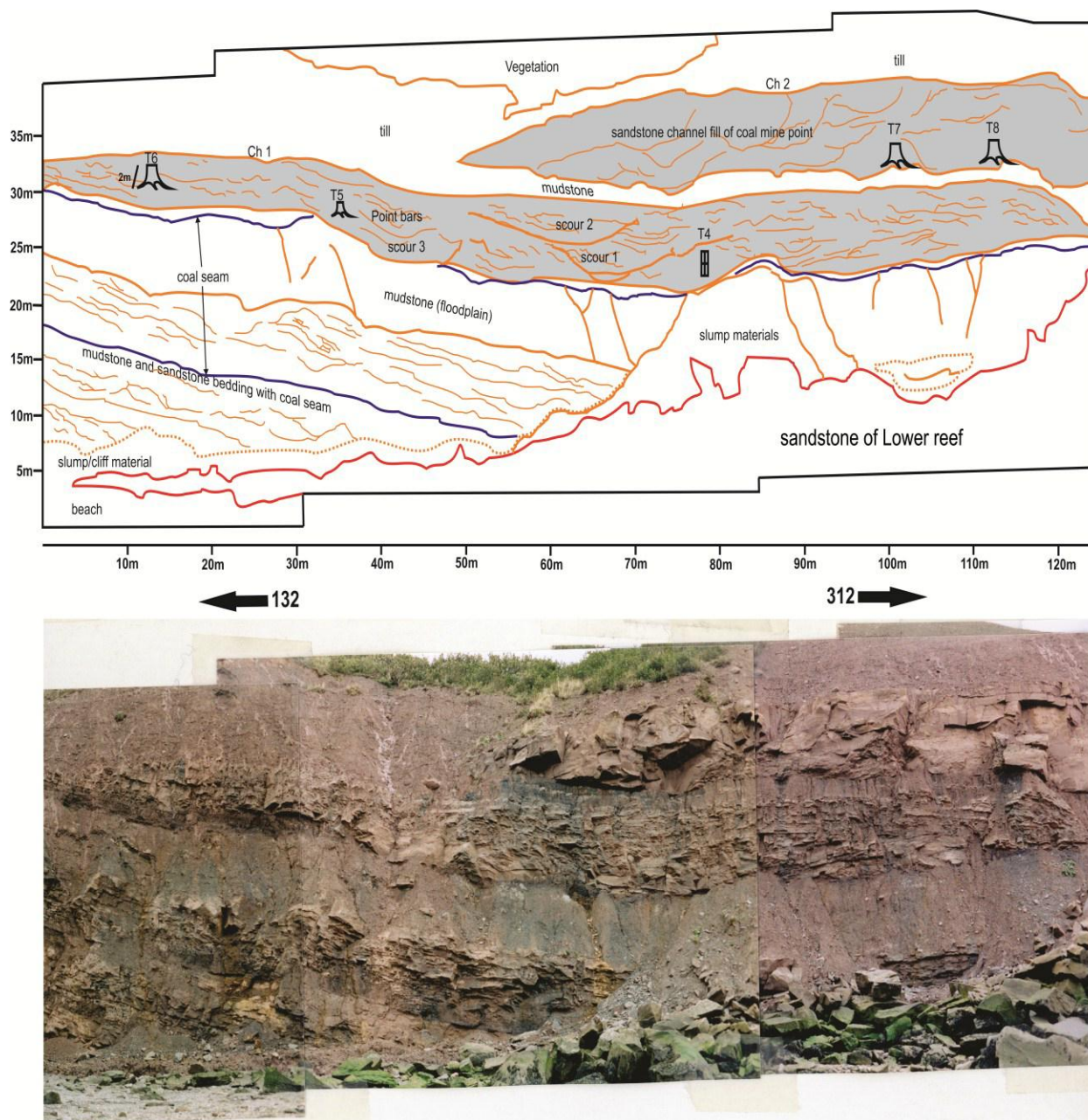


Figure 4.15- Illustrative trace and photograph of Coal Mine Point, showing the two major channel bodies (Ch1 and Ch2), and the three migrating channel fills of Ch2. T4 through T8 above the purple boxes represent the position of tree trunks, whereas the two black arrows represent the cliff orientation. Photograph taken by Gibling in 1998.

Channel-body 2 is the topmost blocky sandstone channel whereas channel body1 is the lower channel body containing three visible scours: scour 1, scour 2 and scour 3, with point bar deposits at the base of scour 1 (Fig. 4.15). Channel-body 1 comprises sandstone-siltstone interbeds. Channel-body 2 is a channel body about 4.7 m thick with trough cross-bedding, ripple cross-lamination, root impressions and fossilized tree trunks. This channel-body 2 forms the main cliff at Coal Mine Point just to the south, and a lot of these structures and features can be seen at the headland. Based on these sedimentary structures, the paleoflow direction is approximated to be into the cliff line as seen in the cove. The fossilized tree trunks in channel-body 2 are mainly noticed within the centre of the channel body which is probably as a result of rapid sedimentation that preserved the tree trunks. Within channel-body 2 are flat-lying wood fragments that were probably carried along in the channel.

Channel-body 1 is the deposit of a single large (~3-4 m deep) channel. There are inclined lateral-accretion surfaces that go through the channel-body from base to top, indicating deposition as a point bar. This channel-body contains three individual scours: scour1, 2 and 3, with tree trunks beneath scours 1 and 3 (Fig. 4.15). The tree trunks in channel body 1 are represented by the tree trunks numbered T1 through 6 (Fig. 4.15 and 4.16), and these are mainly big trees with a few calamites as seen in T4. T1, T2, T3 and T4 are rooted in the floodplain underneath the channel base (Fig. 4.16 and 4.17). The height of T1, T2 and T3 are 0.5 m, 0.8 m, and 0.14 m. The right-side of channel-body 1 appears to be thinning out from the position of T3 at about 40 m to about 55 m on the horizontal scale (Fig. 4.16). T1, T2 and T4 are growing close to what seem to be the position of the right-hand bank of channel-body 1. T5 and T6 are both growing close to scour 3 with T5 closest to the scour (~1.5 m close to scour 3) and T6 about 20 m farther away from the scour but closely adjacent to T5 (Fig. 4.15).

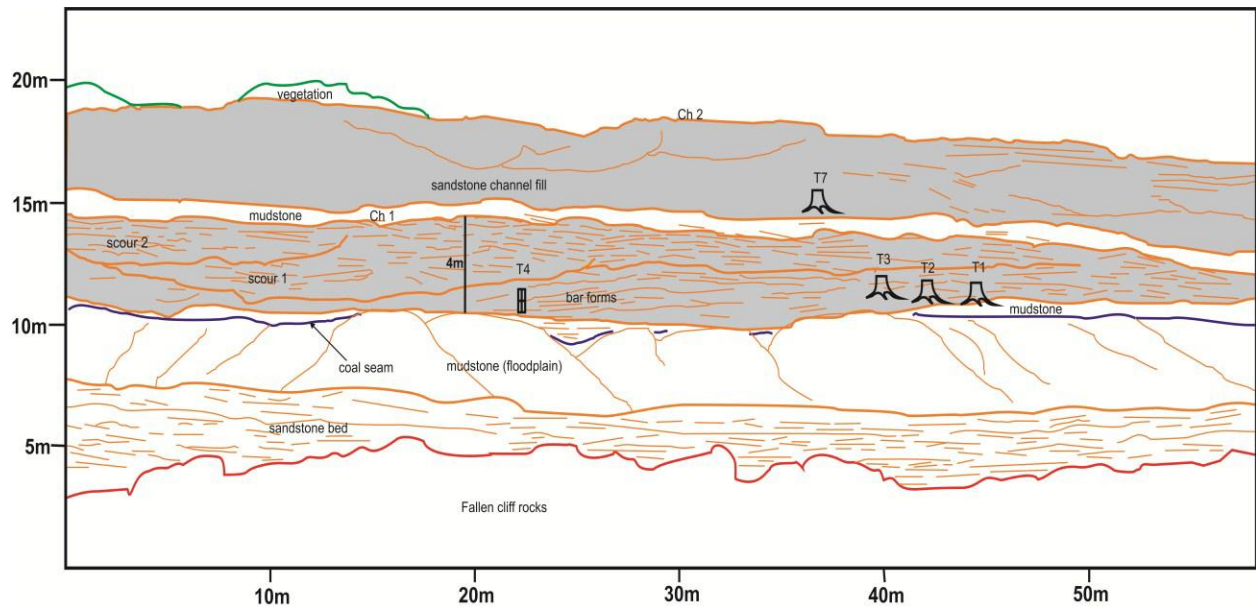


Figure 4.16- Illustrative trace and photograph of central wing of Coal Mine Point, showing the two major channel bodies (Ch1 and Ch2), and two of the three migrating channel fills of Ch1. Photograph taken in 2011.

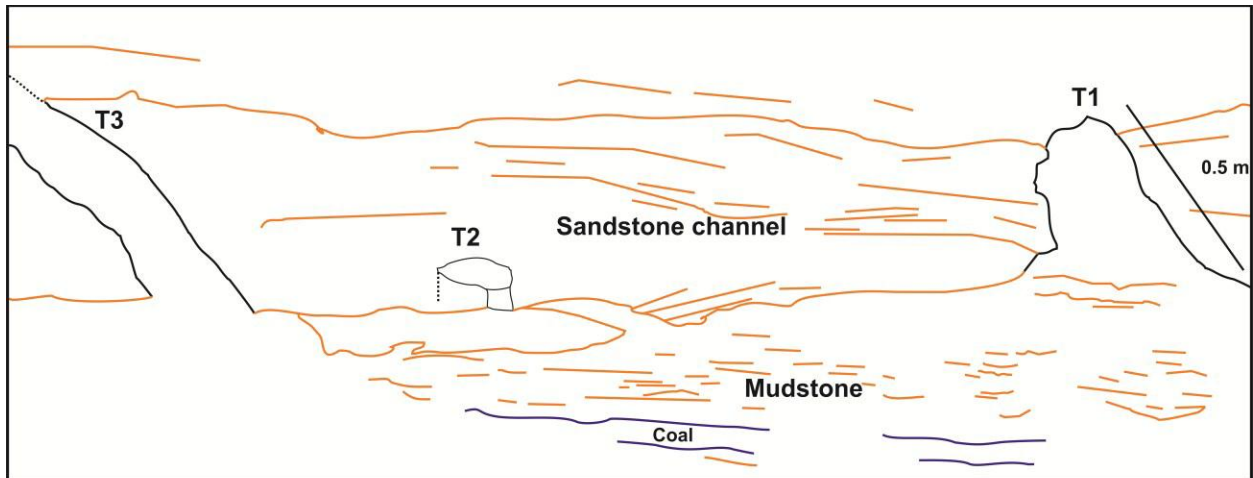


Figure 4.17- Illustrative trace and photograph of tree remains represented by T1, T2 and T3, with T1 showing the flaring base of the trunk representing the root system.

There is a visible erosional surface cut down within 15 m and 35 m of T6 and T5. T6 is a trunk of approximately 2 m height and 70 cm diameter growing above a mudstone-coal seam, implying its growth after a flooding event. T5 and T1 flare at the bottom, showing that the exposure is from the trunk to the root region of the tree, and T3 is tilted towards the channel at a moderate angle and shows about 1 m of exposure (Figs. 4.17 and 4.18).

The photographs of reference were taken 13 years apart. Figure 4.15 was taken in 1998, whereas the rest of the figures were taken in 2011 (Fig. 4.16). Some of the tree stems noticed in Figure 4.15 are not present in Figures 4.16, and some of those present in Figures 4.16 are not present in Figure 4.15 as a result of rapid erosion of the cliff over time. Erosion within this time period when these photographs were taken accounts for the absence of some of the features noticed in Figure 4.15.

Channel-body 2 has a distinct channel bank in the left-side, evidenced by thinning out of the channel body from about 75 m to 47 m where it terminates. However, the right-side does not show any evidence of a channel bank. The photograph of the cliff taken in 1998 shows evidence of two trees (T7 and T8), whereas 2011 photograph shows evidence of only one tree (T7). Both T7 and T8 are situated in the channel-body, but it is difficult to tell exactly where they were rooted. T7 shows a 0.60 m long exposure with a diameter of about 0.55 m, whereas T8 shows an exposure of about 1.43 m with a diameter of about 0.8 m. These tree trunks are situated at a depth of about 5.14 m and 4.57 m below the top of channel-body 2.

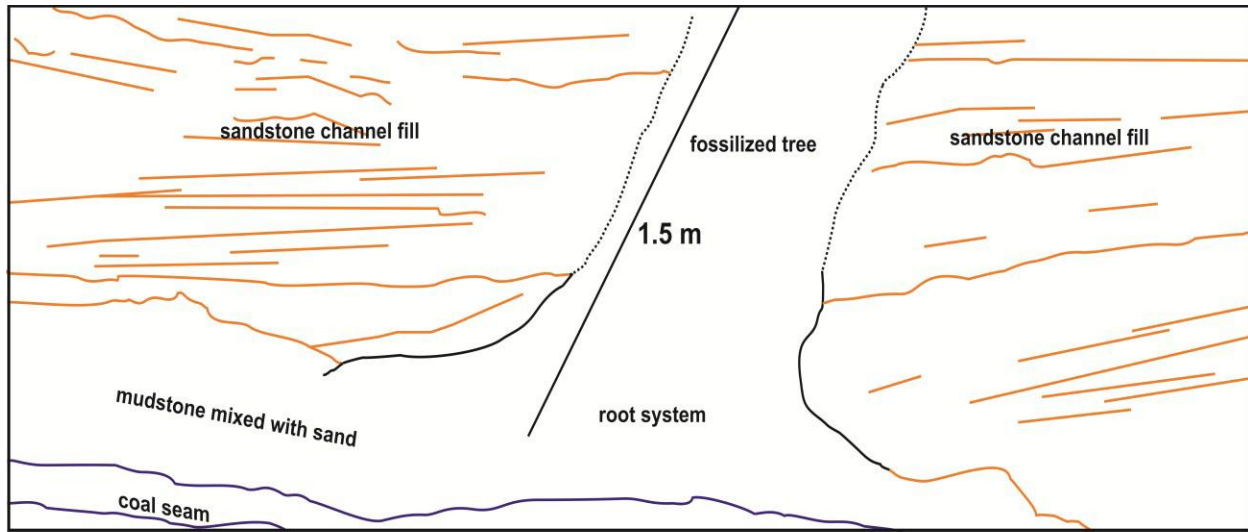


Figure 4.18- Illustrative trace and photograph of tree trunk in Coal Mine Point represented by T5, showing the flaring base indicating root system position.

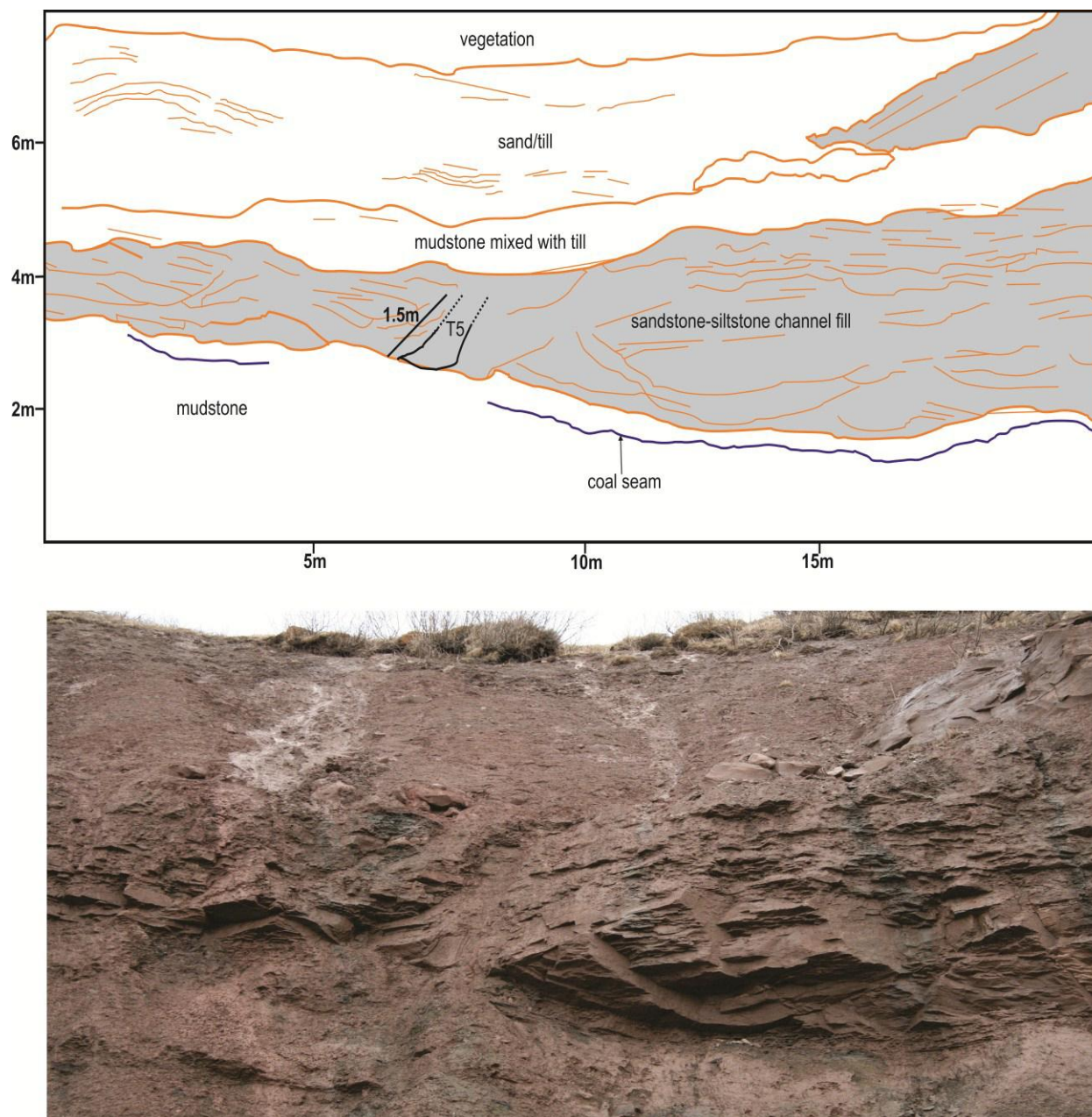


Figure 4.19- Illustrative trace and photograph of left-wing of Coal Mine Point, showing the margins of the two major channel bodies (Ch1 and Ch2).

4.5.2 Interpretation

Coal Mine Point records the largest channel body in the entire Joggins Fossil Cliff. Coal Mine Point cliff is situated stratigraphically above the sandstone of Lower Reef. The cliff comprises two major sandstone channel fills, some flooding surfaces, coal seams and mudstone-sandstone interbeds. The tree trunks in the second channel body were already in existence in the area before being cut through in the channel body, as evidenced by its rooting below channel-body 2. Rapid sedimentation resulted in well preserved trough cross-bedding and ripple cross-lamination on the second sandstone channel of Coal Mine Point.

Channel-body 1 is the main focus of this discussion due to the preservation of the tree trunks along the channel banks. There is evidence of bank vegetation, as depicted by upright tree trunks (T5 and T6) positioned within 15 m and 35 m of the visible cut margin of the original channel (Fig. 4.15). Tree trunk T5 shows a flaring base indicating that the base of the trunk adjacent to the roots is visible. The flaring base position indicates that the tree trunk was growing within the mudstone beneath. The flaring base of the trunk traces along the base of the channel bank of the first channel fill (Fig. 4.18), suggesting that the tree root system has an impact on the channel bank. The tree trunk T5 probably has an impact on the first channel fill due to its position close to the bank. Location of T6 at about 20 m inland from the bank position is also evidence that the tree had an influence in stabilizing the bank.

The thinning out of the right-side of channel-body 1 from the position of T3 to about 55 m, is an indication of the bank. T1, T2 and T3 are growing along the right-side bank of the first channel fill. T1 shows a flaring trunk base, unlike T2 and T3, but T1 is rooted on the mudstone below the channel body and may extend to the coal seam beneath. There is a possibility that T2

and T3 are rooted on the mudstone and coal beneath, but it is not certain. The flaring base of T1 traces along the base of the channel body which is an indication that the tree root system had an impact on the channel. The tilting of T3 towards channel-body indicates resistance to bank erosion. The occurrence of T1, T2 and T3 together indicates abundance of vegetation in the first channel body, which probably extended inland to the bank. Combined influence of vegetation close to the bank and possible vegetation extension beyond the bank may have been sufficient to stabilize the channel bank.

The rooting of most of the trees on coal or mudstone below the channel bodies implies that the trees were growing in the wetlands before the channel was developed. The position of the channel might have been influenced by the trees since they were already growing before the channels were formed. This implies that the trees influenced the channel because the channel body ends close to the position of preserved trees.

The thinning out of the left-side of channel-body 2 until its termination is an evidence of the channel bank. Although it is difficult to tell exactly where the tree trunks in channel-body 2 are rooted, it is probable that they are rooted in the coal or mudstone beneath the channel because of the position of the exposure close to the base, with no evidence of the root system within the channel body. Channel-body 2 is not a good study for channel-body controls for the case study because none of the trees (T7 and T8) are positioned on or close to the channel bank.

4.6.0 Petrography

4.6.1 Description

Microscope petrography observations performed on three thin sections X, Y and Z collected from root casts in Trace 4 locality aided in identification of minerals coarse enough to be identified using their optical and chemical properties. These thin sections are transverse cuts through root casts, thereby exposing materials from immediately around the former root position to the outer margin of the cast. Some minerals in the samples are too fine grained, and their optical properties cannot be measured. These very fine minerals were analysed using X-ray diffraction and electron microprobe.

Thin section X contains fine-grained minerals that can be best analysed using 10x and 40x magnifications. The minerals identified are quartz, calcite, siderite, and kaolinite. The approximate grain size ranges of the minerals are; 62 μm - 150 μm for quartz, 62 μm - 182 μm for calcite, and 56 μm - 188 μm for siderite (Fig. 4.20). Quartz grains constitute 35 % of the sample; calcite constitutes 20 %, siderite 30 %, and kaolinite 15 % (Appendix B). Quartz crystals associated with this thin section are mainly angular to subangular and are randomly distributed. Quartz grains in thin section X appear to be floating in the calcite cement, implying early crystallization of calcite before much compaction had taken place. Some smaller quartz pieces are fragments of a single large crystal. An explanation to the fragmented individual quartz crystals is pressure impact from crystallization of calcite, resulting in expansion and fragmentation of some of the individual quartz crystals. Quartz crystals associated with this thin section are mainly angular to subangular and are randomly distributed.

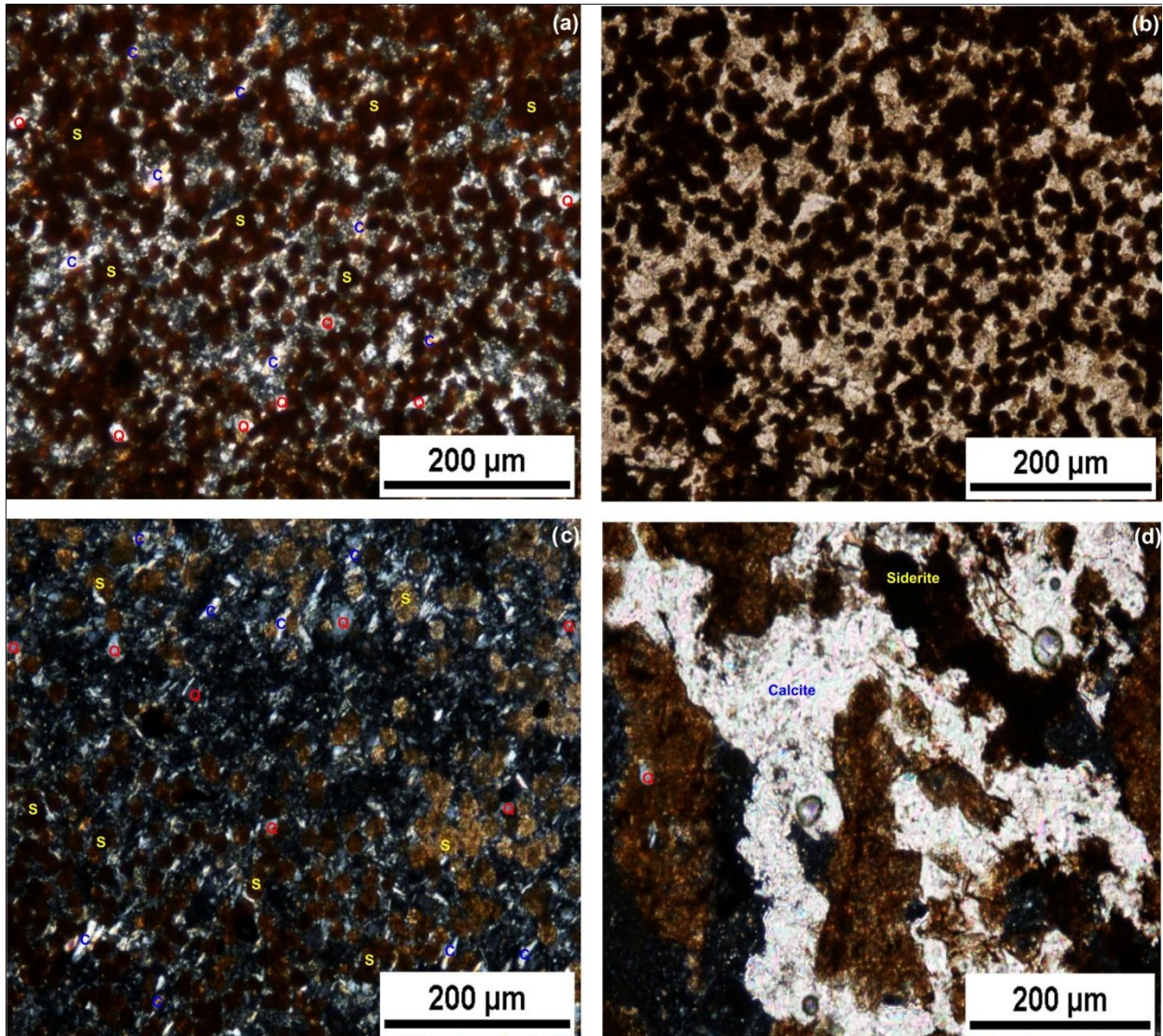


Figure 4.20- Thin section X with codes Q, C and S representing quartz, calcite and siderite. (a) Oolitic and irregular siderite grains hosting quartz, and with calcite and quartz groundmass. (b) Plane-polarised version of (a). (c) Oolitic siderite crystals with angular to subangular quartz grains, and tabular to needle-like calcite crystals. (d) Calcite fillings in cracks and fractures with siderite localised at the margin (Cross-polarised light).

moderate positive relief which changes with rotation. The siderite crystals are predominant along the edges of the root cast, and also on the margins of fractures where they are associated with calcite (Fig. 4.20d).

The mineralogy of thin section Y is quartz, plagioclase, and calcite. Quartz grains in this sample vary in shape from angular to rounded, and in size from 40 μm to 240 μm (Fig. 4.21). The sample is dominated by calcite, which constitutes about 55 % of the sample, followed by 43 % quartz grains, and 2 % plagioclase (Appendix B). The cement is dominated by calcite. Only three plagioclase crystals were noticed in this sample, with well defined twin lamellae, and approximate grain size of 144 μm . These plagioclase crystals are mainly subangular and tabular. Single calcite grains present are tabular with well defined twin lamellae, and approximate grain size range of 142 μm and 184 μm , whereas the groundmass calcite crystals are irregularly shaped and also possess twin lamellae.

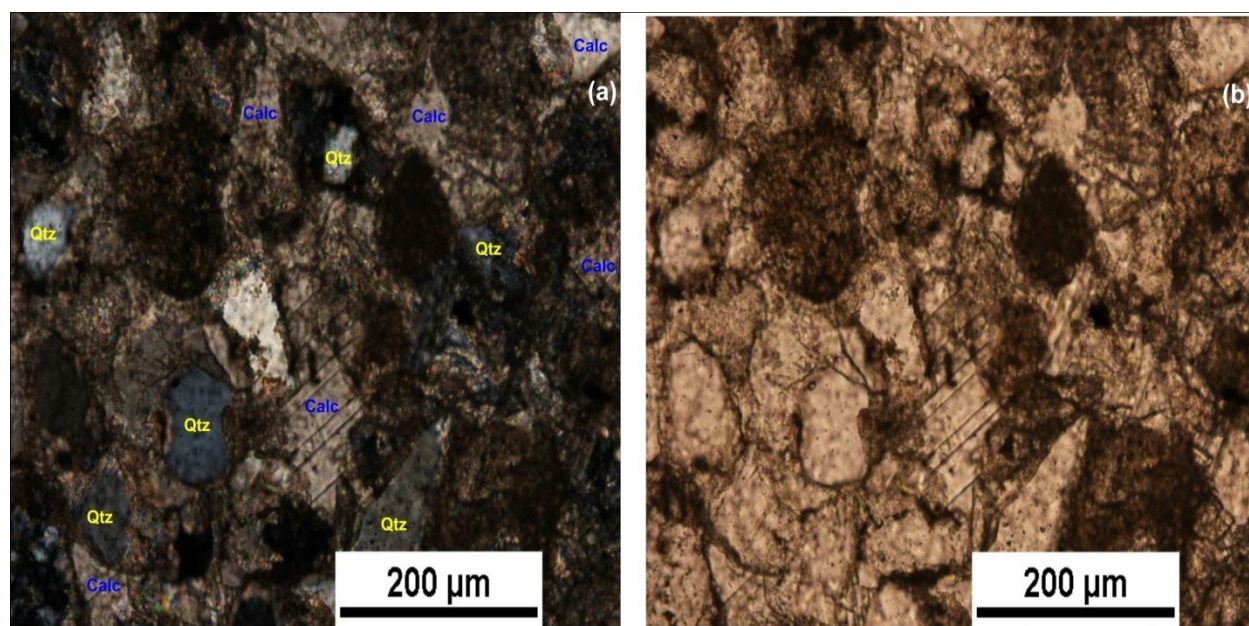


Figure 4.21- Thin section Y showing well defined twinning on calcite crystals, and angular quartz crystals. (a) Cross polarised Light (b) Plane polarised Light.

Thin section Z contains similar minerals to thin section X with the exception of plagioclase, which is scarce in thin section Z and not present in thin section X. Quartz, calcite and siderite are all present in sample Z. Siderite exhibits an oolitic-spherulitic shape and is localized at the edge of the sample, in similar pattern as thin section X. Some of the siderite is irregular in shape due to joining of individual grains. Individual siderite crystals have approximate grain size in the range of 15 μm to 20 μm . Calcite shows a poikilotopic texture in some areas where large crystals in optical continuity contain numerous smaller grains of calcite and quartz. There are small amounts of tabular and needle-like crystals of calcite with approximate grain size range of 80 μm to 100 μm . Quartz grains are subangular to angular with grain-size ranging from 20 μm to 160 μm . The middle of the sample contains grains/books of kaolinite occupying cracks probably created by roots (Appendix B). Kaolinite in this thin section has grain size ranging from 9 μm to 15 μm (Fig. 4.22). Fine-grained silt and clay sized materials are present in this sample, but were not identified using this method.

4.7.0 X-ray diffraction

4.7.1 Description

X-ray diffraction is very important for the identification of fine minerals in this research. This mineral identification is essentially a two-step process involving “search” and “match”. The search involves selection of a list of possible phases by comparing the pattern of the unknown to a large set of reference mineral patterns. The match is considered made when a final mineral assemblage is chosen through considerations of peak intensities, chemistry of the sample, and mineral associations. The comparison done in the first step involves comparing the unknown peak with a standard peak and deciding how far the peak angle and intensity can diverge.

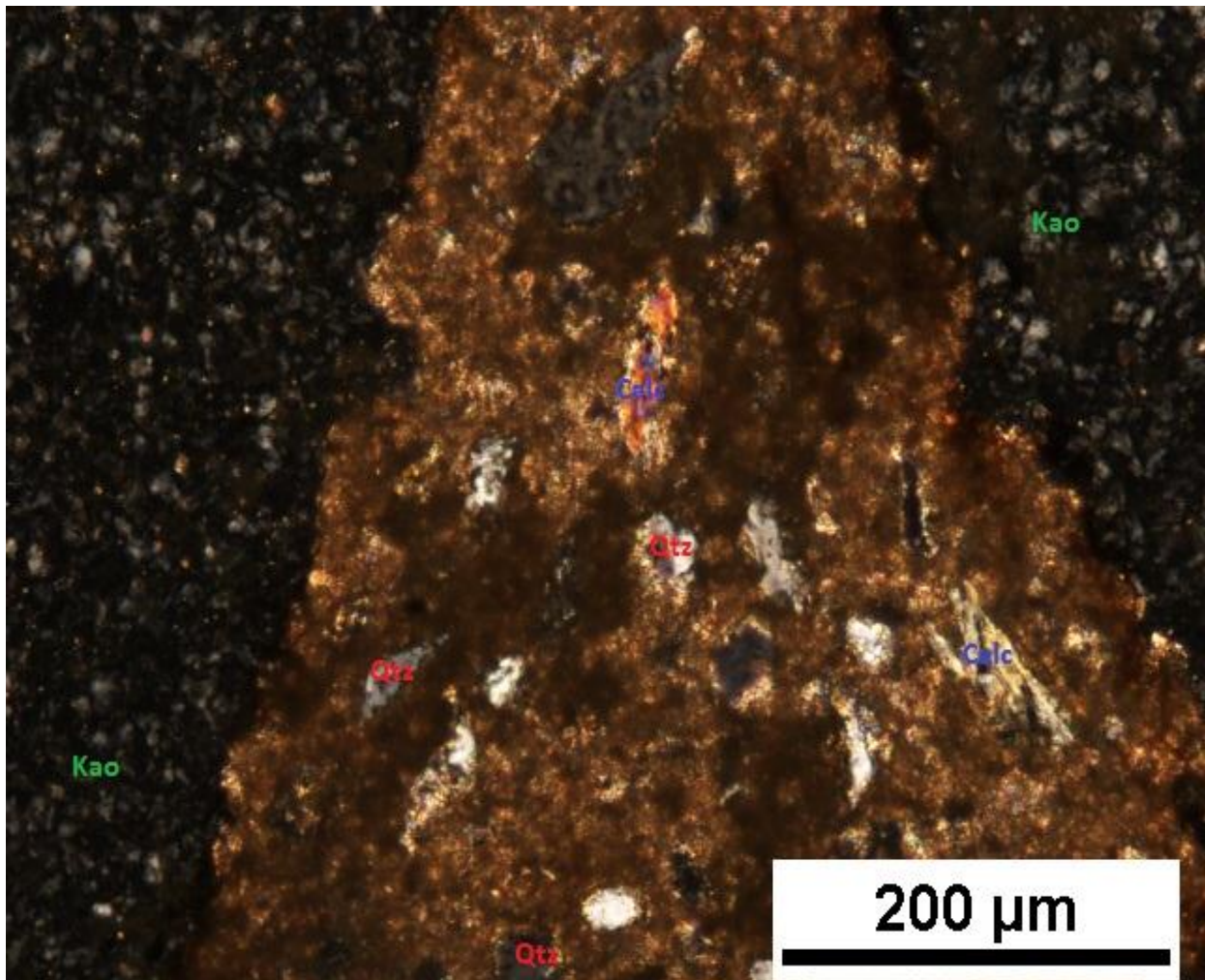


Figure 4.22- Thin section Z showing books of kaolinite in fractures, and angular to subrounded quartz grains and calcite grains.

Some of the minerals identified in the X-ray diffraction analysis of three samples X, Y and Z are similar to those in the petrographic analysis. The samples showed varying numbers of peaks with sample X containing 38 peaks, 44 peaks for sample Y, and 29 peaks for sample Z. The peak lists show the various positions, heights, d-spacing and relative intensities for each of the minerals represented in the samples. The peaks correspond to various minerals, though multiple peaks were identified for individual minerals. The start position for each of the graphical analyses was 5° whereas the end position is 85° . The measurement parameters for all the three samples were the same (Appendix C).

All the five minerals represented in the petrographic analysis are also present in the identified phases of sample X. Kaolinite in the thin section is localised only within cracks, whereas there is little to no muscovite in the thin section. Most of the “muscovite” identified in the X-ray diffraction analysis is probably illite clay. Quartz and calcite are present in both the X-ray diffraction and the petrographic analysis in sample Y, whereas siderite which is present in the X-ray diffraction analysis was not identified in the petrographic analysis, and plagioclase which is present in the petrographic analysis is not evident in the X-ray diffraction analysis. The plagioclase identified in the petrographic analysis is not significant because only three crystals were identified in the thin section. Three peaks in sample Y have no perfect matching minerals, so there are no identified phases for them. The identified phases in sample Z are quartz, siderite and kaolinite (Appendix C). Kaolinite was probably the constituent of the matrix of the thin section, the crystals of which were too fine to be identified using its optical properties. Most of the kaolinite is localised within cracks, as seen in sample X. Very low quantity of plagioclase was identified in the petrographic observation which results in it not being recognised in the X-ray diffraction analysis. Lack of identification of plagioclase in the X-ray diffraction doesn't

necessarily imply its absence in the sample, but the masking of its peak with the surrounding noise disallows for its identification by the software.

4.7.2 Petrographic and X-ray diffraction analysis interpretation

Mineralogical relationship between the three analysed samples gives a good indication of environmental conditions of deposition. Almost all recognized minerals in the petrographic analysis were also identified in the X-ray diffraction analysis, with few exceptions noted in the description. Plagioclase is probably present in proportions that are below resolution to be identified in X-ray Diffraction. There was very little to no muscovite crystals in the thin section, and the material identified using X-ray diffraction is probably illite clay. An explanation for the fragmented quartz crystals noted in the petrographic description is pressure impact from crystallization of calcite, resulting in expansion and pushing apart of some of the quartz grains.

Siderite crystals are mainly localised at the edge of the sample and along the margins of fractures towards the centre of the thin sections. The siderite-rich zone at the edge of the sample has a sharp contact with quartz grains in the outer layer, implying that the siderite-rich zone contact with the outer quartz grains marks the contact between the nodule and the surrounding quartz-rich sandstone. The Fe-component of siderite shows that the nodules probably formed by precipitation under reducing conditions (Browne and Kingston., 1993). Since siderite is associated with calcite in this environment, there is a possibility of iron replacing calcium to form siderite through a replacement reaction. Unidentified Fe-rich clay minerals such as illite with Fe component may account for the presence of Fe in the environment. Calcite and siderite in these samples are coatings that precipitated around roots, and therefore have the potential for generating erosion-resistant armour around the roots.

Semi-quantitative analysis carried out on the sample in X-ray diffraction show mineral proportions different from that of petrography analysis. In the petrography analysis, quartz is the most abundant mineral in sample X with proportion of about 35 %, whereas siderite is the most abundant according to the X-ray diffraction with mineral proportion of about 28%. Calcite which is lower than siderite in petrography analysis appeared to be higher in proportion than quartz in the X-ray diffraction analysis (Appendix B and C). In sample Y, siderite is the most abundant in the petrography analysis with proportion of 55 %. Meanwhile X-ray diffraction analysis portrays quartz as the most abundant mineral with high proportion of about 81.4 % (Appendix C). Siderite is the most abundant mineral in both the petrography analysis and the X-ray diffraction analysis in sample Z. Mineral proportion for quartz in petrography analysis of sample Z is 35 %, and 57.9 % in X-ray diffraction analysis.

4.8.0 Electron microprobe

4.8.1 Description

Electron microprobe analysis was carried out on sample X to confirm the minerals identified in both the petrography and the X-ray diffraction analysis. The probe analysis also aided in identification of unidentified minerals in petrography and X-ray diffraction analysis. The probe analysis focused mainly on WDS (Wavelength Dispersive Spectroscopy) and EDS (Energy Dispersive Spectroscopy) analytical method. Various chemical components of the mineral being analysed in EDS are represented by peaks with the element name above or beside them. Some of these peaks show overlap between elements. The WDS analysis gives better and more precise chemical analysis.

Microprobe analysis performed on sample X shows evidence of siderite localisation along cracks, towards the centre and close to the edge of the sample. These siderite grains range in size from 15 μm to 25 μm along cracks, and 10 μm to 18 μm close to the edges of the sample. The siderite grains along the cracks are irregular, subrounded and subangular in shape (Fig. 4.23), whereas those at the edge of the sample are spherulitic and irregular in places where amalgamated (Fig. 4.23c). EDS analysis for the siderite grains displays one high Fe-peak (Fe^{α}) with one moderate and one low Fe-peak (Fe^{β}), and O-peak overlapping with Fe-peak (Appendix F). Low Ca-, Mn- and Mg- peaks were also identified in the EDS analysis of siderite. The WDS analysis show high mass percentages for other elements in almost all the analyses. Mass percentages for FeO, MnO, MgO, and CaO are 44.177 %, 6.331 %, 2.69 %, and 2.471 % (Table 4.1).

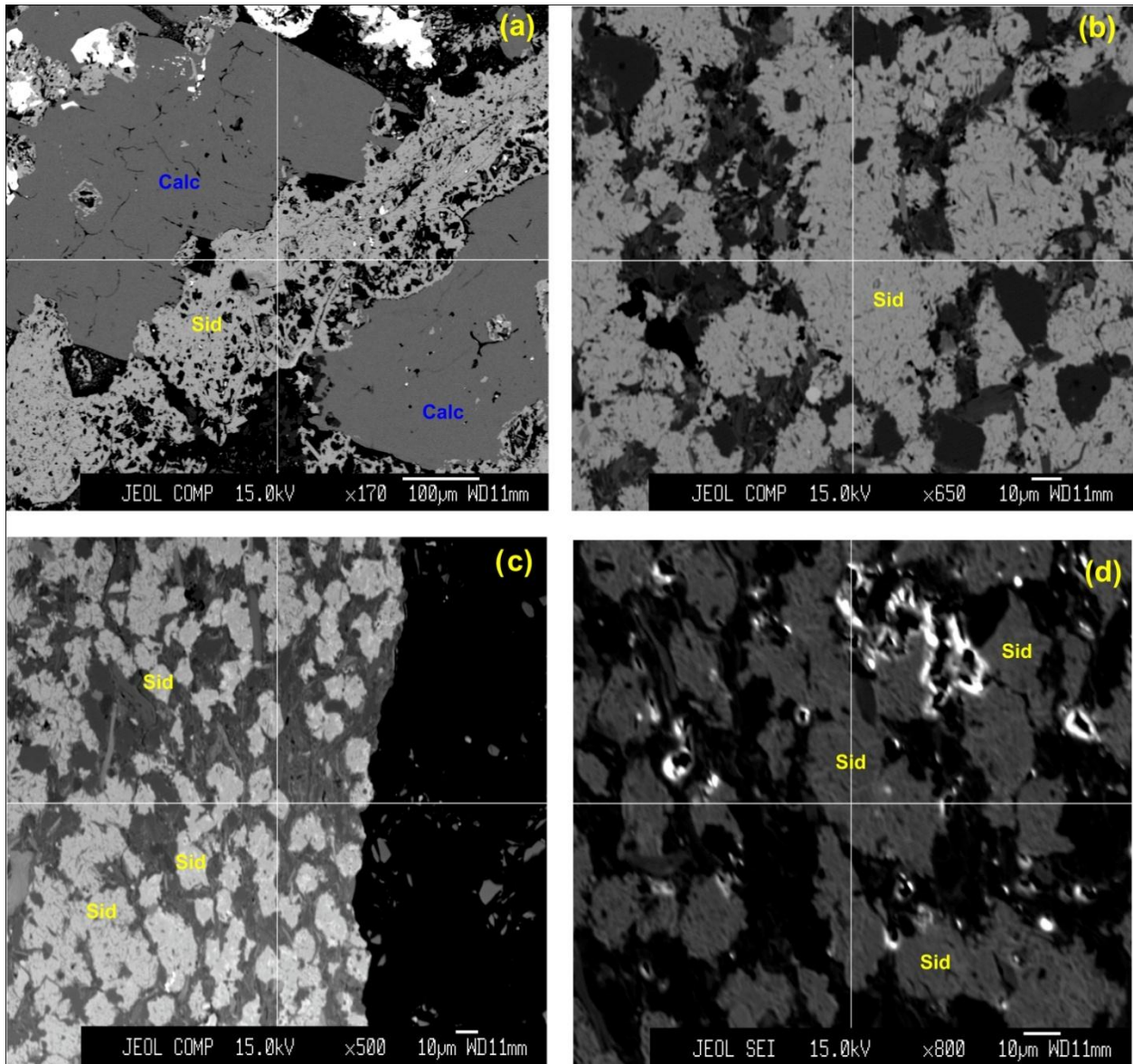


Figure 4.23- Electron microprobe image of siderite in sample X. (a) Siderite interaction with calcite in some cracks. (b) Amalgamated siderite grains close to the edge of the root cast. (c) Spherulitic and irregular siderite grains at the edge of the root cast. (d) Angular and irregular siderite grains.

ZAF	Siderite	Quartz	Alkali feldspar	Calcite	Kaolinite	Illite
Element	Mass (%)	Mass (%)	Mass (%)	Mass (%)	Mass (%)	Mass (%)
K ₂ O	0.038	0.042	15.751	0.016	0.012	5.571
Cr ₂ O ₃	0.081	0	0	0	0	0
Na ₂ O	0.116	0.012	0.712	0.006	0.018	0.107
SiO ₂	0.378	92.137	64.504	0.01	47.191	52.991
MnO	6.331	0.117	0.073	1.787	0	0.098
CaO	2.471	0.077	0	39.204	0	0.133
TiO ₂	0.293	0	0.062	0.202	0	0.046
MgO	2.69	0.558	0.018	0.208	0	1.410
Al ₂ O ₃	0.3	1.545	17.97	0.122	37.979	32.206
FeO	44.117	4.124	0.958	1.232	0.197	3.659
BaO	0.165	0	0.735	0.028	0	0
Total	56.98	98.612	100.783	42.815	85.397	96.221

Table 4.1- Summary of oxide mass percentage of siderite, quartz, alkali feldspar, calcite, kaolinite and illite.

Quartz was also identified in the EDS analysis with very high Si-peak and O-peak, and very low C-peak (Appendix F). Quartz grains in the sample are subangular to angular and range in size from 10 μm to 43 μm (Fig.4.24). The WDS analysis for quartz shows a reasonable total mass percentage of 98.612 %. Mass percentage of 92.137 % for SiO₂ is normal for quartz (Table 4.1). However, the mass percentage of 4.124 %, 1.545 %, 0.558 %, and 0.117 % for FeO, Al₂O₃, MgO and MnO, is high for quartz. Alkali feldspar was also identified in the EDS analysis (Fig. 4.25), but it was not recognised in the thin section and X-ray diffraction. The alkali feldspar grains are subangular to angular in shape, and have approximate grain size of 23 μm . The mass percentage for Al₂O₃, K₂O, and SiO₂ are 17.97 %, 15.751% and 64.504 % (Table 4.1). These percentages are typical for alkali feldspar analysis, but the total mass percentage of 100.783 is high for alkali feldspar.

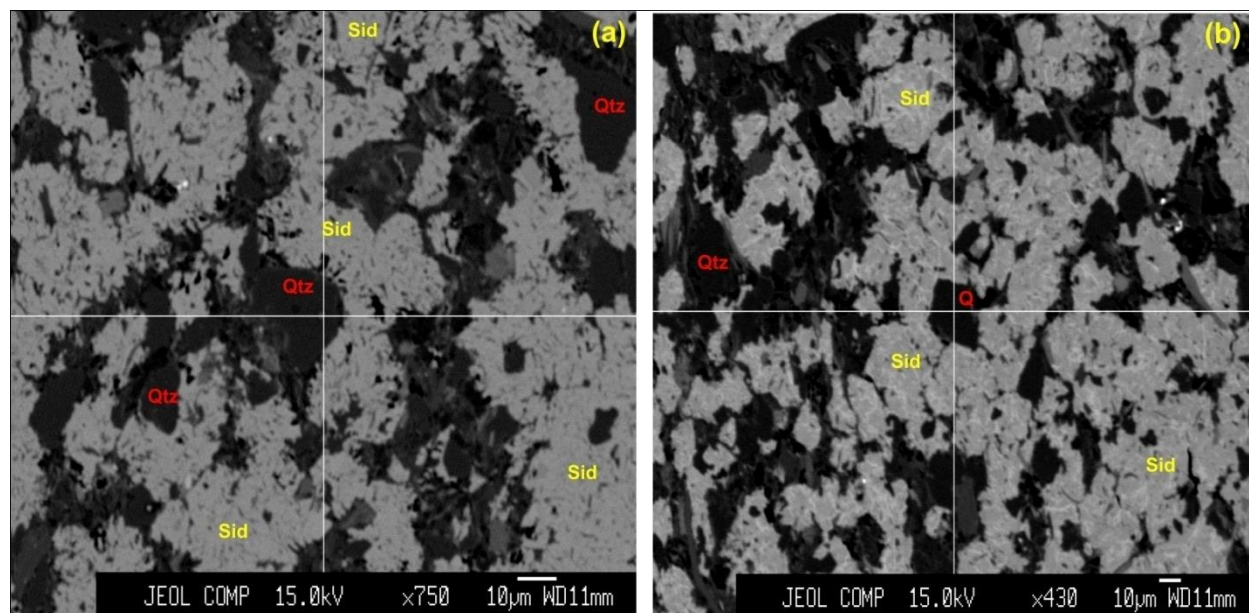


Figure 4.24- Electron microprobe image of quartz in sample X. (a) Subangular quartz crystal at the centre. (b) Quartz interaction with siderite.

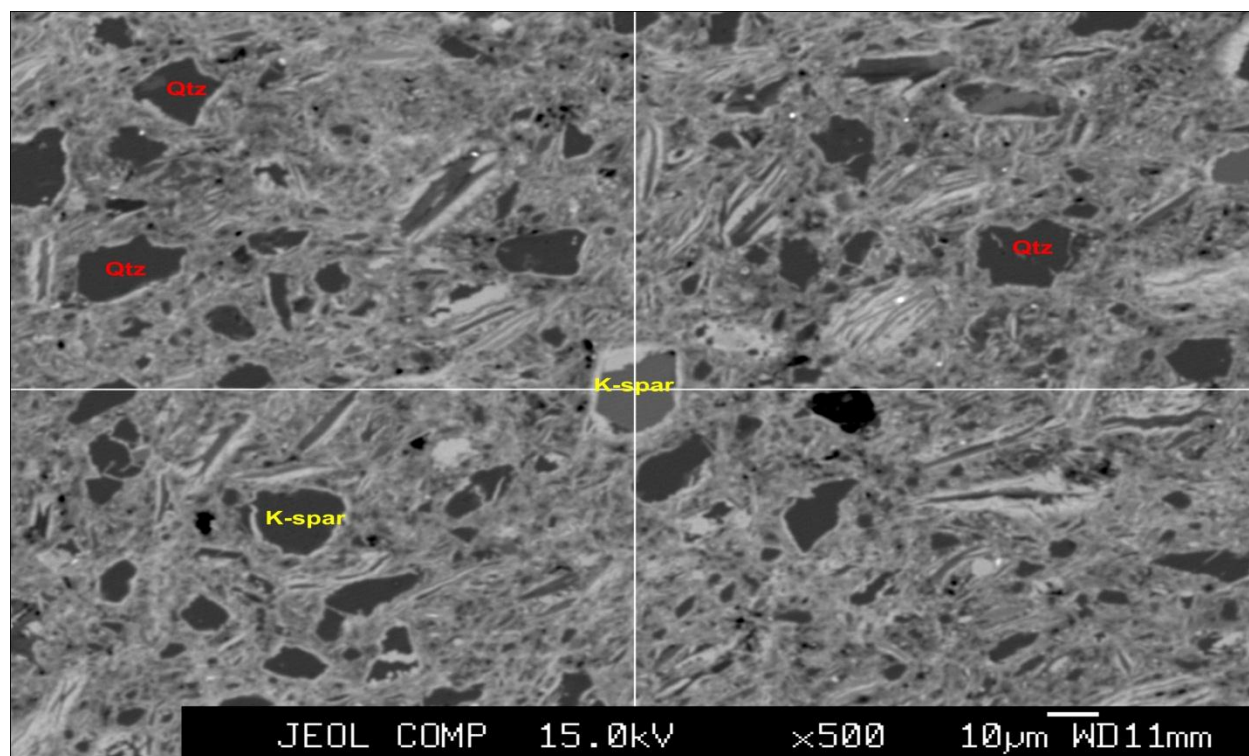


Figure 4.25- Electron microprobe image of alkali feldspar in sample X.

Calcite was also identified in the EDS analysis with high Ca-peak and moderate O-peak (Appendix F). There are other elements present in the EDS analysis such as Mg, Mn and Fe. Calcite was found to be localised between the siderite grains, in cracks and close to the edge (Fig. 4.26). Calcite grains in this sample are subangular to angular, with grain size ranging from about 100 μm to 825 μm (Fig.4.26c). The mass percentage for CaO, MgO, FeO, and MnO are 39.204 %, 0.208 %, 1.232 % and 1.787% (Table 4.1).

Clay minerals such as kaolinite and illite are abundant in the sample. Kaolinite in the sample is localised both within the main root cast and also inside some of the cracks (Fig.4.27). Kaolinite crystals within the root cast are tabular, and are about 37 μm long, whereas kaolinite crystals inside the cracks are angular with approximate grain size of 10 μm . The EDS analysis shows evidence of kaolinite with high Al-, Si, and O- peaks (Appendix F), and low peaks of Fe. The total mass percentage for kaolinite is 85.397 %. Illite was also identified in both the EDS and WDS (Appendix F). The WDS analysis shows illite to have a total mass percentage of 96.221 % (Table 4.1). The EDS analysis also identified minerals such as zircon, rutile, and pyrite (Fig. 4.28.).

The EDS analysis of rutile shows both the alpha- and beta- peaks of Ti, and O (Appendix F). Minor traces of B and Fe are also present. The rutile crystals are subangular in shape, with approximate grain size of 9 μm and 11 μm . Zircon signature shows only the alpha peaks of Zr, S and O, with minor peaks of Fe, Ca, F, Mg and Al (Appendix F). Zircon crystals identified in the root cast are tabular, with approximate grain size of 24 μm . The EDS analysis of pyrite portrays both the alpha- and beta- peaks of S and Fe. Minor elements present in the EDS analysis for pyrite are As and Zr. Pyrite crystals in the root cast are angular to subrounded in shape, with grain size ranging from about 7 μm to 20 μm .

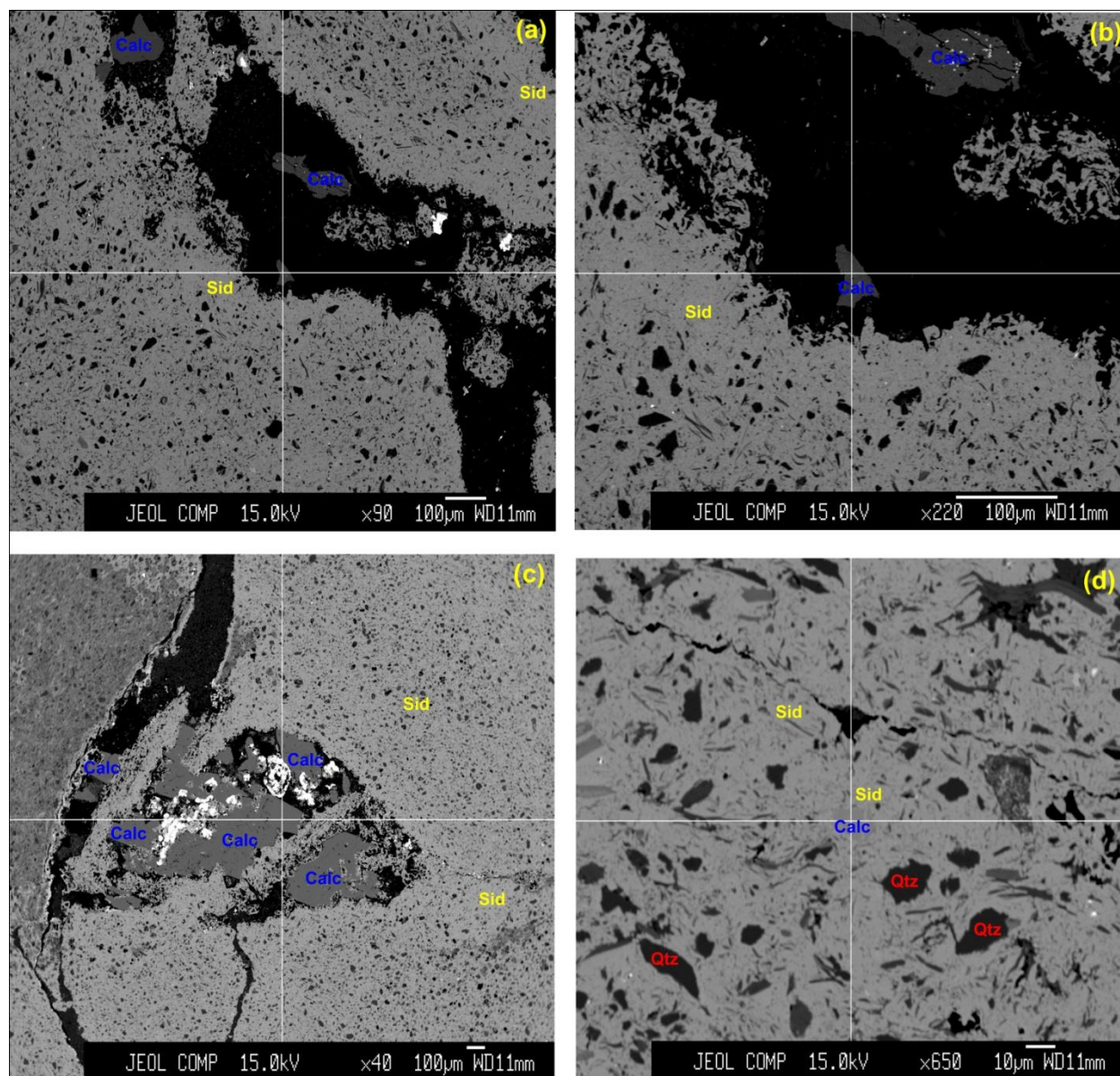


Figure 4.26- Electron microprobe image of calcite in sample X. (a) Calcite grains in cracks. (b) A closer view of angular calcite grain in crack. (c) Calcite grains in crack and their interaction with siderite. (d) Calcite interaction with matrix siderite.

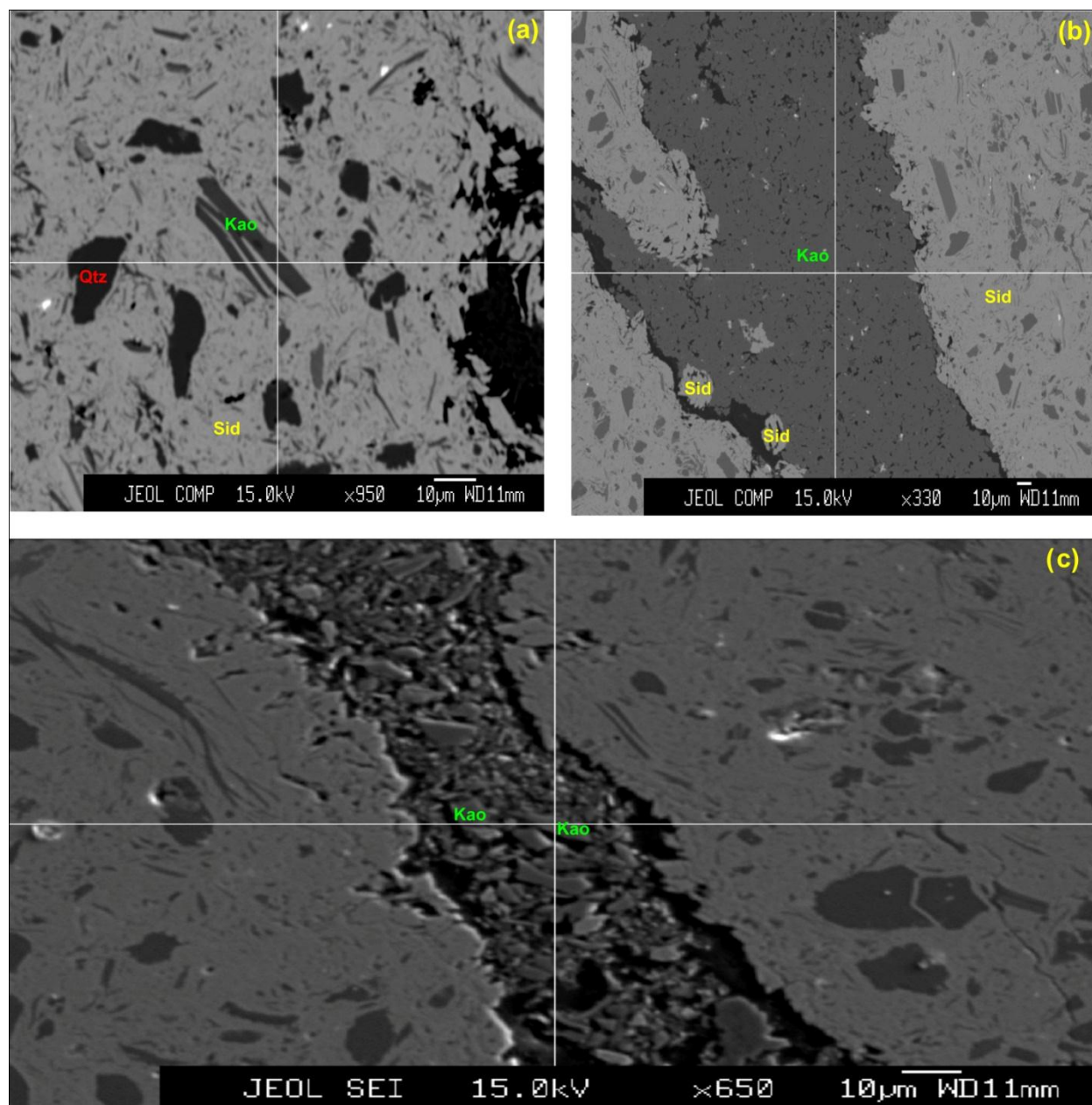


Figure 4.27- Electron microprobe image of kaolinite in sample X. (a) Near-tabular kaolinite crystal in siderite matrix. (b) Kaolinite filling in cracks (c) Angular kaolinite (Kao) crystals in crack.

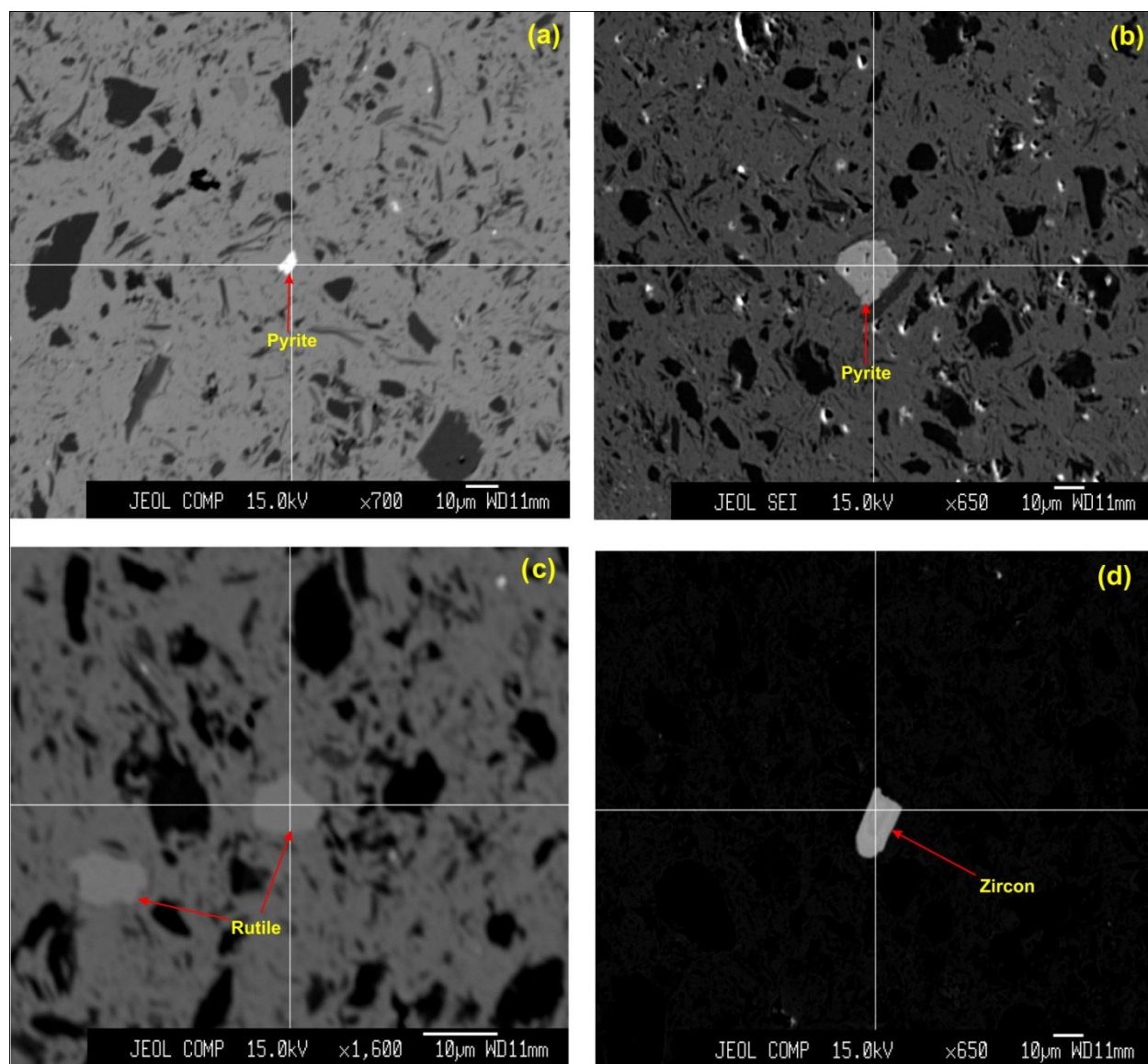


Figure 4.28- Electron microprobe image of pyrite, rutile, and zircon in sample X. (a) Angular pyrite crystal within the root cast. (b) Subrounded pyrite crystal within the root cast. (c) Subangular rutile crystals in siderite matrix. (d) Zoned tabular zircon crystal within the root cast.

4.8.2 Interpretation

The electron microprobe analysis carried out on Sample X shows similar minerals to those noted in petrographic analysis and X-ray diffraction analysis. The microprobe analysis also identified minerals that were not noticed in the petrographic and X-ray diffraction analysis such as alkali feldspar, zircon, rutile and pyrite.

The WDS analyses were abnormal for almost all the minerals due to intergrowth of minerals, resulting in the apparent presence of unusual elements in many of the minerals. The intergrowth between minerals resulted in the inability to acquire normal mass percentages for the WDS analysis. This intergrowth of minerals also resulted in the presence of minor minerals in the EDS analysis. Siderite grains along the edge of the sample are more intergrown with clay minerals (kaolinite and illite), whereas the siderite closer to the middle is more free from the intergrowth. The matrix of the sample is made up of a combination of several elements, making it difficult to identify the exact mineral constituent. However, the EDS analyses of the matrix look more like an intergrowth of siderite and clay minerals. The low total mass percentage of 56.98 % for siderite is probably as result of inability of the microprobe to analyse for carbon. Some of this discrepancy is accounted for by the fact that carbon adds to the mass, but is not reported. Intergrowth of minerals also accounts for this discrepancy. This is also the case for the low total mass percentage for calcite (Table 4.1). Many of the minor elements are in trace amount and therefore do not have any EDS peak.

There are compositional changes from the centre to the margin of the root casts, where there are more intergrowths of minerals. Calcite is more abundant towards the centre of the root cast than near the margins. Chemical composition of the minerals close to the margin shows

more sign of minor elements, whereas the minerals closer to the centre of the root cast tend to show fewer amounts of minor elements. This is to say that there are less contaminations at the centre of the root cast.

CHAPTER 5 – Discussion

5.1.0 Vegetation and sediment influence

This study has investigated the possible influence of vegetation on the stability of channel banks. Vegetation influence on channel bank stability has been evidenced by results from the previous chapter, but the extent of these impacted effects of vegetation on banks is yet to be determined. Results and interpretations have shown evidence of rooting architecture, root mats, and vegetation mass influence on channel bank stability. Table 5.1 summarises evidence in favour of and against vegetation impact on channel stability, and also comments on the various lines of evidence in favour.

Results and interpretations from Tracing 1 (Fig. 4.1) have shown evidence of root architecture effect on the channel banks (Table 5.1). Root tracings along the base and margins of the channel show evidence of root architecture impact, with the root acting as the base and margin line. This implies that the root system played an important role in stabilizing the bank of the channel, thereby shaping the base and margin of the channel. Root architecture impact was also shown by large cordaitalean roots bordering the base of the second sandstone channel fill in Tracing 4 (Fig. 4.10). Tree trunks T5 and T1 have roots that trace along the base of channel fill 1 bank, and provide another line of evidence of root architecture impact on channel bank stability. Roots bordering channel bases in the three localities represented in the traces are similar in the sense that the roots form a root-line. These root-lines act as a sharp boundary between the channel fill and the layer beneath it, and also take the shape of the bank margin in some, as shown in Tracing 1. Siderite coating on roots in Tracing 1 is another line of evidence for mineral impact on channel bank stability and will be discussed in the next section. The evidence noticed in Tracing 1 are only possible and true for the case study if the tree position is actually on a ridge

between the two channels, and if the tree was not drowned by a channel much deeper than is apparent in the outcrop.

Trace #	Evidence in favour	Evidence against	Comment
1	<ul style="list-style-type: none"> -Tree position on ridge -Root tracing along channel bank base. -Siderite nodules coating roots 	<ul style="list-style-type: none"> -Possibility of the channel having been deeper and drowning the tree. 	<ul style="list-style-type: none"> -Tree on ridge and root tracing on channel base suggests that root architecture influenced stability. -Siderite nodules form resistant armour against erosion.
2	<ul style="list-style-type: none"> -Barforms positioned around location of upright trees suggest that trees extended up into channel and influenced sedimentation. 	<ul style="list-style-type: none"> -Possibility of tree not extending into the channel, based on outcrop uncertainties. 	<ul style="list-style-type: none"> -Reasonable evidence that trees caused turbulence up-flow and reduced velocity down-flow, thereby reducing erosion and promoting deposition.
3	<ul style="list-style-type: none"> -Extensive vegetation/dense forestation (tree, stems, roots) adjacent to channel bodies. -Calamites between channels fills 1 and 2. 	N/A	<ul style="list-style-type: none"> -Combined effects of roots from numerous upright trees, still preserved at channel margins may have promoted the presence of narrow channel bodies, by stabilizing banks.
4	<ul style="list-style-type: none"> -Large cordaitalean roots border base of the second channel fill. -Presence of root mat on fallen cliff rocks. -Two tree trunks preserved on the bank of an associated small channel body. -Carbonate minerals (siderite and calcite) coating on roots. 	<ul style="list-style-type: none"> -Vegetation and mineral coated roots on fallen cliff boulders not <i>in situ</i>. -Possibility of rooting system of two trunks on bank being lower, within unit below. 	<ul style="list-style-type: none"> -Tracing of root-line on the base of the sandstone channel fill implies root architecture impact. -Resistant and cementing capability of siderite and calcite would have strengthened channel bank and reduced erosion. -Root mat may have protected channel bank.
5	<ul style="list-style-type: none"> -Bank vegetation prominent (T5 and T6 on left-side bank, and T1, T2 & T3 on right-side bank). -T5 and T1 root tracing along base of channel fill 1 at the bank. 	<ul style="list-style-type: none"> -Possibility of the trees being broken and dead before the channel was emplaced and buried them. -Many trees rooted in underlying peat (coal) and thus their roots would not have influenced sedimentation 	<ul style="list-style-type: none"> -Combined influence of the roots of numerous, closely spaced trees is capable of stabilizing the banks, where trees rooted at bank surfaces. -Root architectural impact as a result of root tracings. -Tree influence may have

	-Channel body ending close to position of preserved trees. -Upright trees at bank tilted towards channel, indicating resistance to bank erosion	strength at level of channel base.	resulted in channel body ending close to preserved trees.
--	--	------------------------------------	---

Table 5.1- Evidence for and against vegetation impact on channel bank stability with brief comment.

There is no clear evidence of vegetation impact on the channel stability of Tracing 2 (Fig. 4.2). The tree trunks in Tracing 2 are rooted in the mudstone beneath the channel fill and do not seem to have a direct impact on the bank. The projections of the trees into the channel probably influenced accumulation of sediment mounds in the channel, but have no impact on bank stability. The sandstone channel-body has no preserved margin on the left-hand side of the cliff, and ends in an abandoned-channel fill with no sign of preserved vegetation near its margins. The tree trunks can have indirect impact on the channel bank by causing extensive turbulence up-flow, possibly promoting erosion, and reducing velocity down-flow, thereby promoting deposition (Table 5.1). This indirect impact on flow is possible only if the tree trunk actually extended up into the channel.

Abundant roots and stems in the locality of Tracing 3 (Fig. 4.8) signify vegetation abundance. Vegetation in this locality is extensive and extends from the floodplain into the channel bank. The combined impact of the roots from the dense vegetation would probably have been capable of stabilizing the bank and reducing erosion. Presence of calamite plants between channel fill 1 and 2 on the locality of Tracing 3 suggests that the channel bodies were probably locked in on both sides by vegetation which probably stabilized the banks.

Aside from root architecture impact discussed earlier concerning Tracing 4 (Fig. 4.8), other lines of evidence include root mat impact, vegetation mass impact and carbonate mineral impact (Table 5.1). The presence of root mats (dense masses of fine roots) noticed on the fallen channel boulders below the cliff (Section 4.4.0) is another possible line of evidence of vegetation influence on channel bank stability. According to Kate and Evans (1999), dense root matting of *S.caprea* stabilizes channel banks and induces bank accretion, resulting in the formation of channel benches. Kate and Evans (1999) noted that *S.caprea* roots extend into water as a thick mat which collects sediments and forms a low shelf. There is a probability of root mats such as these occupying the bank and stretching into the channel. Such root mats may protect the channel bank, making the bank resistant to erosion. The binding power of these roots is capable of increasing bank cohesion and reducing erosion.

Evidence of two big trunks on the bank of the sandstone channel fill along the beach is an example of possible vegetation influence. Vertical and perpendicular forces acting on the trees accounted by root-shoot relationship during growth may add pressure on the bank, thereby resulting in compaction of the surface of growth, depending on the soil type. Trees can compact surface material, but may also promote collapse by putting weight on the bank. However, the negative weighting is counteracted by the increased soil cohesion due to compaction (Simon and Collinson, 2012). The idea of this process impacting on the bank stability is only possible when the gravitational force is greater than the normal force, and the soil type is fine enough with capability of resisting collapse, resulting in compaction of the bank. This process of tree weight impact is very important to ensure bank stability only when larger trees are involved. The presence of large trees on the banks noted in the previous chapter (Sections 4.4.0 and 4.5.0), with well defined margins, are good indications of vegetation mass influence on stability of the

channel banks. Horizontal root expansion during growth on the bank is capable of compressing the surrounding sediments, and thereby stabilizing the bank (Gibling, pers. comm. 2012).

Evidence of carbonate mineral impact was also noticed in the locality of Tracing 4, but will be discussed in more detail in the next section.

For Tracing 5 (Fig. 4.15 and 4.16), bank vegetation as shown by T5 and T6 on the left-side bank, and T1, T2 and T3 along the right-side bank of T4, is evidence of possible vegetation impact on channel bank stabilization. The combined impact of the trees on the channel bank may have been capable of stabilizing the channel bank. T1, T2 and T3 are close together, but there is no evidence of their root length. However, root excavation has shown evidence of lycosid roots up to 8 m long (Gibling, pers. comm. 2012). The original roots of the excavated roots would have been longer than the 8 m length in proximity to Tracing 5 locality. There is a possibility of the roots forming an interconnected network, covering most of the bank areas. Root architecture impact is witnessed by the tracing of tree roots T1 and T5 along the base of channel fill 1. The tilting of T3 towards the channel body is an indication of bank erosion resistance. In general, combined influence of the roots on the bank has the capability of providing very strong binding power on the bank, thereby increasing cohesion and strengthening the bank. Vegetation does not have influence on the bank stability in the case where the trees were broken and dead before the emergence of the channel bank resulting in drowning of the trees. But in the case where the trees were fully functional and alive during the emergence of the channel, it is possible that the trees actually played important roles in shaping the channel and stabilizing the bank. Tree influence is probably responsible for the termination of the channel body close to preserved trees, but since the trees seem to be rooted in the coal and mudstone below, there is a possibility that the roots did not have much effect on the channel banks.

5.2.0 Cementation and compaction

Results from petrographic and X-ray diffraction data obtained from roots in Tracing 4 locality show evidence of mineral impact on channel bank stability. The presence of siderite nodules at the locality of Tracing 1, and siderite and calcite cast around roots in Tracing 4, noted in the previous chapter, is possible evidence that some parts of the bank underwent lithification. Sundby et al (1998) noted that plants extract elements (Fe) from the anoxic bulk sediment and concentrate it into the oxidized microenvironment surrounding each root. This process must have accounted for the formation of some of the cast. It is not clear whether some of these casts formed early or later, but evidence of coarse calcite with floating quartz from petrographic analysis has shown possible early crystallization of calcite in parts of the root cast. The idea of the nodules influencing the strength of the sediments also depends on whether the nodules formed close to the surface. Organic remains of plants are partially preserved by precipitation of diagenetic siderite in concretions. According to Allison and Pye (1994), preservation of plant remains is favoured by the rapidity of siderite crystal growth as coatings, fillings and replacement of cell structure. The description section of Tracing 4 pointed out that the roots are *in situ* at the top of the channel body. This suggests that the nodules were originally close to the surface. However, formation of the siderite nodules on the roots close to the surface is evidence that the nodules might have influenced the strengthening of the sediment since the tree is *in situ*. Petrographic analysis shows “floating grain” textures of framework grains in cement and evidence that calcite crystallization resulted in quartz grain fragmentation. These observations collectively indicate that crystallization of calcite took place while the sediment was loosely compacted, possibly close to the surface. Such relatively early calcite crystallization in the sediments may have resulted in near-surface cementation of the sediments, resulting in bank stability.

It is possible that calcite crystallization penetrated through the pore spaces in the bank sediment, acting as general sandstone cement, increasing the strength of the bank, thereby making it resistant to erosion. There is not much information to know exactly when the calcite cement filled the sandstone or whether the calcite cement was emplaced during burial.

Siderite is present as dark coloured, heavy, iron-carbonate nodules capable of acting as erosion-resistant armour. In the study case, siderite is prominent around tree roots as nodules. The siderite nodules on the roots are secondary diagenetic minerals which formed during or after the growth of the trees. The petrographic and X-ray diffraction interpretation identifies siderite, which is commonly associated with reducing environments (Brown and Kingston, 1993). Siderite can form very early, close to the surface in some settings (Pye et al., 1990). Some of these siderite nodules are probably replacement minerals, with a possibility of the Fe-component of siderite replacing the Ca-component of calcite (Nesse, 2000). This replacement process is only a possibility, as it is rare (~15%) due to the difference in cation size. Siderite nodule existence on the banks of some of the channels (Tracing 1 and Tracing 2) is capable of stabilising the channel banks, thereby resisting erosion of the banks. Both calcite and siderite could have acted to stabilize channel banks in different ways, by strengthening the bank and resisting bank erosion. Estimation of root cast volume on the rock surface has shown that the root casts on fallen beach boulders in Tracing 4 locality occupy about 21% of the rock volume (Appendix D). This percentage shows that the root casts are abundant enough to have impacted on strengthening of the channel bank.

5.3.0 Literature on similar issues

Over the past decades, scientists have paid little attention to vegetation influence on channel body form, but recent research has created awareness of its importance, resulting in considerable present research. Much research has been focused on vegetation influence on stabilizing and shaping channel bodies, but few studies have paid attention to vegetation influence on channel bank stability.

“The ability of vegetation to stabilize a bank is dependent upon factors such as plant vigour, density, and rooting depth” (Robert, 2000, p.21). Robert (2000) noted that different vegetation forms have varying root-shoot architecture, and show both surface and underground rooting which influence the ability of vegetation to stabilize banks of streams and rivers. The surface and underground rooting pattern was also noticed in section 4.4.0 of the previous chapter. Robert also mentioned that the ability of vegetation to stabilize rivers and streams is dependent on scale - the vegetation size relative to the size of the watercourse and absolute size of vegetation.

Vegetation can stabilize river banks and at the same time result in erosion, depending on scale. “Large trees can stabilize banks along large rivers, but on smaller streams those same trees may cause acceleration of water flow, resulting in local bank erosion” (Robert, 2000, p.22). Gray and MacDonald (1989) explain the same concept by stating that the interaction of vegetation with flowing water influences bank erosion through disturbance of the flow field. Reference notes from Robert (2000) portray that channel bank resistance to lateral erosion is the dominant factor in controlling sinuosity, and this dominant factor is influenced primarily by the nature of riparian vegetation and secondarily by the silt/clay percentage in the channel bank sediment (Ebisemiju, 1994). Experiments by Smith (1976) suggest that roots are able to accumulate

rapidly and decay slowly in cool environments with aggrading river conditions where overbank deposition of silt, clay and fine sand dominate the valley fill. According to Smith (1976), rapid accumulation and slow decay of roots protects the banks from erosion. Kate and Evans (1999) noted that dense root matting of *S. Caprea* protects and stabilises channel banks.

Gibling and Davies (2012) commented on the effects of root strength in stabilization of landscape by emphasizing how roots impart tensile strength, and provide cohesive strength to the soil; this implies that vegetation promotes channel stability by increasing bank cohesion and reducing erosion. Gibling and Davies (2012) also mentioned that both woody trees and smaller plants such as grasses and shrubs can stabilize banks and reduce erosion. They also pointed out that woody debris acts as drivers of landscape evolution (Gibling and Davies, 2012), and emphasized that “parallel evolution of meandering rivers and rooted vegetation is clear evidence that vegetation stabilizes banks” (Gibling and Davies, 2012).

Fluvial analogue and numerical modeling carried out in St. Anthony Falls Laboratory in Minnesota has shown the combined impact of vegetation and clay in stabilizing landscapes by promoting island-braided and single-thread channel, as well as shifting braided planform towards an anabranching pattern (Tal and Paola, 2007). According to the experiments, bank mobility and number of active channels were reduced when the fluvial analogue modeling experiment was setup with vegetation, resulting in lower migration rates and narrower and deeper channels (Tal and Paola, 2007). Seeding of sparse alfalfa during simulated low-flow stages resulted in generation of a meandering channel that migrated and maintained its form by balancing erosion and deposition (Tal and Paola, 2007). It was also noted that island-braided style was generated by splitting of flow around stable islands with introduction of sparse alfalfa cover. Deposition of fine-grained sediments in chute channels of vegetation systems did not develop into full-scale

cutoffs, but rather they maintained the meandering style and prevented rapid destruction of channel belts (Gibling and Davies, 2012).

5.4.0 W DFA versus PDF A

There has been a reasonable amount of evidence to support the hypothesis of vegetation influence on channel stability in the Joggins Formation. This study focused on the Poorly Drained Floodplain association (PDF A) because of the presence of well preserved upright trees and channel bodies. The study yielded evidence that vegetation had an impact on channel stability. Although no attempt was made to investigate the Well Drained Floodplain Association (W DFA), it is reasonable to consider whether the vegetation impact on channel stability is the same as for the PDF A.

Past studies have shown vegetation to be abundant in some parts of the W DFA, but none has pointed out their relationship with the channel bank. Due to poor preservation of trees within the W DFA, it is difficult to determine the impact of vegetation on channel banks. Although tree preservation is poor, roots, stems and finely comminuted fragments of plants are abundant throughout the channel fills in the W DFA (Falcon-Lang, 2003; Rygel and Gibling, 2006). Abundant root compressions and dryland vegetation within meandering channel bodies in the W DFA is good evidence in consideration of vegetation impact on shaping and controlling the paleochannel system. It is possible for vegetation to have played an important role in stability of channel banks in W DFA, for which the abundance of plant fragments, roots and dryland vegetation implies an extensive vegetation cover. The presence of plant fragments in W DFA is possible evidence that vegetation may have impact on the channel bank stability.

The presence of reworked carbonate rhizoconcretions and pedogenic carbonate nodules (Rygel and Gibling, 2006) on erosion surfaces in WDFa is evidence for early cementation, which may have had a considerable impact on channel bank stability. Similar to that of PDFa, carbonate minerals have the ability to fill in pore spaces and strengthen the channel bank. There is not enough information to show the direct association of these carbonates with the roots.

The Well Drained Floodplain Association is known to be dominated by red mudstone and sandstone. As mentioned earlier in the case of PDFa, finer grained sediments have more cohesive ability, making them capable of undergoing compaction and resisting pressure. This may also have been the case for the WDFa. The combined impact from vegetation, cementation, and sediment type may have been effective in stabilizing channel banks, although the evidence is not yet conclusive.

CHAPTER 6 – Conclusions

6.1.0 Summary and Conclusions

This thesis focused mainly on investigation of vegetation influence in strengthening and stabilizing channel banks. This investigation was carried out in the Pennsylvanian Joggins Formation by analysing five parts of the Joggins fossil cliff. The analysis was done using photomosaics, supplemented by petrographic, X-ray diffraction and electron microprobe analysis. Field work and careful tracing of the photomosaics helped in identification of relevant parts of the cliff. Analytical work was used in identification of minerals and also in determination of chemical environment and reactions. So far, there have been a number of results evidencing the effects of vegetation on channel bank stability. The case study has shown numerous convincing examples and lines of evidence of vegetation impact on channel bank stability.

The discussion section has considered the effect of root architecture and root mats on channel bank stability. Evidence provided in the previous chapter generally supports the impact of vegetation roots on channel bank stability. It was also mentioned that root architecture and root mats play a big role in channel bank stability. Clues such as sub-horizontal roots acting as the base and margin line of channel banks is an evidence of root architecture effect of roots shaping and stabilizing the banks, but the overall impact of this is not known. There has also been a discussion on root mat impact on bank stability based on evidence seen in fallen cliff rocks from some of the channel bodies. Since no root mat was seen directly on the cliff, evidence from the fallen cliff rocks is not enough to prove the impact of root mats on the channel banks. Positive impacts of these root mats as pointed out in the discussion include bank protection as a

result of the mats, and ability to increase bank cohesion due to the binding power of the roots. Horizontal root thickening during growth can also result in bank stability by compaction of the surrounding sediments, thereby increasing strength. The fact that channel bodies in some of the localities end very close to trees is possible line of evidence that the trees had some impact on the strengthening and formation of the banks.

Calcite and siderite crystallization shows evidence of mineral crystallization impact on channel bank stability. These minerals both noticed as nodules and casts show varying mechanisms of stabilizing the bank. Evidence mentioned in the discussion depicts that calcite crystallization results in cementation and reduction of pore spaces in the soil, therefore strengthening the sediment. These also describe the influence of siderite on bank stability as erosion-resistant armour.

This study has been successful but brief due to time and other unfavourable factors such as weather. So far, this research has shown a body of evidence that provides reasonable support for the hypothesis that vegetation impacted bank stabilization. However, it is also suggested that vegetation is particularly effective in stabilizing channel banks where other factors (mineral cementation) has influenced the banks. This is to say that combined effect of vegetation and mineral growth (calcite and siderite) are likely to be effective in stabilizing a bank. Roots bind the sediments together, thereby strengthening and stabilizing the bank. Overall, vegetation plays a very important role in channel bank stabilization, but at the same time, vegetation can also trigger bank erosion. According to Robert (2000), large trees have the capability of stabilizing banks along large rivers, but at the same time, they can cause acceleration of water flow in smaller streams, resulting in localised bank erosion.

6.2.0 Recommendation for future work

Although this research has been successful, more research is required to effectively investigate vegetation influence on channel bank stability. This research hypothesis of vegetation impact on channel bank stability cannot be satisfactorily proven with the available results and evidence provided, but requires more in-depth study to effectively investigate the effect of vegetation on bank stability. The results of this research can be a working hypothesis for further research in the case study.

More photographs and tracings are required for the entire cliff section, for both the W DFA and P DFA. Attempts should be made to trace more photographs of representative channels with vegetation on the bank. This requires more field work for more observations on the cliff. A lot of the study in this research has been focused on P DFA, whereas there has been none on W DFA. It will be very important to focus more future studies on the W DFA to evaluate whether it supports the hypothesis of the case study.

Advanced mineral and chemical analysis is necessary for better understanding of the chemical reactions in the environment. In order to do so, geochemical data should be collected from the cliff and analysed carefully, and more advanced analytical equipment and methods are required for accuracy purpose. Although thin section, X-ray diffraction and microprobe analysis done in this research provided data on the chemistry of the environment, it is not enough to completely explain the chemistry of the Joggins Formation environment.

REFERENCES

- Allison, A.P. and Pye, K., 1994. Early diagenetic mineralization and fossil preservation in modern carbonate concretions: *Palaios*, v. 9. p. 561-575.
- Browne, G.H. and Kingston, D.M. 1993. Early diagenetic spherulitic siderites from Pennsylvanian palaeosols in the Boss Point Formation, Maritime Canada: *Sedimentology*, v. 40, p. 467-474.
- Calder, J.H., Rygel, M.C., Ryan, R.J, Falcon-Lang, H.J., and Herbert, B.L., 2005, Stratigraphy and sedimentology of early Pennsylvanian red beds at Lower Cove, Nova Scotia, Canada: the Little River Formation with redefinition of the Joggins Formation: *Atlantic Geology*, v. 41, p. 115-142.
- Calder, J.H., Gibling, M.R., Scott, A.C., Davies, S.J., and Hebert, B.L., 2006, A fossil lycopsid forest succession in the classic Joggins section of Nova Scotia: Paleocology of a disturbance-prone Pennsylvanian wetland, in Greb, S.F., and DiMichele, W.A., eds., *Wetlands Through Time: Boulder, Colorado, Geological Society of America Special Paper 399*, p. 169-194.
- Canadell, J., Jackson, R.B., Ehleringer, J.R., Mooney, H.A., Sala, O.E., and Schulze, E.-D., 1996, Maximum rooting depth of vegetation types at the global scale: *Oecologia*, v. 108, p. 583-595.
- Davies, S.J., Gibling, M.R., Rygel, M.C., Calder, J.H., and Skilliter, D.M., 2005, The Pennsylvanian Joggins Formation of Nova Scotia: sedimentological log and stratigraphic framework of the historic fossil cliffs: *Atlantic Geology*, v. 41, p. 115-142.

- Davies, N.S., and Gibling, M.R., 2010, Paleozoic vegetation and the Siluro-Devonian rise of fluvial lateral accretion sets: *Geology*, v. 38, p. 51-54.
- Davies, N.S., and Gibling, M.R., 2011, Evolution of fixed-channel alluvial plains in response to Carboniferous vegetation: *Nature Geoscience*, v. DOI: 10.1038/NGEO1237.
- DiMichele, W.A., Cecil, C.B., Montanez, I.P., and Falcon-Lang, H.J., 2010, Cyclic changes in Pennsylvanian paleoclimate and effects on floristic dynamics in tropical Pangaea: *International Journal of Coal Geology*, v. 83, p. 329-344.
- Dupuy, L., Fourcaud, T., and Stokes, A., 2005, A numerical investigation into the influence of soil type and root architecture on tree anchorage: *Plant and Soil*, v. 278, p. 119-134.
- Falcon-Lang, H., 1999, Fire ecology of a Late Carboniferous floodplain, Joggins, Nova Scotia: *Journal of the Geological Society of London*, v. 156, p. 137-148.
- Falcon-Lang, H.J., 2003, Late Carboniferous tropical dryland vegetation in an alluvial-plain setting, Joggins, Nova Scotia, Canada: *Palaios*, v. 18, p. 197-211.
- Falcon-Lang, H.J., and Bashforth, A.R., 2004, Pennsylvanian uplands were forested by giant cordaitalean trees: *Geology*, v. 32, p. 417-420.
- Falcon-Lang, H.J., and Bashforth, A.R., 2005, Morphology, anatomy, and upland ecology of large cordaitalean trees from the Middle Pennsylvanian of Newfoundland: *Review of Palaeobotany and Palynology*, v. 135, p. 223-243.
- Falcon-Lang, H.J., and Scott, A.C., 2000, Upland ecology of some Late Carboniferous cordaitalean trees from Nova Scotia and England: *Palaeogeography, Palaeoclimatology, Palaeoecology*, v. 156, p. 225-242.

Falcon-Lang, H.J., Rygel, M.C., Gibling, M.R., and Calder, J.H., 2004, An Early Pennsylvanian waterhole deposit and its fossil biota in a dryland alluvial plain setting, Joggins, Nova Scotia: *Journal of the Geological Society of London*, v. 161, p. 209-222.

Gibling, M.R., 2000, Fluid evolution and diagenesis of Carboniferous channel sandstone in Prince Colliery, Nova Scotia, Canada: *Bulletin of Canadian Petroleum Geology*, v. 48, p. 102-109.

Gibling, M.R. and Davies, N.S., 2012, Palaeozoic landscape shaped by plant evolution, *Natural Geoscience*, doi: 10. 1038/NGEO 1376.

Hales, T.C., Ford, C.R., Hwang, T., Vose, J.M., and Band, L.E., 2009, Topographic and ecologic controls on root reinforcement: *Journal of Geophysical Research*, v. 114, p. F03013. doi: 10.1029/2008JF001168.

Harwood, K., and Brown, A.G., 1993, Changing in-channel and overbank flood velocity distributions and the morphology of forested multiple channel (anastomosing) systems: *Earth Surface Processes and Landforms*, v. 18, p. 741-748.

McCarthy, T.S., Ellery, W.N., and Stanistreet, I.G., 1992, Avulsion mechanisms on the Okovango fan, Botswana: the control of a fluvial system by vegetation: *Sedimentology*, v. 39, p. 779-795.

Nesse, W. D. 2000, Introduction to X-ray crystallography, in Nesse W.D, *Introduction to Mineralogy*. Oxford Printing Press, New York, p. 160-168.

- Pye, K., Dickson, A.D., Schiavon, N., Coleman, M.L., and Cox., 1990. Formation of siderite-Mg-calcite-iron sulphide concretions in intertidal marsh and sandflat sediments, north Norfolk, England: *Sedimentology*, v. 37, p. 325-343.
- Rowntree, K.M. and Dollar, E.S.J. 1999, Vegetation controls on channel stability in the Bell River, Eastern Cape, South Africa. *Earth Surface Processes and Landforms*, 24 (2). p. 127-134.
- Robert, A.O., 2000, Factors affecting stream bank and river bank stability, with emphasis on vegetation influences: Region III Forest Practices Riparian Management Committee: Bank Stability. Alaska, p. 21-40.
- Rygel, M.C., and Gibling, M.R., 2006, Natural geomorphic variability recorded in a high-accommodation setting: fluvial architecture of the Pennsylvanian Joggins Formation of Atlantic Canada: *Journal of Sedimentary Research*, v. 76, p. 1230-1251.
- Rygel, M.C., Gibling, M.R., and Calder, J.H., 2004, Vegetation-induced sedimentary structures from fossil forests in the Pennsylvanian Joggins Formation, Nova Scotia: *Sedimentology*, v. 51, p. 531-552.
- Simon, A., and Collinson, A.J.C., 2002, Quantifying the mechanical and hydrologic effects of riparian vegetation on streambank stability. *Earth Surface Processes and Landforms*, v. 27, p. 527-546.
- Sundby, B., Vale, C., Cacador, I., Catarino, F., Madureira, M., and Caetano, M., 1998, Metal-rich concretions on the root of salt marsh plants: Mechanism and rate of formation, 43 (2). p. 245-252.

Tal, M., and Paola, C., 2007, Dynamic single-thread channels maintained by the interaction of flow and vegetation: *Geology*, v. 35, p. 347-350.

Tooth, S., and Nanson, G.C., 2000, The role of vegetation in the formation of anabranching channels in an ephemeral river, Northern plains, arid central Australia: *Hydrological Processes*, v. 14, p. 3099-3117.

Tooth, S., Jansen, J.D., Nanson, G.C., Coulthard, T.J., and Pietsch, T., 2008, Riparian vegetation and the late Holocene development of an anabranching river: Magela Creek, northern Australia: *Geological Society of America Bulletin*, v. 120, p. 1021-1035.

APPENDIX A - PHOTOGRAPHS



A: Parallel roots on fallen cliff boulders on cliff front of Trace 4 locality.



B: More parallel roots on fallen cliff boulders on cliff front of Trace 4 locality



C: Mineral casted roots on fallen cliff boulders on cliff front of Trace 4 locality.



D: Closer view of one of the mineral casted roots.



E: Big tree trunk on the bank of a small channel on the beach of Trace 4 locality, with the red arrow showing the original position of the tree trunk.



F: Tree trunk hidden between rocks representing the same beach bank of Trace 4 locality.

APPENDIX B – PETROGRAPHIC DATA

Thin Section: X

Rock Name: Siltstone

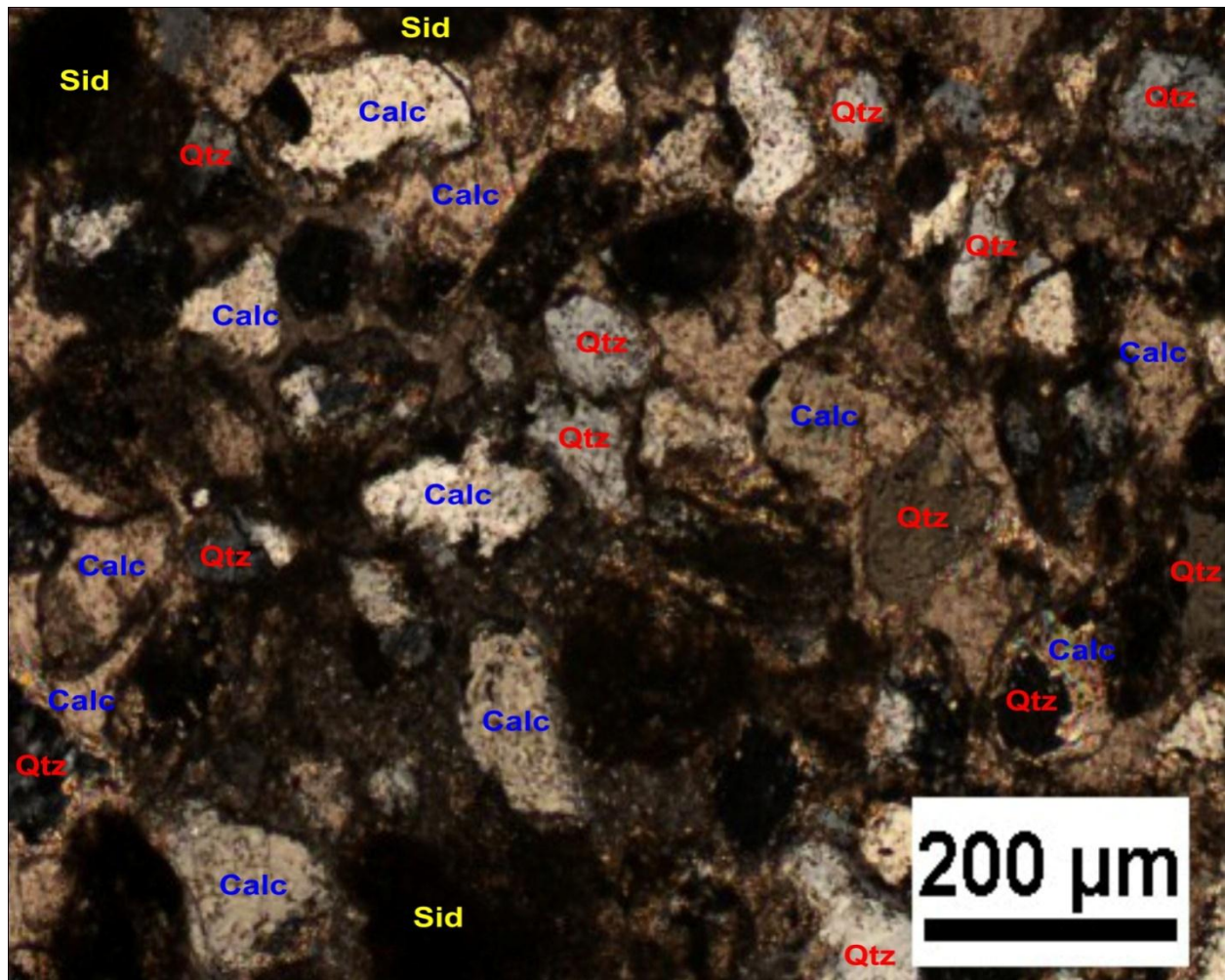
Locality: Joggins Fossil Cliff

Mineralogy

Mineral name	Shape	Color	Abundance
Quartz (Qtz)	Angular to subangular	Colorless	~ 35%
Siderite (Sid)	Oolitic to subrounded And irregular	Pale-yellowish brown to rusty brown	~ 30%
Calcite (Calc)	Fibrous, needle-like and tabular	Colorless	~ 20%
Kaolinite (Kao)	Angular to subangular	Grey	~15%

Texture

- Very fine grained.
- Siderite crystals are localized along the edges of the sample, and also on the margins of fractures.
- Cracks occupied by kaolinite, quartz, calcite, and siderite.
- Oolitic-spherulitic texture in siderite

Thin Section-X Image

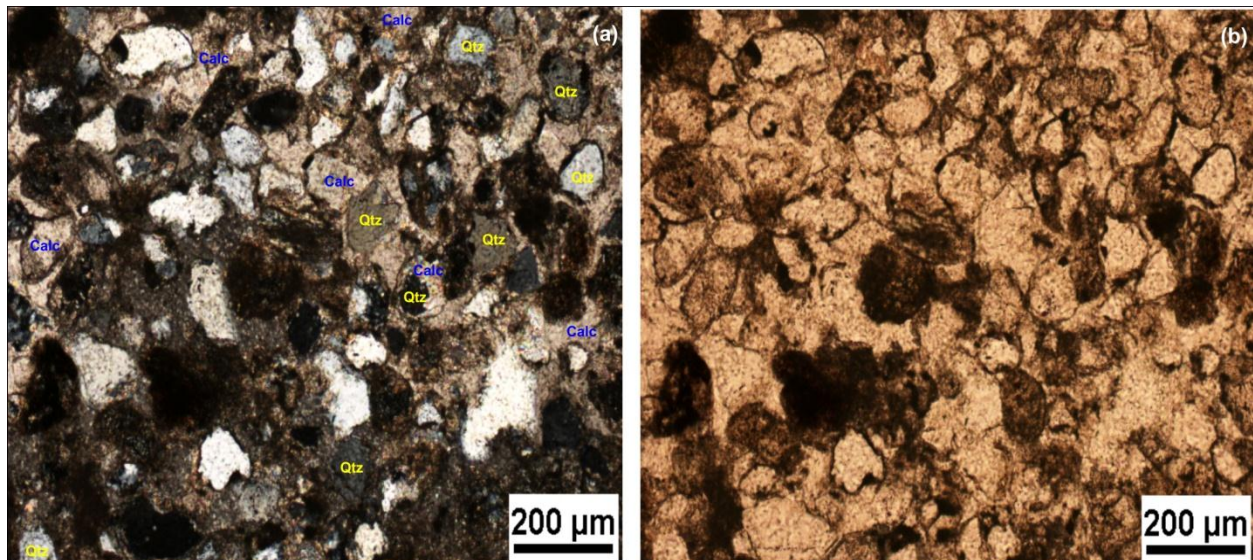
Cross polar representation of thin section X, showing the various mineral and their shapes.

Thin Section: Y**Rock Name:** Sandstone with carbonate cement**Locality:** Joggins Fossil Cliff**Mineralogy**

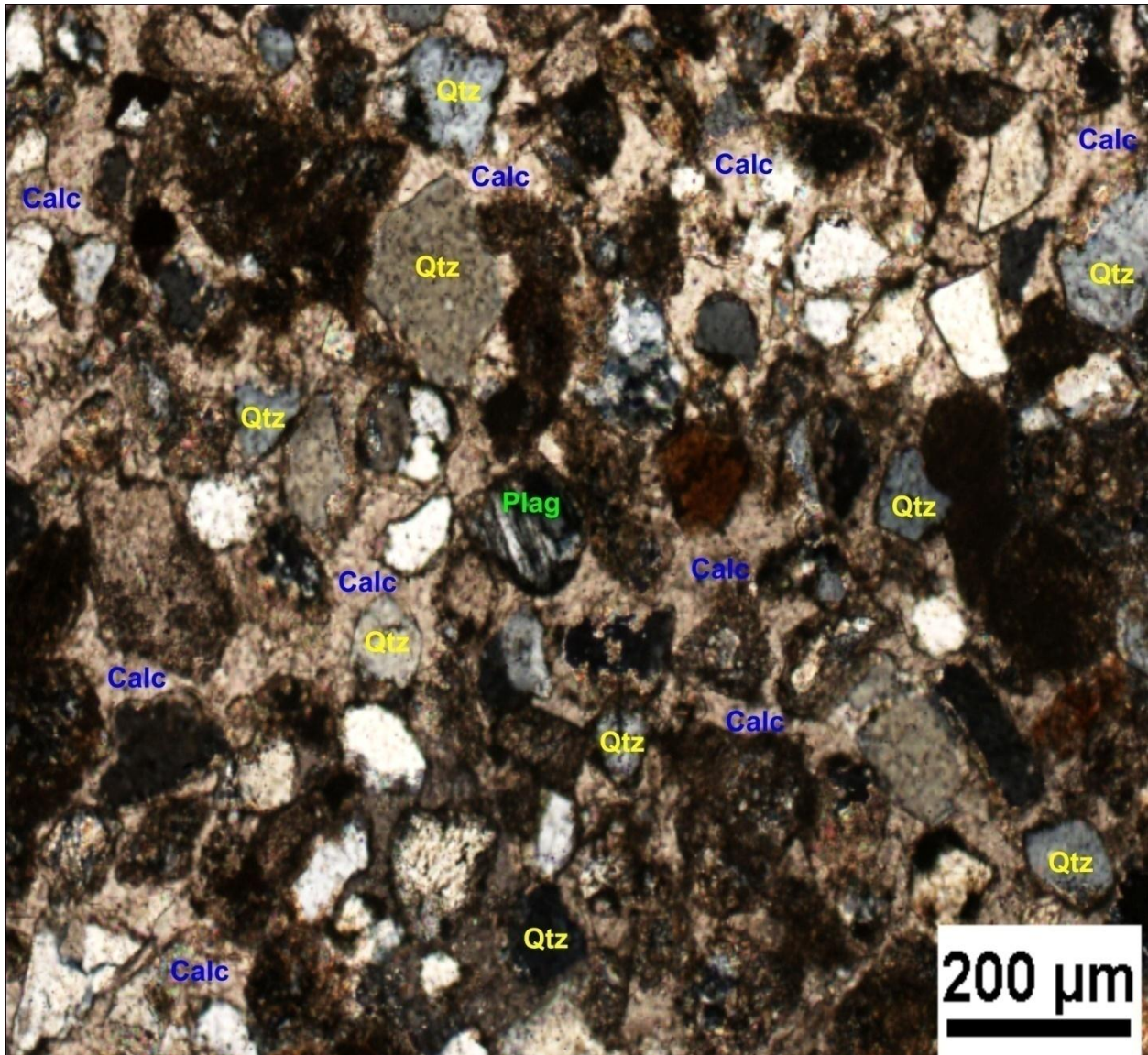
Mineral name	Shape	Color	Abundance
Quartz (Qtz)	Angular to subrounded	Colorless	~ 43%
Calcite (Calc)	Tabular to irregular	Colorless	~ 55%
Plagioclase (Plag)	Subangular, subrounded and tabular	Colorless	~ 2%

Texture

- Fine grained at the centre of the sample and medium grained along the edge.
- Well defined twin lamellae in plagioclase and calcite.
- Calcite cement.

Thin Section-Y Image

Various minerals present in thin section Y represented in cross polarized light (left) and plane polarised light (right).



Closer view of minerals present in thin section X, represented in cross polarised light with matrix dominantly calcite cement.

Thin Section: Z

Rock Name: Siltstone

Locality: Joggins Fossil Cliff

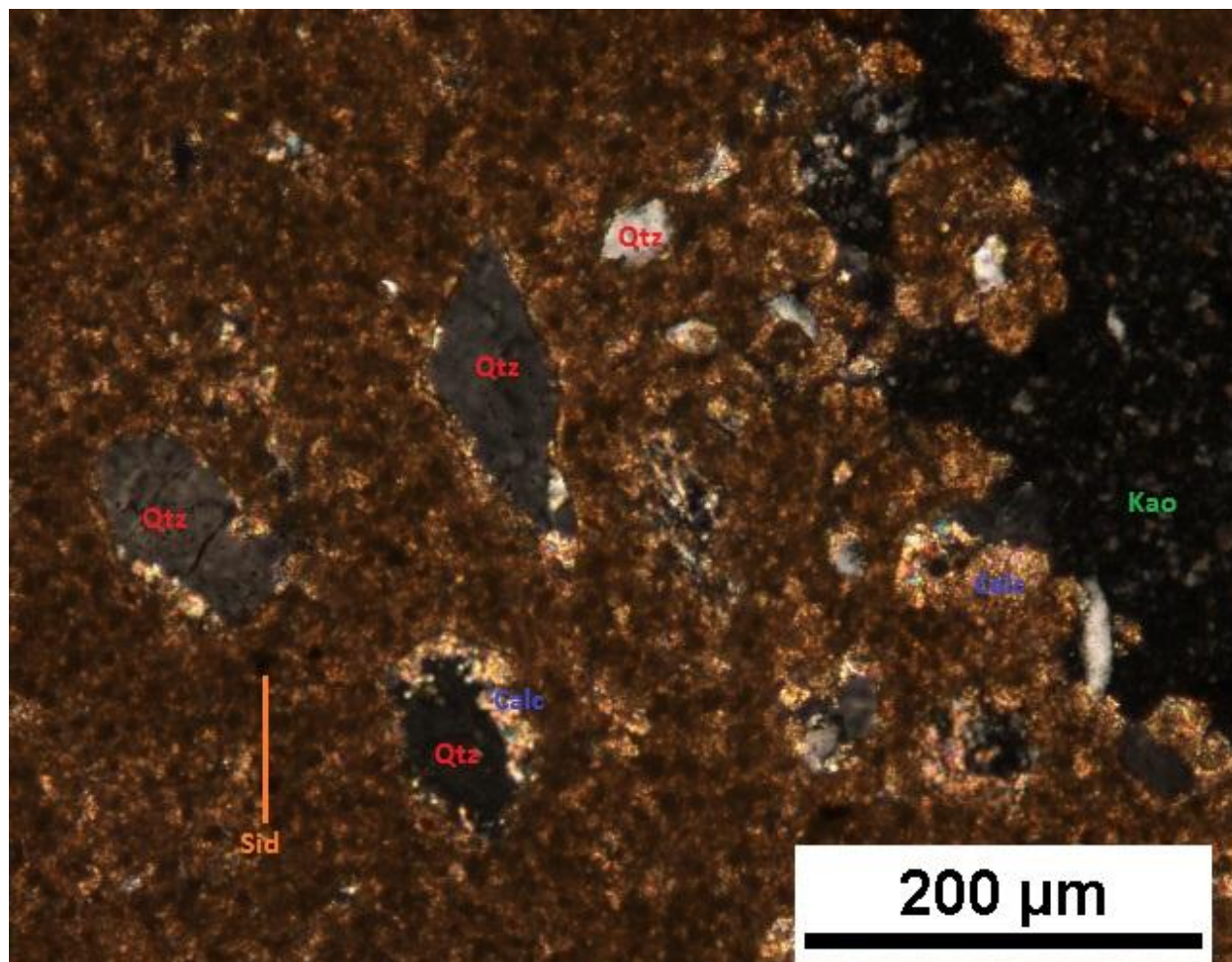
Mineralogy

Mineral name	Shape	Color	Abundance
Quartz (Qtz)	Angular to subangular	Colorless	~30%
Siderite (Sid)	Oolitic to subrounded and irregular	pale-yellowish brown to rusty brown	~35%
Calcite (Calc)	Tabular and needle-like	Colorless	~20%
Kaolinite (Kao)	Angular to subangular	Grey	~15%

Texture

- Very fine grained
- Calcite show poikilotopic texture; hosting smaller grains of calcite and quartz
- Cracks occupied by quartz and kaolinite crystals.
- Siderite crystals are localized along the edge and margin of the sample.
- Oolitic-spherulitic texture in siderite.

Thin Section-Z Image



Cross polarised representation of thin section Z, showing the various minerals present in the sample.

APPENDIX C – XRD CHARTS

Measurement Parameters:

Sample Name X;Y;Z
 Measurement Date / Time 12/2/2011 12:42:58 PM; 12/2/2011 2:01:39 PM; 12/7/2011
 12:31:06 PM
 Start Position [$^{\circ}$ Th.] 5.0000
 End Position [$^{\circ}$ Th.] 85.0000
 Step Size [$^{\circ}$ Th.] 0.0200
 Scan Step Time [s] 1.0000
 Scan Type Pre-set time
 Divergence Slit Type Fixed
 Divergence Slit Size [$^{\circ}$] 1.0329
 Specimen Length [mm] 10.00
 Receiving Slit Size [mm] 0.1000
 Measurement Temperature [$^{\circ}$ C] 25.00
 Anode Material Cu
 K-Alpha1 [\AA] 1.54060
 K-Alpha2 [\AA] 1.54443
 K-Beta [\AA] 1.39225

Peak List X:

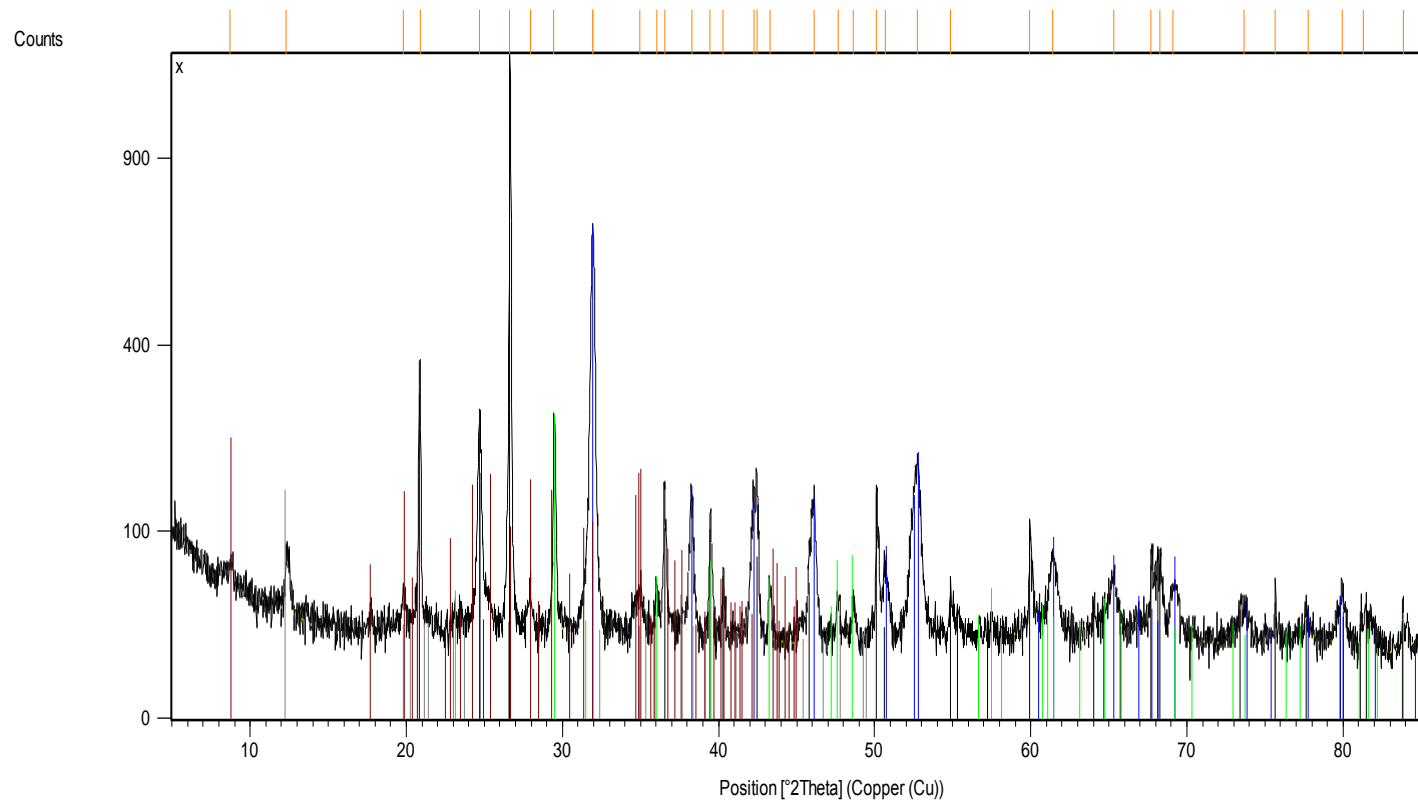
Pos. [$^{\circ}$ Th.]	Height [cts]	d-spacing [\AA]	Rel. Int. [%]
8.7053	16.42	10.15795	1.32
12.2924	32.83	7.20056	2.65
19.8311	19.32	4.47708	1.56
20.8661	349.36	4.25728	28.19
24.6817	248.71	3.60711	20.07
26.6326	1239.37	3.34714	100.00
27.9456	30.30	3.19280	2.44
29.4600	242.96	3.03203	19.60
31.9246	661.04	2.80104	53.34
32.0262	551.90	2.79932	44.53
34.9557	24.51	2.56478	1.98
36.0321	28.64	2.49059	2.31
36.5301	129.42	2.45777	10.44
38.2617	119.77	2.35043	9.66
39.4683	104.82	2.28131	8.46
40.3017	44.20	2.23604	3.57
42.2450	124.84	2.13756	10.07
42.4888	116.60	2.12586	9.41
43.2975	30.44	2.08801	2.46
46.1296	137.42	1.96619	11.09
47.6496	18.16	1.90696	1.46
48.6431	20.85	1.87031	1.68
50.1306	127.98	1.81824	10.33

50.6563	45.88	1.80060	3.70
52.7588	167.86	1.73369	13.54
54.8531	30.00	1.67234	2.42
59.9528	79.78	1.54170	6.44
61.4087	52.44	1.50859	4.23
65.2934	36.15	1.42791	2.92
67.7187	61.66	1.38255	4.97
68.2736	45.00	1.37266	3.63
69.0839	28.16	1.35853	2.27
73.6362	16.89	1.28538	1.36
75.6591	37.83	1.25596	3.05
77.7482	8.38	1.22735	0.68
79.9492	32.11	1.19901	2.59
81.3049	9.94	1.18240	0.80
83.8347	26.92	1.15304	2.17

Identified Phases:

Ref. Code	Score	Compound Name	Chemical Formula
01-070-3755	70	Quartz	Si O ₂
01-083-1764	62	Siderite	Fe (C O ₃)
00-047-1743	26	Calcite	Ca C O ₃
00-058-2028	15	Kaolinite-1A	Al ₂ Si ₂ O ₅ (O H) ₄
00-034-0175	7	Muscovite-2M2	(K , Na) Al ₂ (Si , Al) ₄ O ₁₀ (O H) ₂

Mineral	Window (degrees 2θ)	Peak Height	Peak Width	Peak Area	Intensity Factor	Area x I.F	Abundance (%)
Quartz	26.6326	7.4	0.05	0.185	1.00	0.185	18.8
Siderite	32.0262	4.8	0.1	0.24	1.15	0.276	28.1
Calcite	29.4600	2.75	0.1	0.1375	1.65	0.227	23.1
Kaolinite	12.2924	0.9	0.1	0.045	2.25	0.101	10.3
Mica	19.8311	0.65	0.1	0.0325	6.00	0.195	19.8
				Total		0.984	



Peak List
01-070-3755
01-083-1764
00-047-1743
00-058-2028
00-034-0175

Peak List Y:

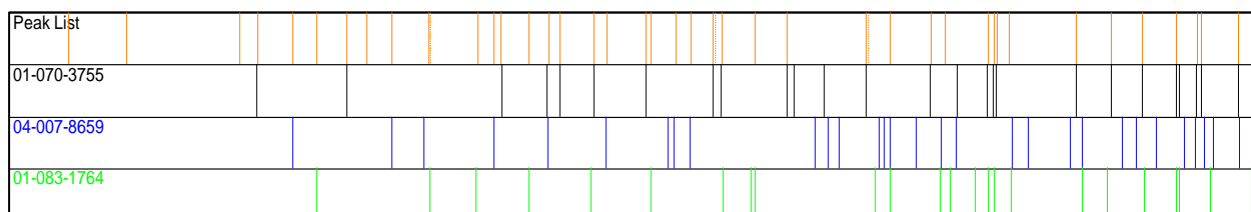
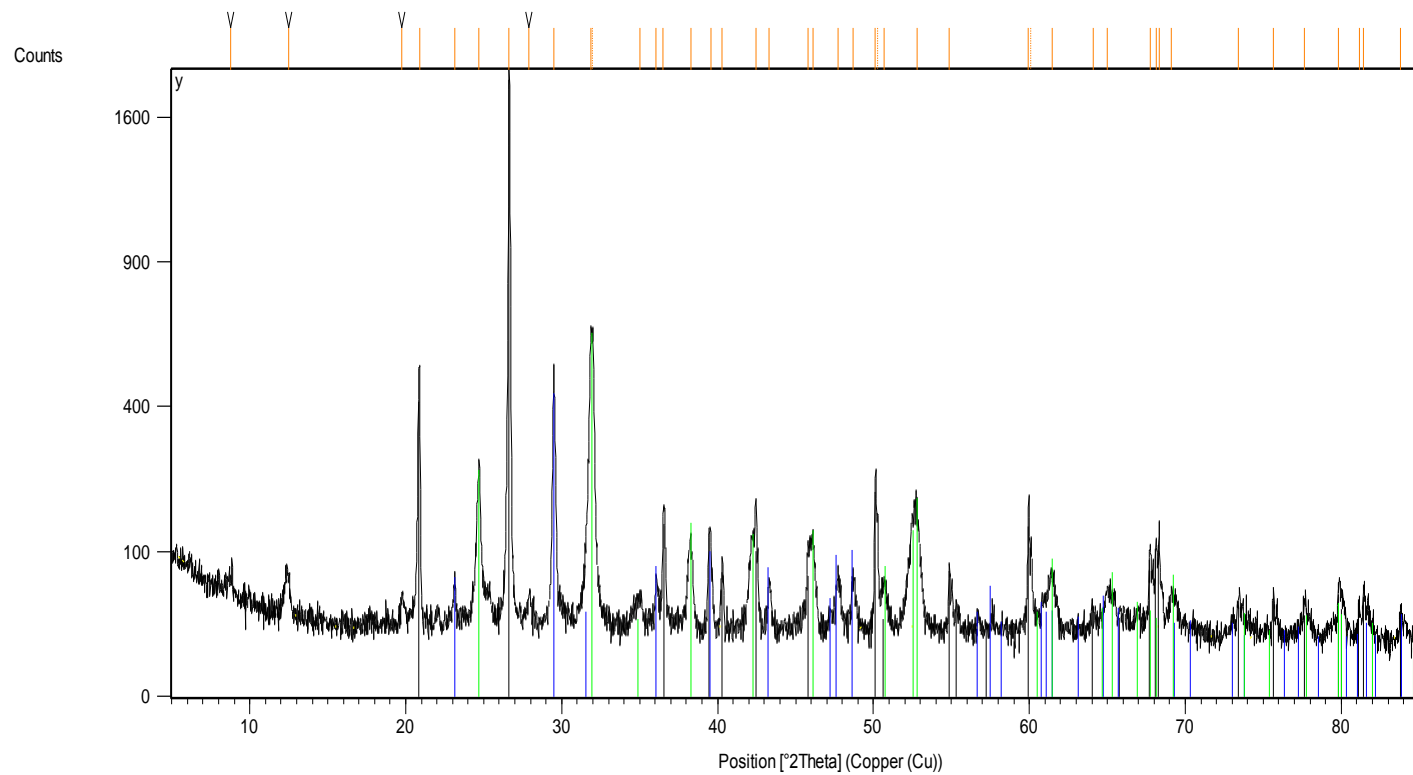
Pos. [$^{\circ}$ 2 θ .]	Height [cts]	d-spacing [\AA]	Rel. Int. [%]
8.7855	19.25	10.06537	1.03
12.4733	34.11	7.09659	1.83
19.7747	22.39	4.48973	1.20
20.8679	495.38	4.25692	26.59
23.1527	38.23	3.84175	2.05
24.6986	241.83	3.60468	12.98
26.6385	1862.98	3.34642	100.00
27.9051	21.02	3.19734	1.13
29.4812	425.41	3.02989	22.83
31.8874	610.79	2.80422	32.79
32.0218	564.43	2.79970	30.30
35.0240	17.99	2.55994	0.97
36.0672	39.29	2.48825	2.11
36.5217	135.31	2.45832	7.26
38.3096	84.85	2.34760	4.55
39.5594	104.20	2.27627	5.59
40.2830	72.58	2.23703	3.90
42.4483	165.74	2.12779	8.90
43.3204	40.07	2.08696	2.15
45.7938	86.05	1.97982	4.62
46.1174	90.67	1.96669	4.87
47.6953	46.52	1.90524	2.50
48.6829	42.57	1.86887	2.28
50.1102	190.50	1.81893	10.23
50.2658	136.06	1.81817	7.30
50.7034	38.46	1.79903	2.06
52.7784	149.58	1.73309	8.03
54.8766	63.58	1.67168	3.41
59.9491	156.10	1.54179	8.38
60.1223	95.95	1.54158	5.15
61.4307	47.50	1.50810	2.55
64.0920	10.94	1.45175	0.59
64.9859	30.50	1.43393	1.64
67.7491	84.29	1.38201	4.52
68.1338	88.00	1.37514	4.72
68.3209	123.40	1.37183	6.62
69.1322	29.73	1.35770	1.60
73.4235	31.70	1.28858	1.70
75.6287	31.35	1.25639	1.68
77.6590	23.61	1.22854	1.27
79.8505	46.00	1.20024	2.47
81.1669	22.66	1.18406	1.22
81.4527	39.80	1.18063	2.14

83.8219	18.55	1.15319	1.00
---------	-------	---------	------

Identified Phases:

Ref. Code	Score	Compound Name	Chemical Formula
01-070-3755	77	Quartz	Si O ₂
04-007-8659	37	Calcite, syn	Ca (C O ₃)
01-083-1764	53	Siderite	Fe (C O ₃)

Mineral	Window (degrees 2θ)	Peak Height	Peak Width	Peak Area	Intensity Factor	Area x I.F	Abundance (%)
Quartz	26.6385	7.15	0.05	1.7875	1.00	1.7875	81.4
Calcite	29.4812	2.8	0.09	0.126	1.65	0.2079	9.46
Siderite	31.8874	3.5	0.1	0.175	1.15	0.2013	9.16
Total						2.1967	



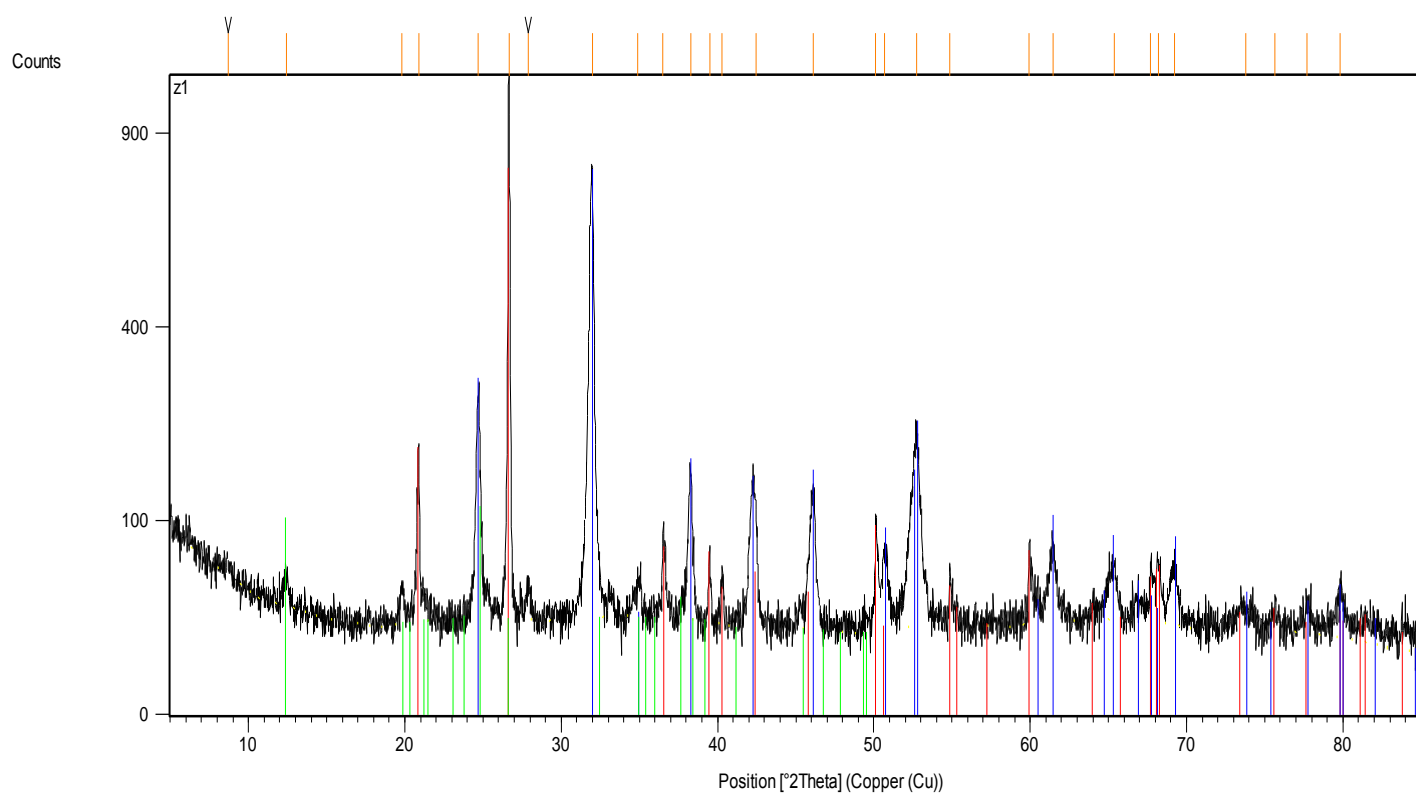
Peak List Z:

Pos. [$^{\circ}$ 2 θ .]	Height [cts]	d-spacing [\AA]	Rel. Int. [%]
8.6920	8.96	10.17349	0.83
12.4258	19.61	7.12359	1.82
19.8195	21.53	4.47968	2.00
20.8846	168.17	4.25355	15.62
24.7073	254.50	3.60343	23.64
26.6520	1076.66	3.34475	100.00
27.9142	22.29	3.19632	2.07
31.9907	754.98	2.79771	70.12
34.8914	20.67	2.57149	1.92
36.5241	64.22	2.46020	5.96
38.3229	128.12	2.34876	11.90
39.4880	40.28	2.28211	3.74
40.3058	31.15	2.23767	2.89
42.4720	83.14	2.12842	7.72
46.1440	109.25	1.96724	10.15
50.1304	86.50	1.81975	8.03
50.7061	47.28	1.80043	4.39
52.7410	191.51	1.73566	17.79
54.8495	38.30	1.67383	3.56
59.9262	49.20	1.54360	4.57
61.4462	58.58	1.50901	5.44
65.3713	34.03	1.42758	3.16
67.7183	39.60	1.38371	3.68
68.2166	35.03	1.37481	3.25
69.2375	34.05	1.35701	3.16
73.7841	11.17	1.28423	1.04
75.6442	11.63	1.25721	1.08
77.7020	11.98	1.22898	1.11
79.8376	24.56	1.20040	2.28

Identified Phases:

Ref. Code	Score	Compound Name	Chemical Formula
01-070-3755	67	Quartz	Si O ₂
01-083-1764	63	Siderite	Fe (C O ₃)
00-058-2028	12	Kaolinite-1A	Al ₂ Si ₂ O ₅ (O H) ₄

Mineral	Window (degrees 2θ)	Peak Height	Peak Width	Peak Area	Intensity Factor	Area x I.F	Abundance (%)
Quartz	26.6520	7.4	0.05	0.185	1.00	0.185	31.9
Siderite	31.9907	5.8	0.1	0.29	1.15	0.3335	57.5
Kaolinite	12.4258	0.55	0.1	0.0275	2.25	0.0619	10.7
Total						0.5804	

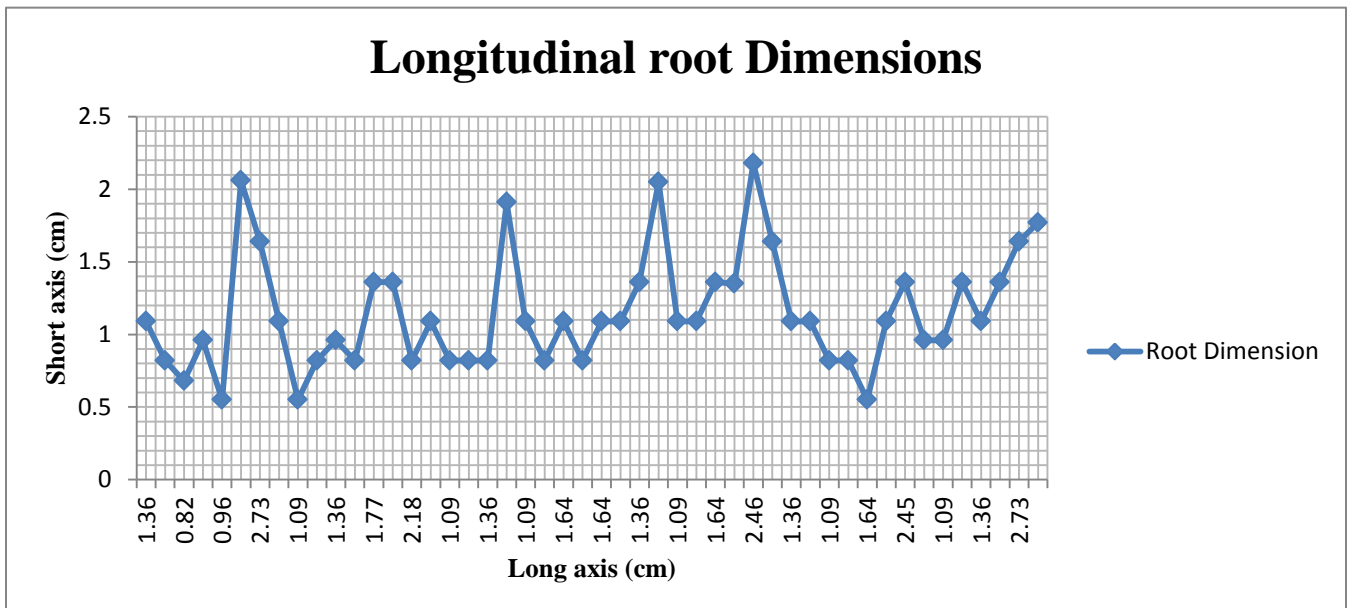
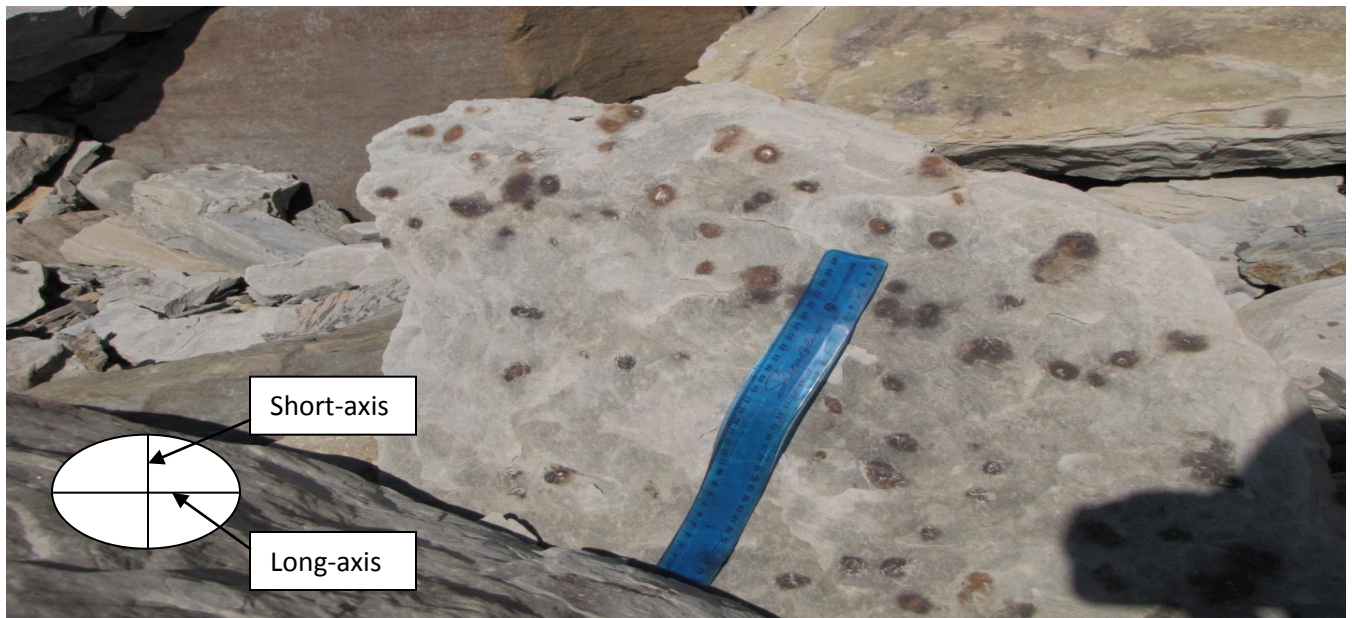


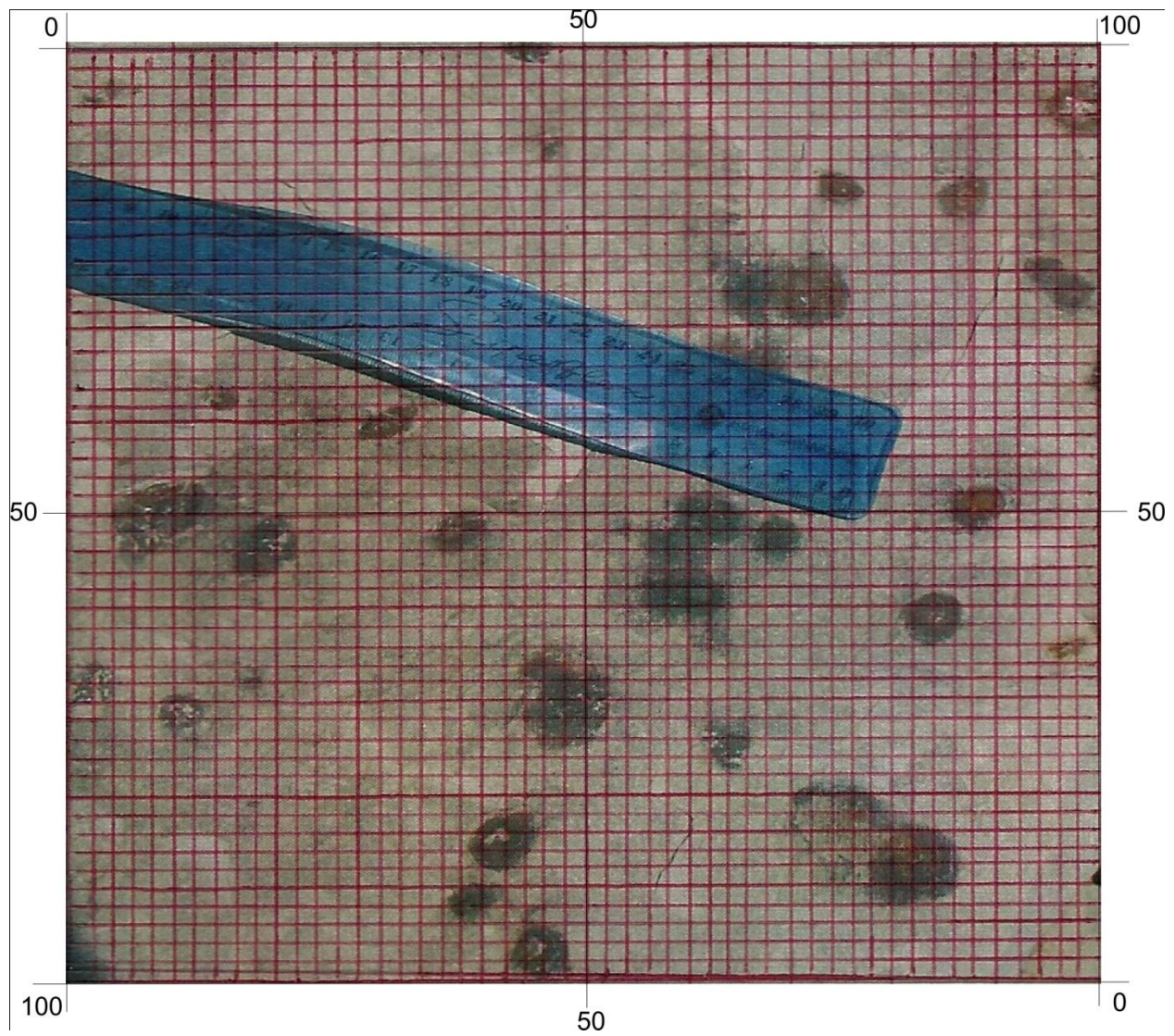
Peak List
01-070-3755
01-083-1764
00-058-2028

**APPENDIX D - LONGITUDINAL ROOT DIMENSION AND AREA ESTIMATION
DATA**

Root dimension	
long-axis (cm)	short-axis (cm)
1.36	1.09
1.64	0.82
0.82	0.68
1.09	0.96
0.96	0.55
2.18	2.06
2.73	1.64
1.77	1.09
1.09	0.55
0.82	0.82
1.36	0.96
0.82	0.82
1.77	1.36
1.36	1.36
2.18	0.82
1.36	1.09
1.09	0.82
0.82	0.82
1.36	0.82
2.05	1.91
1.09	1.09
1.36	0.82
1.64	1.09
1.09	0.82
1.64	1.09
1.36	1.09
1.36	1.36
2.18	2.05
1.09	1.09
1.09	1.09
1.64	1.36
2.06	1.35
2.46	2.18
2.18	1.64
1.36	1.09

1.64	1.09
1.09	0.82
1.5	0.82
1.64	0.55
1.77	1.09
2.45	1.36
0.96	0.96
1.09	0.96
2.18	1.36
1.36	1.09
2.45	1.36
2.73	1.64
2.05	1.77



Estimate of root area

Total vertical intersection = 100

Total horizontal intersection = 100

Total intersections = $100 * 100 = 1000$

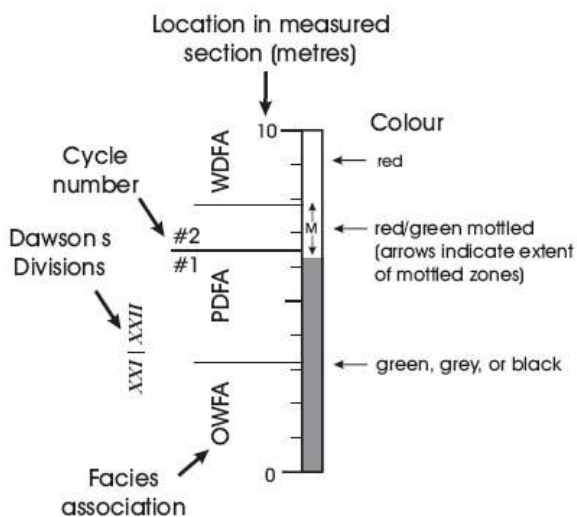
Total root intersections = 200

Percentage volume covered by root = $(210/1000) * 100$

= 21 %

APPENDIX E – TRACE LOCATION ON STRATIGRAPHIC LOG

EXPLANATION OF SEDIMENTOLOGICAL LOG



TIDAL FLAT OUTCROPS

- CB # = channel body
- SBS # = sharp-based sandstone
- SS # = sheet sandstone
- LS # = limestone

indicates meterage at top of the bed (to the nearest metre)

FACIES ASSOCIATIONS







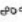


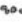



- OWFA = open-water facies association
- PDFA = poorly drained facies association
- W DFA = well drained facies association

ORGANIC HORIZONS












- ← LS = limestone
- ← Coal (Logan # if applicable)
- ← CS = carbonaceous shale
- ← OR = organic-rich horizon

SYMBOLS USED IN SEDIMENTOLOGICAL LOG









SEDIMENTARY FEATURES

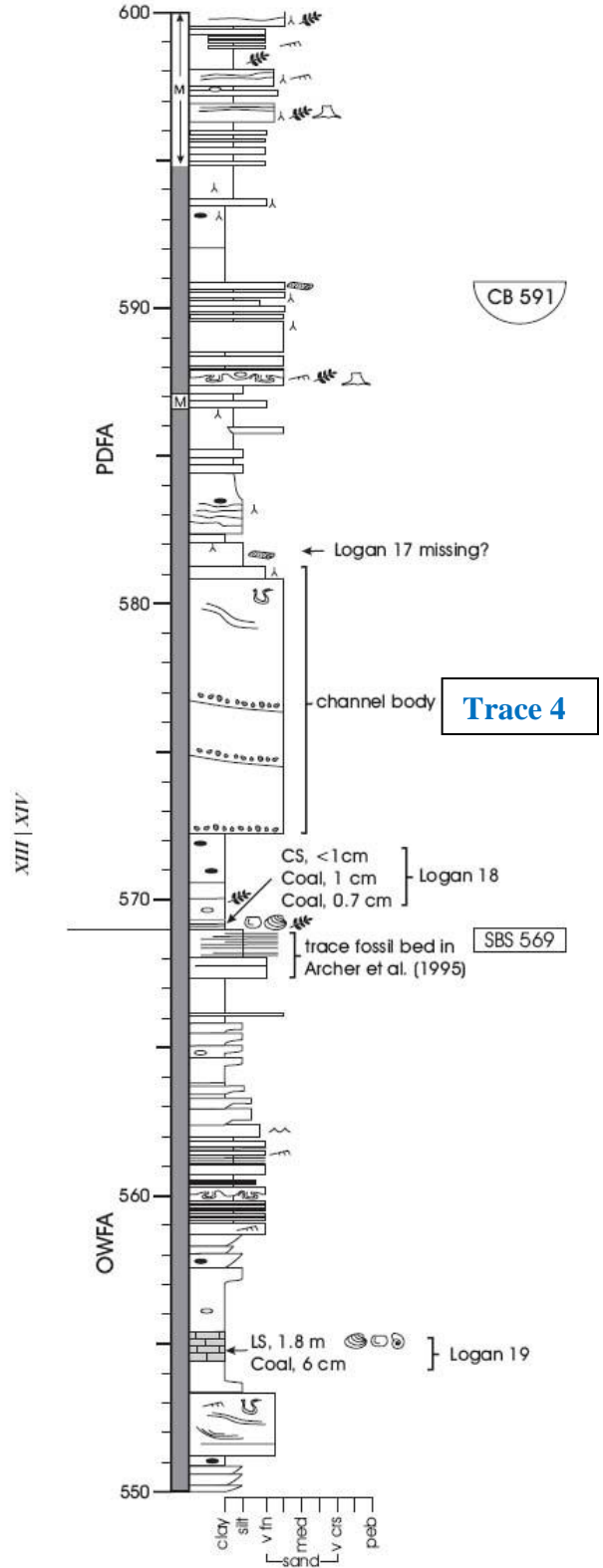
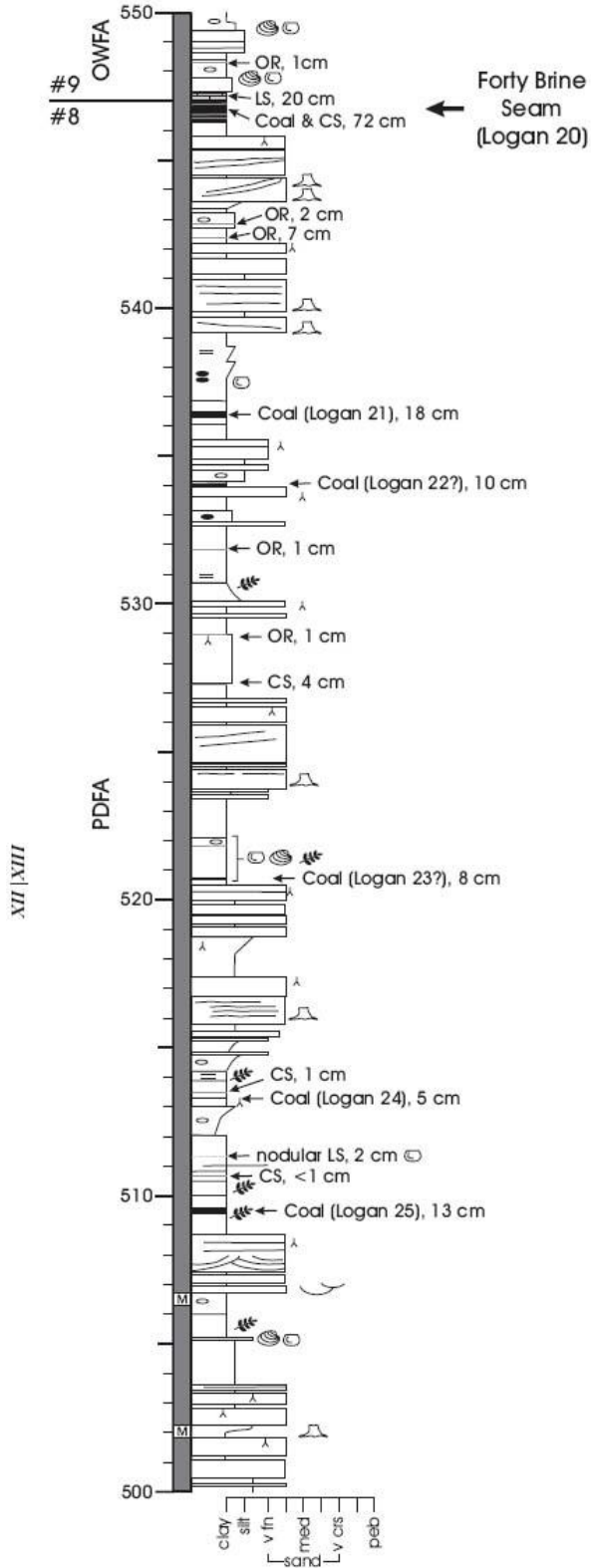
 concretion or nodule (calcareous)	 wave ripple	 horizontal lamination
 concretion or nodule (non-calcareous)	 ripple cross-lamination	 groove cast or tool mark
 calcareous rip-up clast	 trough cross-bedding	 pedogenic slickenside
 mud-chip rip-up clast	 planar cross-bedding	 convolute bedding
 climbing ripple cross-lamination		

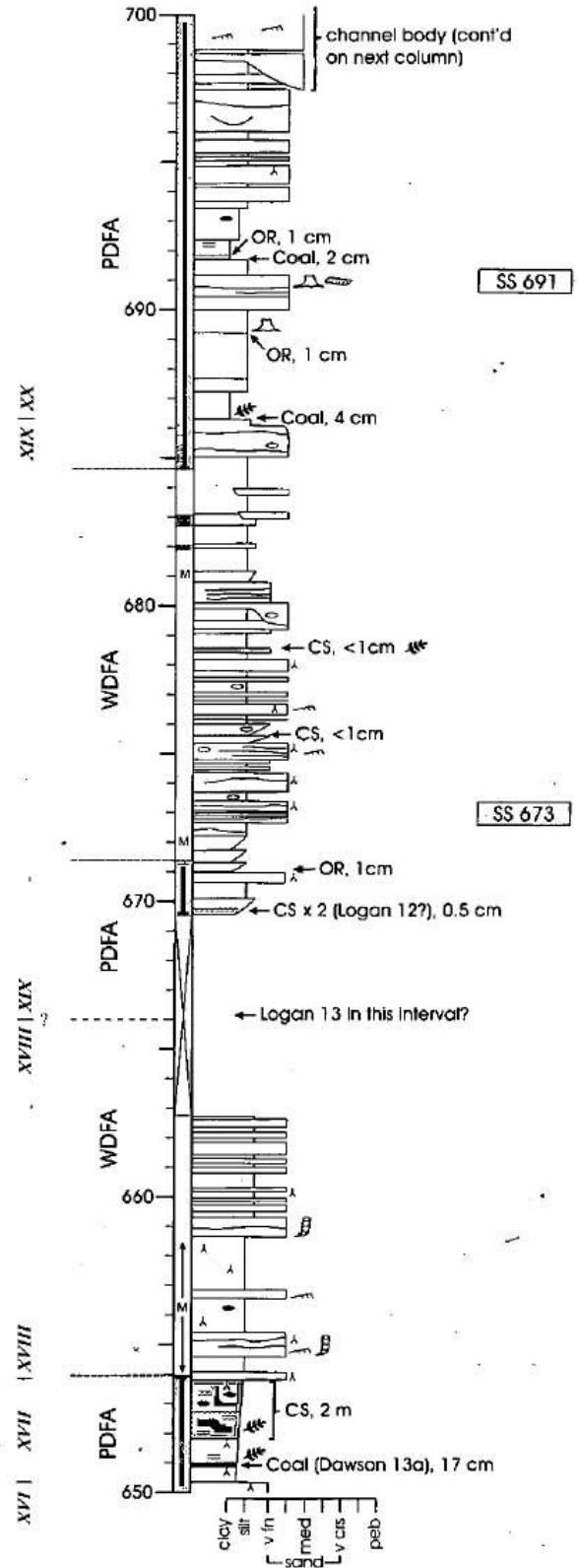
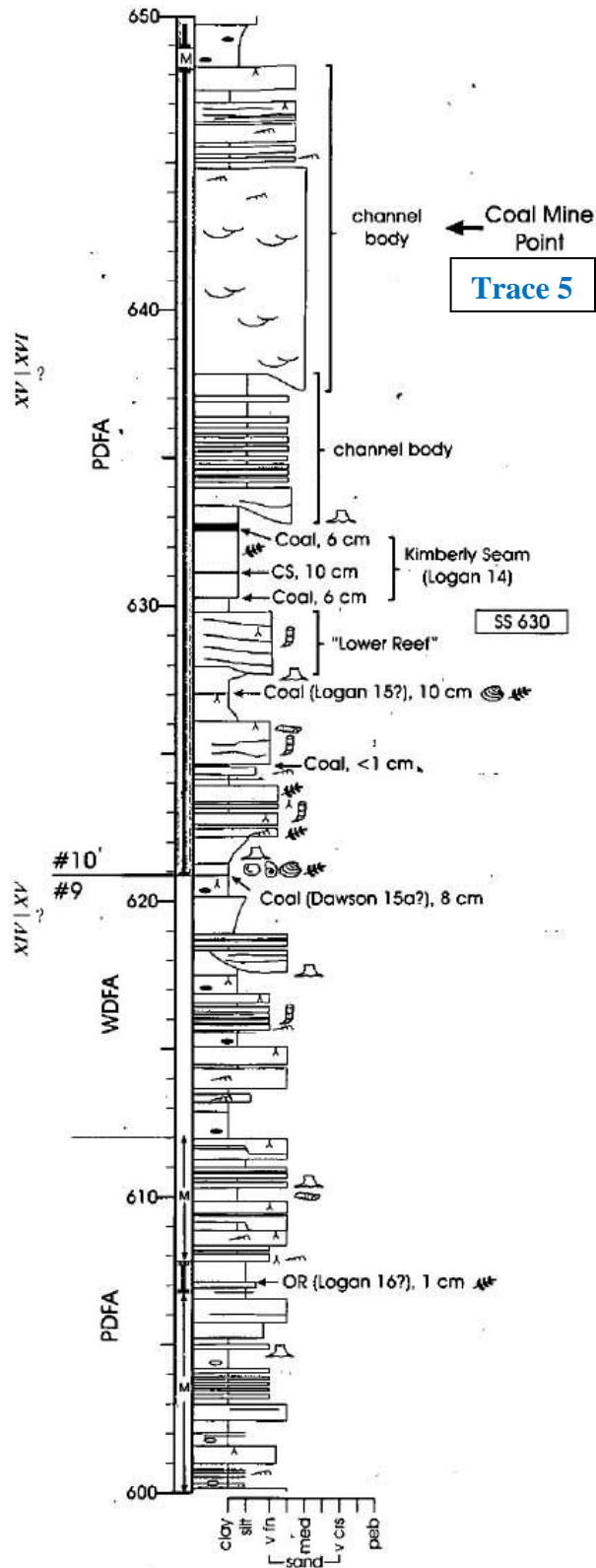
FLORA

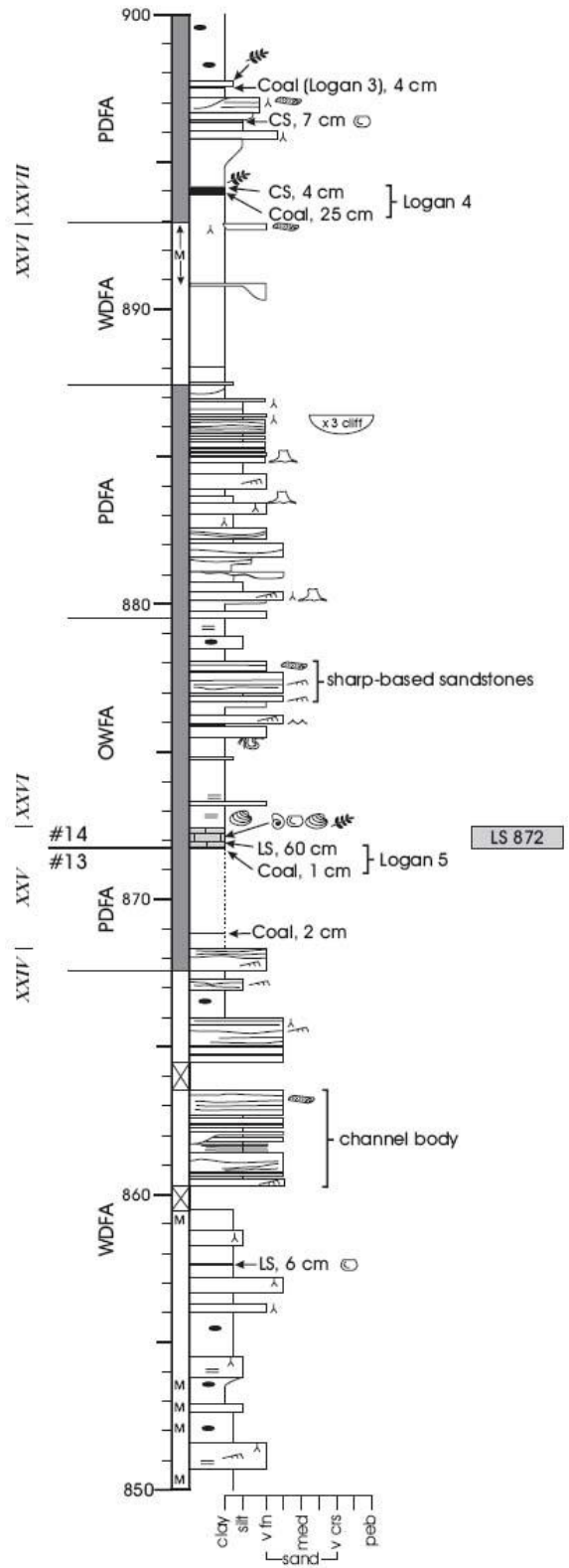
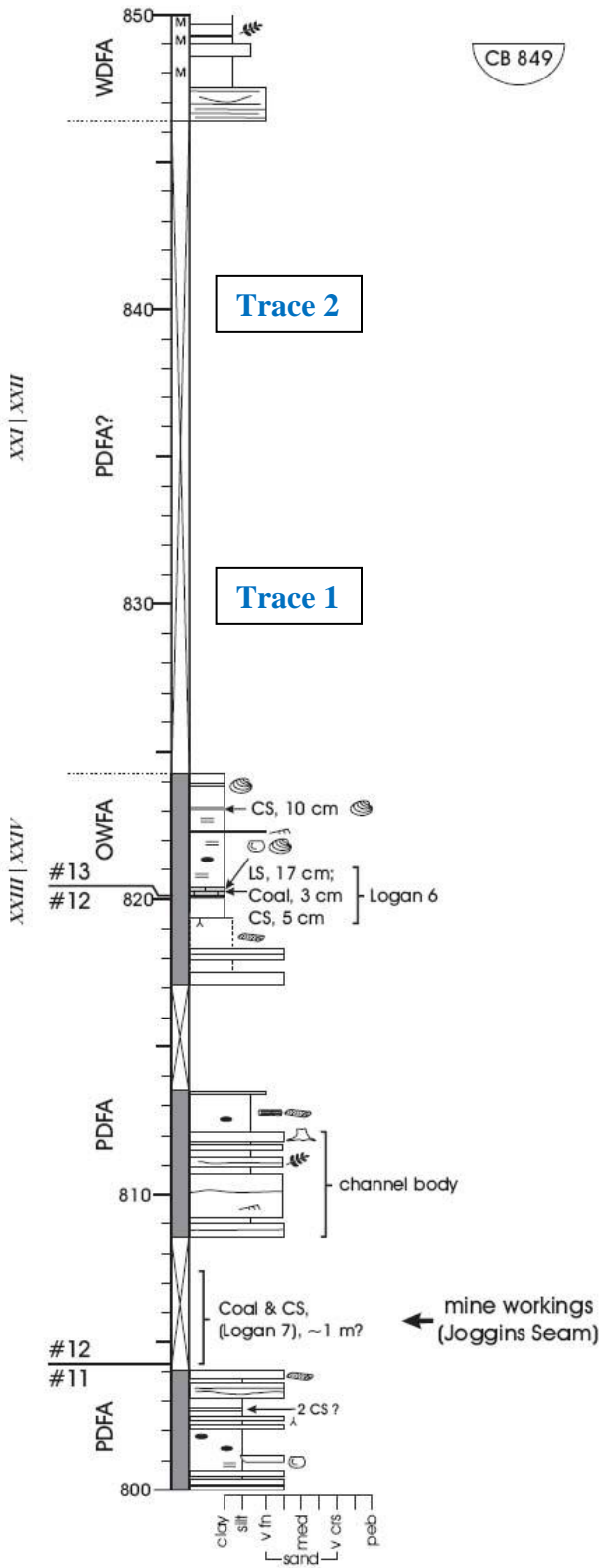
 calamite (<i>in situ</i>)	 <i>Stigmaria</i> Sp.	 finely macerated plant material
 calamite (transported)	 cordaite gymnosperm (<i>in situ</i>)	 root compression
 lycopsid trunk (<i>in situ</i>)	 <i>Artisia transversa</i> (cordaite pith cast)	 charcoal
 lycopsid trunk (transported)	 <i>Cordaites principalis</i> (cordaite leaf)	

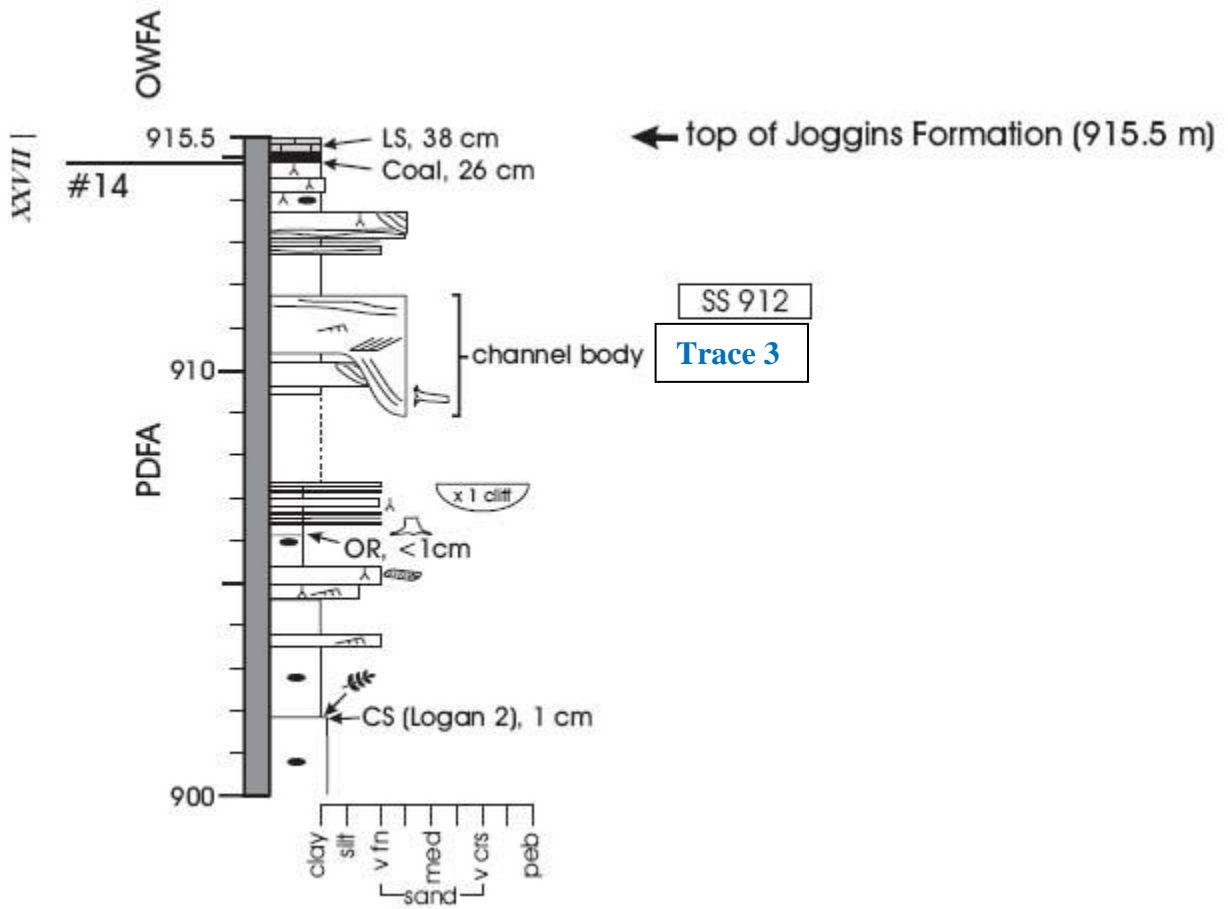
FAUNA

 <i>Diplichnites</i> (<i>Arthropleura</i> trackway)	 <i>Spirorbis</i>	 tetrapod trackway
 bivalve	 <i>Dendropupa vetusta</i>	 fish bone or scale
 ostracode	 tetrapod bone	







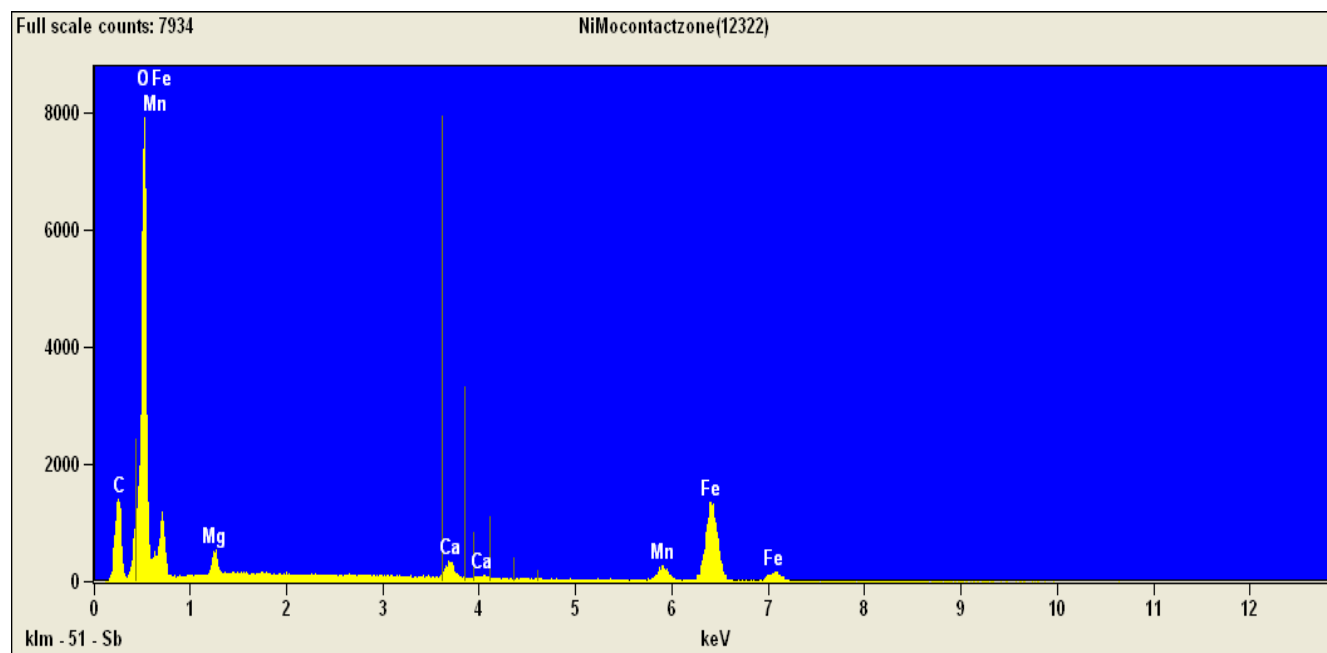


Stratigraphic log modified from Davies et al., 2005.

APPENDIX F - MICROPROBE DATA

WDS data for siderite

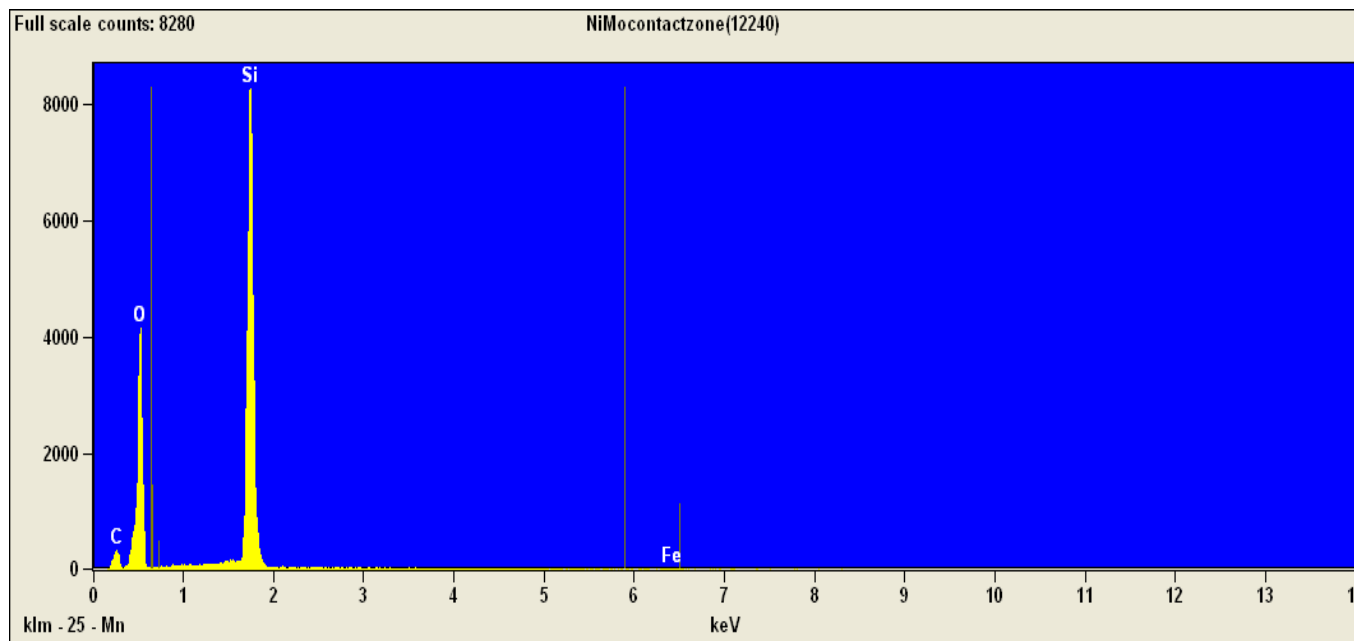
Group :	Dalhousie	Sample :	Chi01					
Stage :	X=	44.1676	Y=	47.4731	Z=	9.984		
Acc. Volta	15 (kV)	Probe Dia.	1	Scan :	On	Mag:	4000	
WDS only	No. of acci	1						
Curr.(A) :	2.00E-08							
Element	Peak(mm)	Net(cps)	Bg-	Bg+	S.D.(%)	D.L.(ppm)		
1 K		120.241	3.9	9.5	3.3	6.97	86	
2 Cr		72.606	10.2	50.9	33.6	3.07	181	
3 Na		129.628	8.4	18.5	12.8	4.56	81	
4 Si		77.339	49.7	49	30.4	2.38	129	
5 Mn		146.558	606	16.1	12.9	0.9	126	
6 Ca		108.088	248.3	0.3	0.5	1.42	22	
7 Ti		87.422	25.7	0.1	0.3	4.4	20	
8 Mg		107.584	353	0	0.8	1.19	10	
9 Al		90.519	31.7	0	0.2	3.96	7	
10 Fe		135.029	4588.3	0.3	0.4	0.33	20	
11 Ba		88.241	8	20.4	15.9	4.39	300	
Overlap	correction							
24.55 (Ti	cps)	=						
7.65 (Ba	cps)	=						
25.7 (Ti	Net)	0	0.13783	x		8 (Ba	Net)	
8 (Ba	Net)	0	0.01223	x		24.6 (Ti	Net)	
ZAF	Oxide							
Element	Mass(%)	Cation	K(%)	K-raw(%)	ZAF	Z	A	F
K2O	0.038	0.0009	0.042	0.348	0.8969	0.9206	0.9889	0.9852
Cr2O3	0.081	0.0013	0.089	0.061	0.9038	1.0609	1.006	0.8468
Na2O	0.116	0.0044	0.054	0.355	2.1338	0.919	2.3131	1.0038
SiO2	0.378	0.0074	0.326	0.504	1.1589	0.9234	1.2543	1.0006
MnO	6.331	0.1053	6.353	7.787	0.9965	0.9904	1.0062	1
CaO	2.471	0.052	2.721	26.42	0.9083	0.9274	0.9933	0.9861
TiO2	0.293	0.0043	0.341	7.218	0.8599	0.9252	0.9879	0.9407
MgO	2.69	0.0787	1.818	14.205	1.4796	0.9307	1.5812	1.0053
Al2O3	0.3	0.0069	0.208	1.107	1.4427	0.9235	1.5389	1.0151
FeO	44.117	0.7243	47.737	216.743	0.9242	0.9245	0.9996	1
BaO	0.165	0.0013	0.171	0.261	0.9603	1.0666	0.9776	0.9209
Total	56.98	0.9868	59.86	275.007	Total	O	=	1
						Iteration	=	4



EDS chart for Siderite

WDS data for quartz

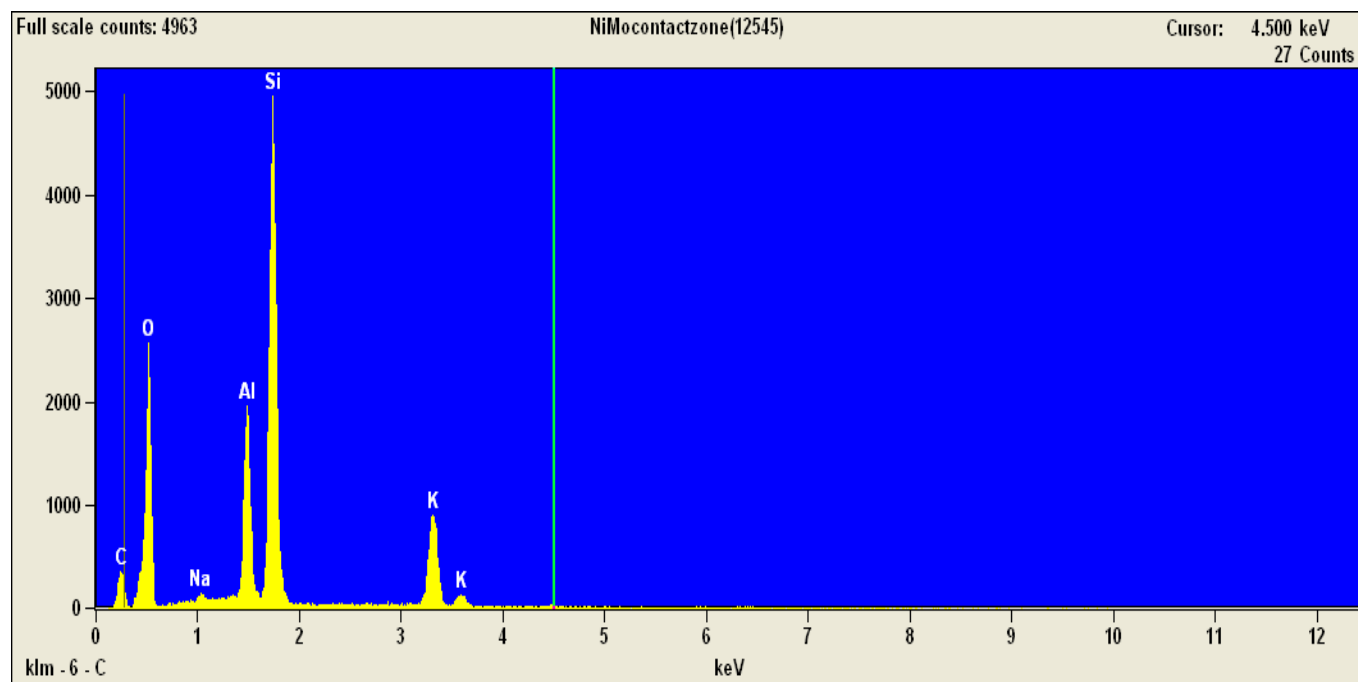
Group :	Dalhousie	Sample :	Chi01					
Stage :	X=	26.9251	Y=	49.962	Z=	10.0305		
Acc. Volta	15 (kV)		Probe Dia	1	Scan :	On	Mag:	4000
WDS only	No. of acc	1						
Curr.(A) :	2.00E-08							
Element	Peak(mm)	Net(cps)	Bg-	Bg+	S.D.(%)	D.L.(ppm)		
1	K	120.281	3.8	8.7	3.5	7.12	86	
2	Cr	72.616	-4.5	50.5	34.8	3.6	185	
3	Na	129.606	1.5	18.9	13.5	5.31	85	
4	Si	77.334	14983.5	40.1	35.1	0.18	129	
5	Mn	146.565	10	15.7	12	4.58	126	
6	Ca	108.108	6.7	12.1	8.1	5.45	113	
7	Ti	87.421	-0.8	27.5	17.4	4.81	207	
8	Mg	107.595	117.2	34.9	27	1.84	92	
9	Al	90.535	234.3	32.9	19.2	1.39	106	
10	Fe	135.023	383.5	22.6	16.8	1.11	146	
11	Ba	88.247	-1.5	28.7	16.3	4.94	337	
Overlap	correction							
	-0.8 (Ti	cps)	=					
	-1.49 (Ba	cps)	=					
	-0.8 (Ti	Net)	0	0.13783 x		-1.5 (Ba	Net)	
	-1.5 (Ba	Net)	0	0.01223 x		-0.8 (Ti	Net)	
ZAF	Oxide							
Element	Mass(%)	Cation	K(%)	K-raw(%)	ZAF	Z	A	F
K2O	0.042	0.0003	0.041	0.34	1.02	1.0092	1.0109	0.9998
Cr2O3	0	0	0	0	0	0	0	0
Na2O	0.012	0.0001	0.01	0.068	1.1226	1.0045	1.1176	1
SiO2	92.137	0.4811	99.778	154.292	0.9234	1.009	0.9145	1.0007
MnO	0.117	0.0005	0.106	0.13	1.1032	1.0961	1.0064	1
CaO	0.077	0.0004	0.075	0.726	1.0314	1.0178	1.0092	1.0041
TiO2	0	0	0	0	0	0	0	0
MgO	0.558	0.0043	0.61	4.768	0.9136	1.017	0.9029	0.9949
Al2O3	1.545	0.0095	1.558	8.305	0.9915	1.009	0.9934	0.9891
FeO	4.124	0.018	4.022	18.263	1.0252	1.0256	0.9996	1
BaO	0	0	0	0	0	0	0	0
Total	98.612	0.5143	106.201	186.892	Total	O	=	1
						Iteration	=	4



EDS chart for Quartz

WDS data for alkali feldspar

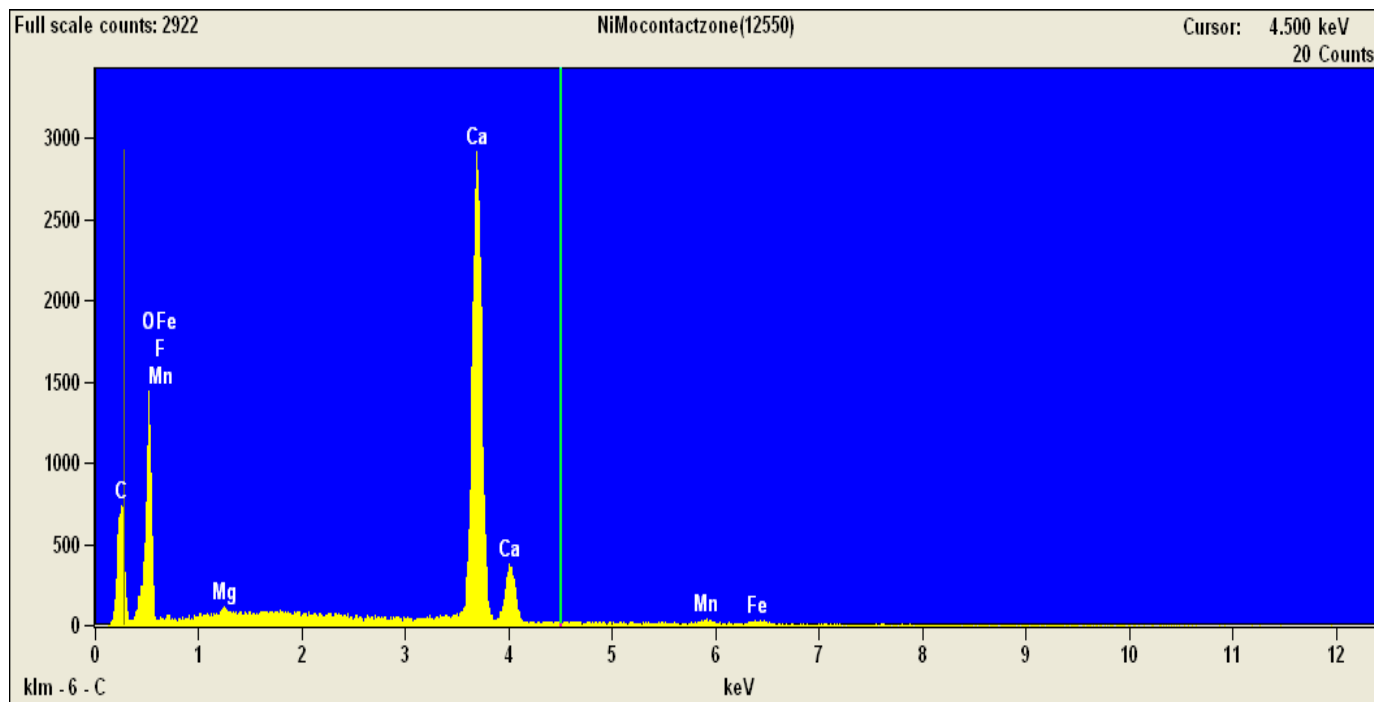
Group :	Dalhousie	Sample :	Chi01					
Stage :	X=	45.0646	Y=	46.4394	Z=	9.9835		
Acc. Volta	15	(kV)	Probe Dia.	1	Scan :	On	Mag:	4000
WDS only	No. of acci	1						
Curr.(A) :	2.00E-08							
Element	Peak(mm)	Net(cps)	Bg-	Bg+	S.D.(%)	D.L.(ppm)		
1	K	120.241	1465.7	7.2	3.3	0.58	78	
2	Cr	72.606	-2.8	51.7	33.1	3.53	181	
3	Na	129.628	99.4	17.5	11.7	2.09	79	
4	Si	77.339	9947.9	47.1	30.4	0.22	128	
5	Mn	146.558	6.3	16.3	12.9	4.89	127	
6	Ca	108.088	-0.7	14.6	9.5	6.59	121	
7	Ti	87.422	8.3	24.3	16.5	4.17	198	
8	Mg	107.584	3.9	27.1	19.1	4.29	78	
9	Al	90.519	2771.1	24.1	16.1	0.42	92	
10	Fe	135.029	90.3	24.1	18	2.12	149	
11	Ba	88.241	28.4	23.8	17.2	3.21	318	
Overlap	correction							
4.39	(Ti cps)	=						
28.35	(Ba cps)	=						
8.3	(Ti Net)	0	0.13783	x		28.4	(Ba Net)	
28.4	(Ba Net)	0	0.01223	x		4.4	(Ti Net)	
ZAF	Oxide							
Element	Mass(%)	Cation	K(%)	K-raw(%)	ZAF	Z	A	F
K2O	15.751	0.1163	15.812	130.739	0.9961	0.9986	0.9975	1
Cr2O3	0	0	0	0	0	0	0	0
Na2O	0.712	0.008	0.646	4.221	1.1018	0.9942	1.1079	1.0003
SiO2	64.504	0.3733	65.212	100.841	0.9891	0.9987	0.9907	0.9998
MnO	0.073	0.0004	0.066	0.081	1.1	1.0837	1.015	1
CaO	0	0	0	0	0	0	0	0
TiO2	0.062	0.0003	0.061	1.288	1.0212	1.0072	1.0078	1.0061
MgO	0.018	0.0002	0.02	0.158	0.9063	1.0066	0.9044	0.9956
Al2O3	17.97	0.1226	18.126	96.606	0.9914	0.9987	0.993	0.9997
FeO	0.958	0.0046	0.939	4.264	1.0201	1.0137	1.0062	1
BaO	0.735	0.0017	0.634	0.966	1.1581	1.162	0.9973	0.9993
Total	100.783	0.6273	101.517	339.164	Total	O	=	1
						Iteration	=	4



EDS chart for Alkali Feldspar

WDS data for calcite

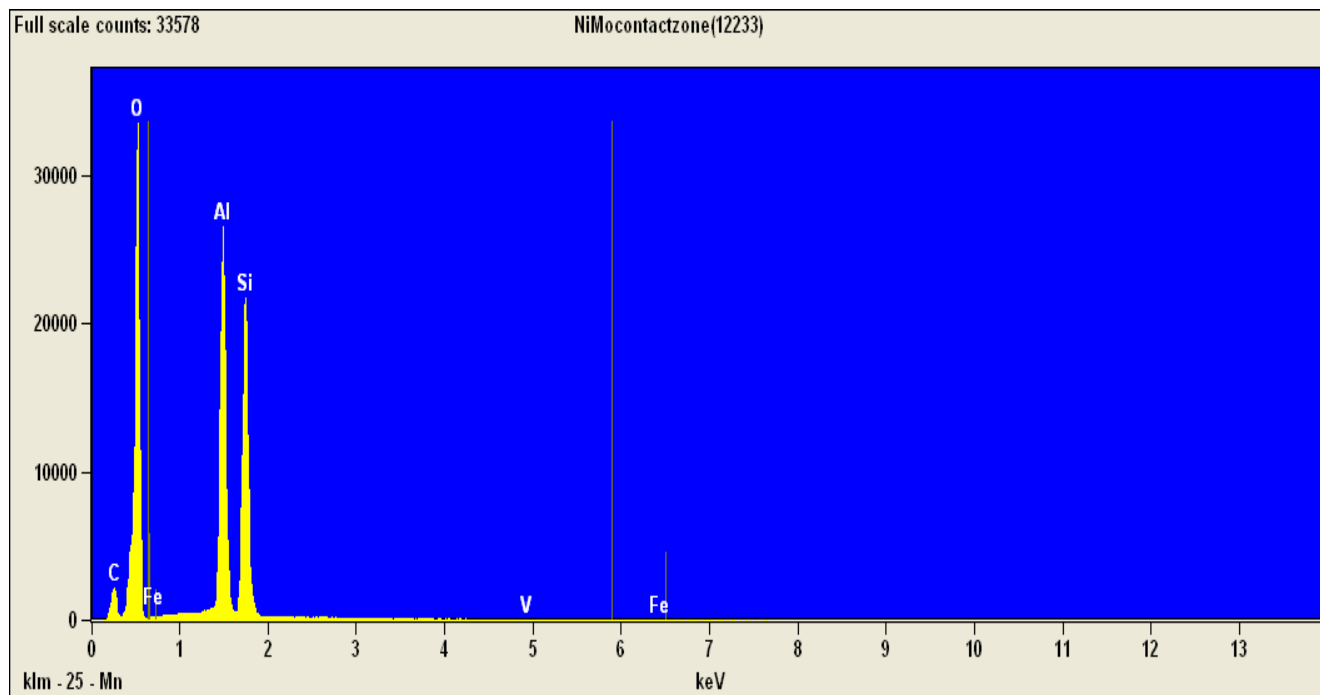
Group :	Dalhousie	Sample :	Chi01					
Stage :	X=	44.1368	Y=	47.3129	Z=	9.9855		
Acc. Volta	15	(kV)	Probe Dia.	1	Scan :	On	Mag:	4000
WDS only	No. of acci	1						
Curr.(A) :	2.00E-08							
Element	Peak(mm)	Net(cps)	Bg-	Bg+	S.D.(%)	D.L.(ppm)		
1	K	120.241	1.9	9.5	3.3	45.12		86
2	Cr	72.606	-1	50.9	33.6	100		181
3	Na	129.628	0.6	18.5	12.8	194.6		81
4	Si	77.339	1.5	49	30.4	131.91		129
5	Mn	146.558	154.2	16.1	12.9	1.96	126	
6	Ca	108.088	3786.3	0.3	0.5	0.36	22	
7	Ti	87.422	13.7	0.1	0.3	6.13	20	
8	Mg	107.584	37.2	0	0.8	3.7	10	
9	Al	90.519	16.4	0	0.2	5.56	7	
10	Fe	135.029	116.6	0.3	0.4	2.08	20	
11	Ba	88.241	1.2	20.4	15.9	112.93		300
Overlap	correction							
13.53	(Ti cps)	=						
1.04	(Ba cps)	=						
13.7	(Ti Net)	0	0.13783	x		1.2 (Ba Net)		
1.2	(Ba Net)	0	0.01223	x		13.5 (Ti Net)		
ZAF	Oxide							
Element	Mass(%)	Cation	K(%)	K-raw(%)	ZAF	Z	A	F
K2O	0.016	0.0004	0.021	0.17	0.7795	0.9743	0.9435	0.848
Cr2O3	0	0	0	0	0	0	0	0
Na2O	0.006	0.0003	0.004	0.028	1.4129	0.9715	1.4485	1.0041
SiO2	0.01	0.0002	0.01	0.015	0.9794	0.976	1.0067	0.9969
MnO	1.787	0.0333	1.616	1.981	1.1057	1.0523	1.0508	1
CaO	39.204	0.9247	41.481	402.797	0.9451	0.9819	0.9592	1.0035
TiO2	0.202	0.0033	0.188	3.978	1.0735	0.9807	1.09	1.0042
MgO	0.208	0.0068	0.192	1.498	1.0859	0.9837	1.098	1.0054
Al2O3	0.122	0.0032	0.107	0.572	1.1333	0.9761	1.1455	1.0137
FeO	1.232	0.0227	1.213	5.506	1.0158	0.9832	1.0332	1
BaO	0.028	0.0002	0.023	0.035	1.217	1.131	1.0791	0.9972
Total	42.815	0.9952	44.854	416.58	Total	O	=	1
						Iteration	=	3



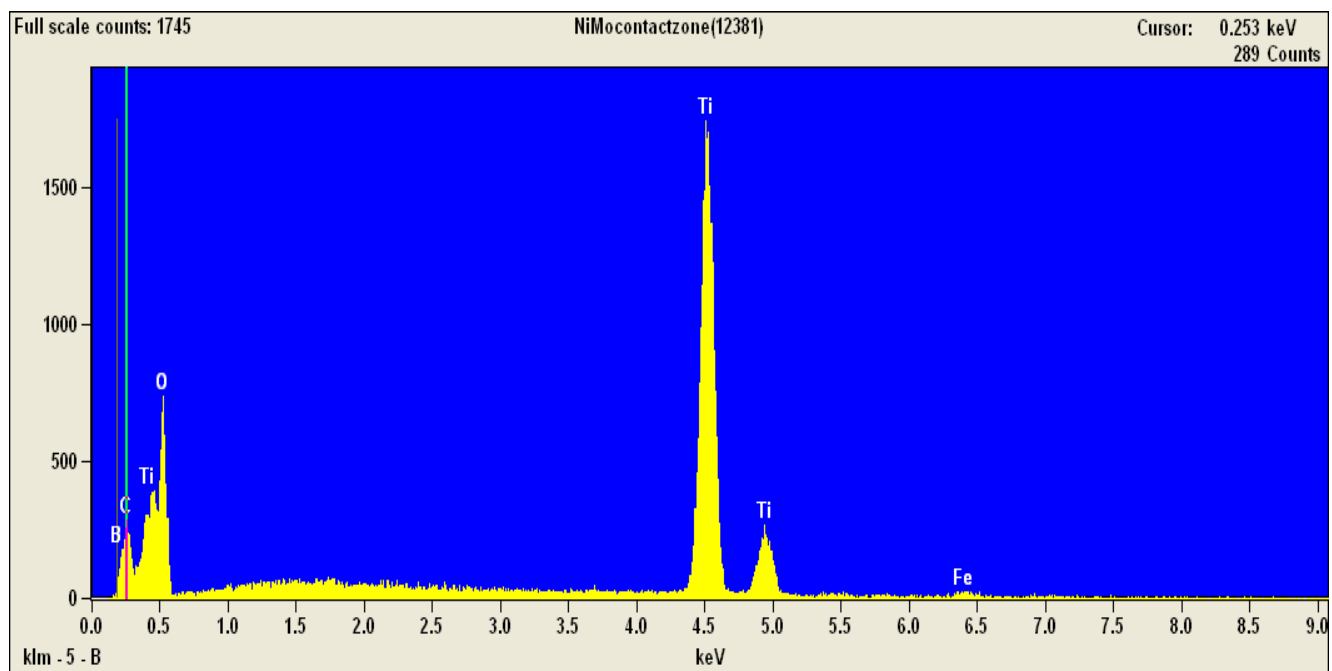
EDS chart for Calcite

WDS data for kaolinite

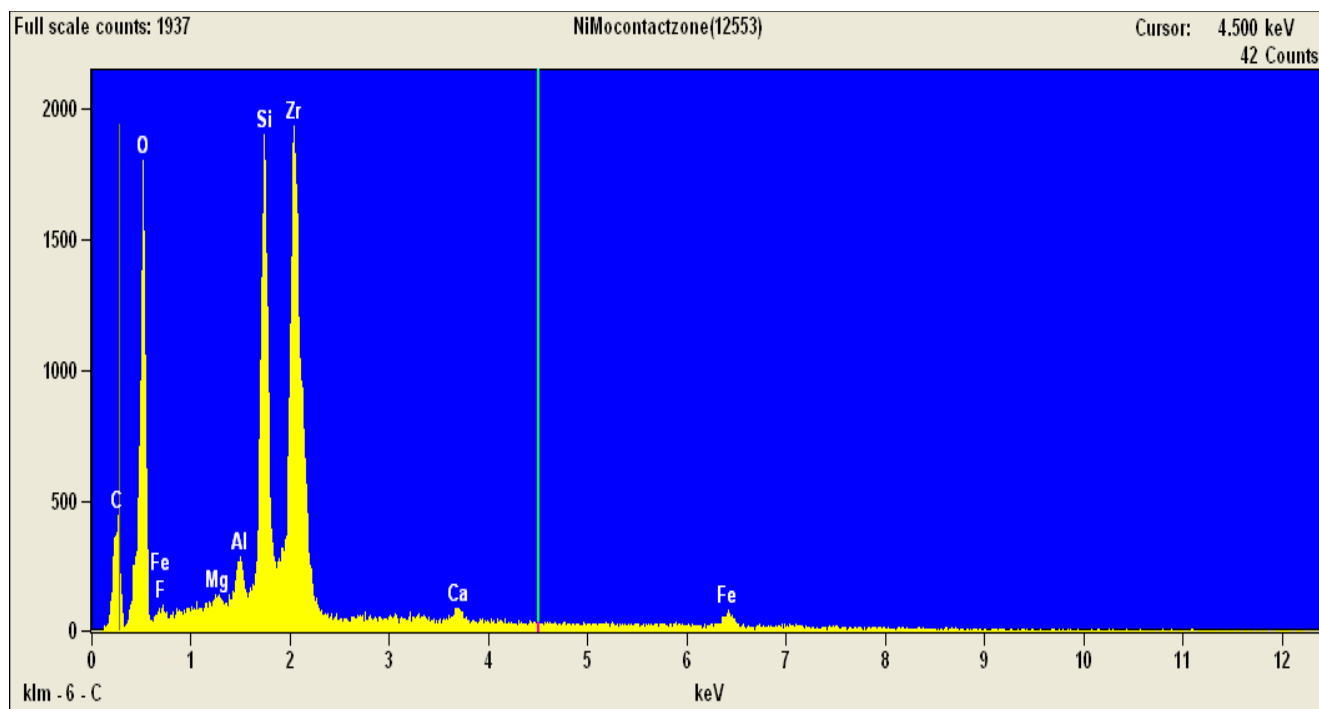
Group :	Dalhousie	Sample :	Chi01					
Stage :	X=	25.2685	Y=	49.7978	Z=	10.0255		
Acc. Volta	15	(kV)	Probe Dia	1	Scan :	On	Mag:	4000
WDS only	No. of acc	1						
Curr.(A) :	2.00E-08							
Element	Peak(mm)	Net(cps)	Bg-	Bg+	S.D.(%)	D.L.(ppm)		
1	K	120.281	1.1	8.7	3.5	8.33	86	
2	Cr	72.616	-6.5	50.5	34.8	3.7	185	
3	Na	129.606	2.6	18.9	13.5	5.16	85	
4	Si	77.334	6446.2	40.1	35.1	0.28	129	
5	Mn	146.565	-0.2	15.7	12	6.05	126	
6	Ca	108.108	-0.4	12.1	8.1	7.16	113	
7	Ti	87.421	-4.4	27.5	17.4	5.26	207	
8	Mg	107.595	-1.1	34.9	27	4.09	92	
9	Al	90.535	5949.3	32.9	19.2	0.29	106	
10	Fe	135.023	18.4	22.6	16.8	3.64	146	
11	Ba	88.247	-6.7	28.7	16.3	5.74	337	
Overlap	correction							
-4.35	(Ti	cps)	=					
-6.74	(Ba	cps)	=					
-4.4	(Ti	Net)	0	0.13783	x	-6.7	(Ba	Net)
-6.7	(Ba	Net)	0	0.01223	x	-4.4	(Ti	Net)
ZAF	Oxide							
Element	Mass(%)	Cation	K(%)	K-raw(%)	ZAF	Z	A	F
K2O	0.012	0.0001	0.012	0.1	1.0138	1.0058	1.0077	1.0003
Cr2O3	0	0	0	0	0	0	0	0
Na2O	0.018	0.0002	0.017	0.111	1.0311	1.0009	1.0321	0.9982
SiO2	47.191	0.2918	42.905	66.346	1.0999	1.0054	1.0932	1.0007
MnO	0	0	0	0	0	0	0	0
CaO	0	0	0	0	0	0	0	0
TiO2	0	0	0	0	0	0	0	0
MgO	0	0	0	0	0	0	0	0
Al2O3	37.979	0.2768	39.545	210.759	0.9604	1.0054	0.9515	1.004
FeO	0.197	0.001	0.193	0.875	1.0218	1.0227	0.9991	1
BaO	0	0	0	0	0	0	0	0
Total	85.397	0.5699	82.672	278.191	Total	O	=	1
						Iteration	=	5



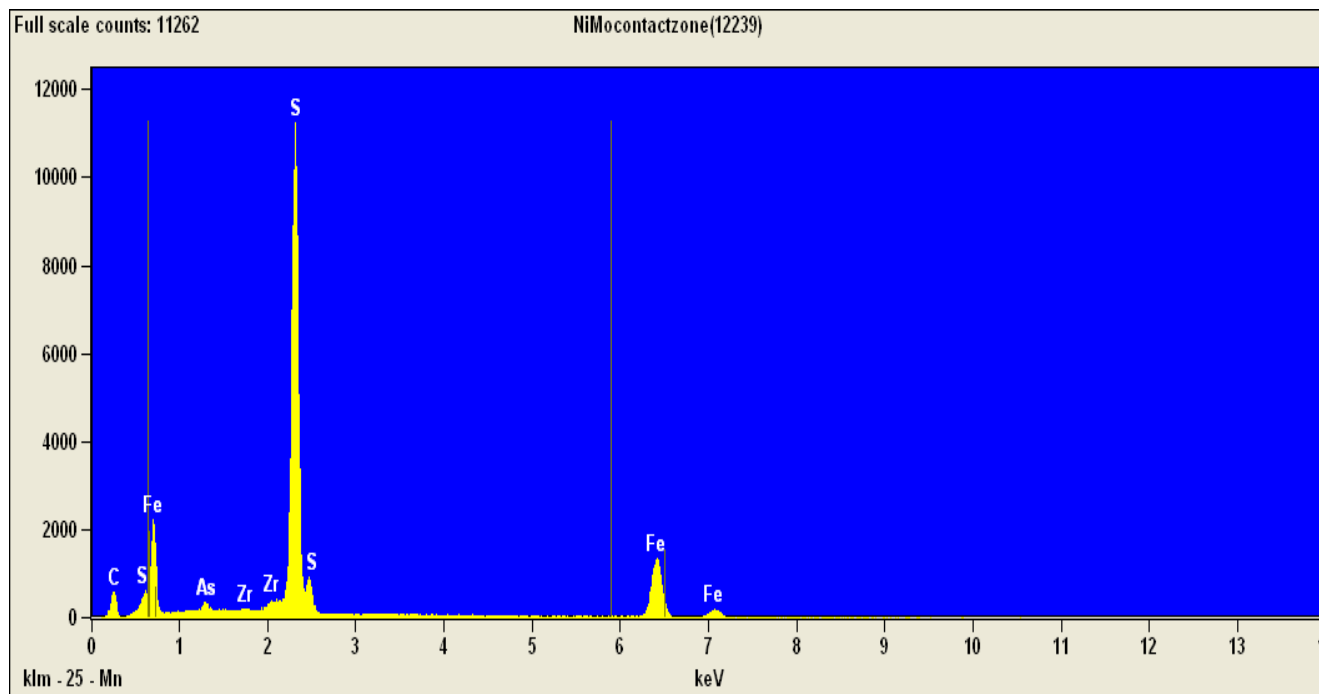
EDS chart of Kaolinite



EDS chart of Rutile



EDS chart for Zircon



EDS chart for Pyrite